The Sediment, River Plume, and Inner Shelf Variability in a Bay with Multiple Fluvial Inputs

A thesis

submitted in fulfilment

of the requirements for the degree

of

Doctor of Philosophy in Earth Science

at

The University of Waikato

by

TED CONROY

THE UNIVERSITY OF
WAIKATO
Te Whare Wānanga o Waikato

2024

Abstract

Small mountainous rivers deliver considerable sediment loading to the coastal ocean and play a disproportionate role in marine sediment deposition globally. Discharge in these rivers is often driven by short episodic events and they typically deliver sediment to energetic coastal environments where in-situ observations of cross-shelf sediment transport are spatially limited and are difficult to maintain over representative periods of time. How these river plumes respond to environmental conditions, and where sediment is initially deposited from the river plumes are essential to understanding long-term sediment transport and deposition patterns in the coastal ocean. This thesis explores this problem using three approaches applied to Hawke Bay (Aotearoa New Zealand) and its river plumes: remote sensing (paper 1), large-scale numerical modelling (paper 2) and high resolution in situ observations at one of the river mouths (the Tukituki River) (paper 3).

Using ocean colour remote sensing to determine the length scales of sediment transport from small mountainous river plumes

Satellite ocean colour records now extend >20 years and have the potential to facilitate spatially-explicit, long-term studies of suspended sediment variability in river plumes in many coastal regions of the world. In this work, I developed a local algorithm for total suspended sediment (TSS) concentration and applied it to the daily MODIS ocean colour record to characterize river plume dynamics, determine their drivers, and identify likely sediment deposition sites in Hawke Bay, Aotearoa New Zealand. This natural embayment, located in a temperate region, is an energetic coastal environment receiving sediments inputs from multiple small mountainous rivers, making it an ideal test site for this study. Our analysis revealed that the river plume length scales were found to be 2–8 km, varying with river size and river discharge. Waves driving sediment resuspension also contributed to the observed concentration signal. Wind was an important factor determining the plume directionality.

Circulation and cross-shelf sediment fluxes in an energetic bay with multiple small mountainous rivers

Understanding the source to sink transport of sediment from rivers into the coastal ocean is a key process that has implications for marine ecology and land and river management. In locations with multiple rivers that have episodic, high intensity discharge events, the response to inner shelf conditions and the transit of sediment is a highly relevant issue both in Aotearoa New Zealand and for small mountainous river systems worldwide. In this chapter, a three dimensional, realistic numerical

ocean model that couples hydrodynamics and waves is used to simulate these patterns in Hawke Bay, Aotearoa New Zealand over multi-year time scales. The developed model is well validated with a broad range of oceanographic data, and is used to characterise the understudied circulation in Hawke Bay, the river plume dynamics, and the resulting cross-shelf sediment flux. The mean circulation and stratification largely influenced by buoyancy input, with river plumes and coastal currents commonly present in the nearshore. Wind was found to be a key driver of plume transport and mixing. Both event time scale and multi-year sediment deposition and erosion patterns were detailed throughout the Bay, finding that longer term deposition primarily occurs in depths greater than 40 m, due to persistent wave resuspension of sediment.

The variability of cross-shelf flows offshore of a small mountainous river

The response of a river plume circulation, stratification, and mixing to common inner shelf forcings ultimately impacts the cross-shelf flux of terrestrial material. In particular, for small mountainous river systems, the magnitudes of river discharge can be high, the coastal ocean receiving environment can be energetic with strong wind and large wave conditions, and the spatial scales are typically smaller than classic river plume studies have presented. In this chapter, an in-situ dataset of density and circulation throughout the water column was collected offshore of the Tukituki River in Aotearoa New Zealand. This dataset captured a broad range of environmental conditions that was uniquely situated in the near-field river plume for a large portion of the deployment. This chapter characterised the response to varying wind conditions on river plume vertical structure, finding that upwelling winds, along with offshore winds, the latter which has not been studied in detail prior, can drive the largest cross-shelf fluxes in the surface layer. This chapter additionally highlighted the importance of inlet morphology for setting the river plume directionality, and the implications for cross-shelf sediment transport.

Acknowledgements

This thesis would not have been possible without the unrelenting support, positivity, and help of Karin Bryan. Cedric Fichot was instrumental in developing my knowledge of remote sensing and working with satellite data. Thank you to Joe O'Callaghan for the continual advice regarding physical processes in river plumes and the inner shelf. Thank you to Hayden Moffitt at Ocean Adventures for being an amazing boat captain, wealth of maritime and local knowledge, and being nice to me when I got seasick. A huge thank you to Ben Roche for helping with the instrument deployment, that was a massive undertaking that wouldn't have been possible without your help. Thank you to Moritz Lehmann for the advice on how to use the hyperspectral radiometer. Thank you to Becky Shanahan and Jose Beya for the advice throughout the project regarding Hawke Bay. Lastly, thank you to my family for the support.

Table of Contents

List of Figures

List of Tables

Chapter 1: Introduction

1.1 Introduction to thesis

The flux of sediment and terrestrial material to the coastal ocean is linked through river outflows and buoyant river plumes which transit material across the nearshore and inner shelf (e.g. Fig. 1.1). Many rivers in Aotearoa New Zealand yield high suspended sediment concentrations and transit millions of tons of sediment to the coastal ocean annually (Hicks et al. 2011), where flood events typically occur over short time scales related to episodic storm systems (Walsh and Nittrouer 2009). Small mountainous rivers, which have drainage basins less than 10,000 km^2 and are found on active margins with steep coastal topography, in particular transit large amounts of sediment to the coastal ocean relative to their watershed size (Milliman and Syvitski 1992). For example, Aotearoa New Zealand rivers have been estimated to contribute 1.7% of the global sediment flux to the ocean although its land area covers 0.2% of the global land area (Hicks et al. 2011). The delivery of terrestrial sediment into the coastal ocean can cause impacts on the shelf and nearshore ecosystem, such as limiting light penetration and blanketing the benthic environment with fine sediments, ultimately changing the structure and function of these areas (Thrush et al. 2004). Characterizing the sediment pathway from rivers, to transit within river plumes, to deposition on the inner shelf and beyond is important for understanding potential future changes due to land use changes and climate change.

Figure 1.1 The Tukituki River in Hawkes Bay, Aotearoa New Zealand, during a flood event. Image from Hawkes Bay Regional Council.

This work is focused on understanding the circulation and suspended sediment transport from small mountainous rivers to the coastal ocean. The study site is Hawke Bay, in Aotearoa New Zealand (Fig. 1.2), a large bay with multiple rivers that yield a significant flux of terrestrial material to the coastal ocean. There are major knowledge gaps regarding the circulation of Hawke Bay and the transport of fine sediment from rivers to the coastal ocean, with implications to coastal ecosystems. Additionally, the dynamics of small to medium sized rivers with episodic river discharge (that are typically produced by small mountainous rivers) have received less attention than larger rivers with steadier river discharge (Horner-Devine et al. 2015). For a comprehensive understanding of dynamics for these river plumes and impacts to the suspended sediment transport, an assessment of the impacts of common inner shelf processes and environmental conditions is needed at a multitude of temporal and spatial scales. Relevant to this thesis are the topics of inner shelf circulation, river plume dynamics, and suspended sediment transport, each of which are reviewed in this introduction.

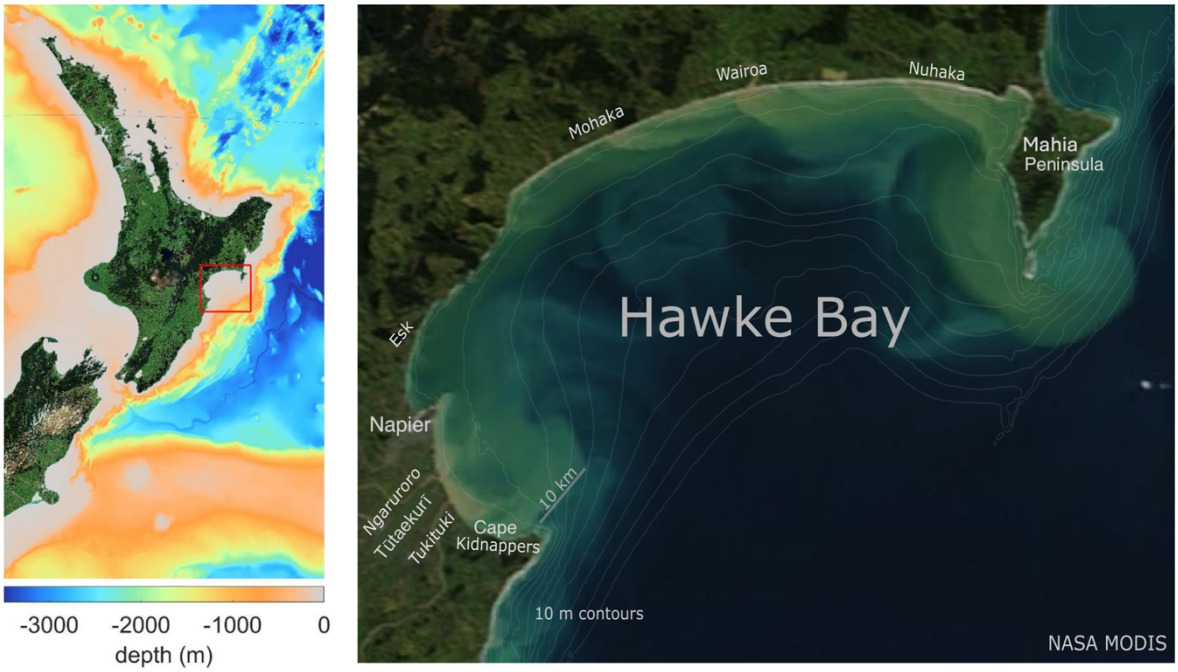

Figure 1.2 Spatial overview of the study site. The left plot shows the bathymetry (m) of the North Island of Aotearoa New Zealand. The red box marks the region of Hawkes Bay. On the right is a satellite image of Hawke Bay, including the names of the major rivers and places throughout the region, and 10 m depth contour lines from 10 to 100 m depth (grey). Image from NASA MODIS.

1.2 Inner shelf and river plume circulation

The currents on the inner shelf are influenced by wind, waves, tide, and offshore forcings (Lentz and Fewings 2012, Kumar et al. 2016). Tides are a key driver of coastal circulation in New Zealand (Stevens et al. 2021) and rotate counter clockwise around the North Island. Wind stress can drive upwelling and downwelling which in turn drive cross-shelf currents, and wave induced currents can drive cross-shelf, vertical and alongshore currents in the nearshore. The additional input of

buoyancy from rivers drives river plume circulations and can create regions of freshwater influence (e.g. O'Callaghan and Stevens 2017).

River plumes are formed due to the input of buoyancy from rivers into the coastal ocean, and are persistent features of Hawke Bay which can be commonly identified from satellite imagery (e.g. Fig. 1.2). River plumes are the initial transport mechanism for sediment and other terrestrial material from land to the coastal ocean, and the currents associated with river plumes can greatly alter coastal circulation patterns (Horner-Devine et al. 2015). The plume dynamics are dependent on the outflow strength of the river, the intensity of stratification, and mixing processes which act to slow the river plume and dilute the river plume water. A river plume can be characterised by three regions, which are the near field, mid-field, and far field (Fig. 1.3; Horner-Devine et al. 2015, Hetland 2005).

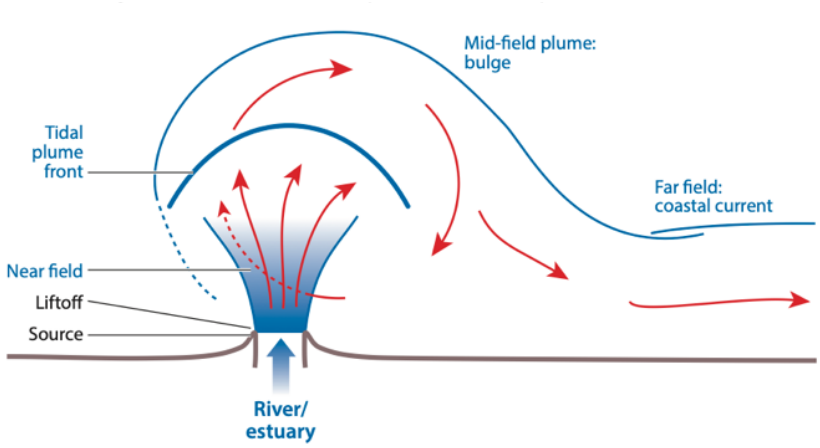

Figure 1.3 Schematic of river plume dynamical regions. The schematic includes the near field, mid-field, and far field regions. Figure is sourced from Horner-Devine et al. (2015).

In the near field region, transport is dictated by the outflow momentum at the river mouth and behaves as a jet, being slowed down by shear mixing at the base of the plume (Fig. 1.3). A near field plume will occur if the flow becomes supercritical at the mouth of the river. In the mid-field region, other processes become important as the momentum flux decreases due to shear driven mixing. The density contrast between the fresh and ocean water produces lateral spreading at the rate of the internal wave speed, and local winds can create surface currents which transport the freshwater as well as provide vertical mixing if the Ekman layer depth is greater than the plume depth. In the far field plume, winds become the dominant mixing and transport mechanism, as well as other inner shelf currents and the Coriolis force which can drive rotation and the formation of a coastal current (Fig. 1.3).

Upwelling winds that are directed alongshore have been shown to enhance the cross-shore river plume transport and thin the plume, while downwelling winds have been shown to inhibit the cross-shore transport and thicken the plume vertically (Fong and Geyer 2001). The role of cross-shelf winds has received less attention, as cross-shore transport related to Ekman dynamics is expected to

be more important. However, Hunter et al. (2010) noted the relation between direct cross-shore wind and associated cross-shore plume transport in the Hudson River plume, and Kakoulaki et al. (2014) similarly showed direct relations between wind and plume directions for wind speeds greater than 4 m s^{-1}. These studies showed that smaller scales plumes are likely more susceptible to cross-shelf winds than larger river plumes such as the Columbia River (e.g. Hickey et al. 2010).

1.3 Sediment transport from rivers into the coastal ocean

The transport of sediment from rivers into the ocean is dependent on the plume circulation and sediment characteristics (Geyer et al. 2004), and the dispersal and deposition of sediment is largely dependent on the characteristics of the coastal ocean receiving environment and plume circulation (Wright and Nittrouer 1995). For example, Walsh and Nittrouer (2009) classify varying types of dispersal settings, with the *marine dispersal dominated* setting most relevant for small mountainous rivers in New Zealand (as studied here). Small mountainous rivers are characterised by steep coastal mountain ranges that generally drain into energetic coastal oceans and have episodic discharge events, and make up a large portion of the sediment transported into the ocean globally (Milliman and Syvitski 1992). In these systems, buoyant river plumes advect suspended sediment horizontally until it falls out of the plume into a region with sufficient bottom stress to be resuspended and further transported at depth to longer-term depositional areas (Fig. 1.4). Rivers that fit the *marine dispersal dominated* category include the Eel River (Geyer et al. 2000), the Po River (Harris et al. 2008), and the Waipaoa River in Poverty Bay (Kuehl et al. 2016).

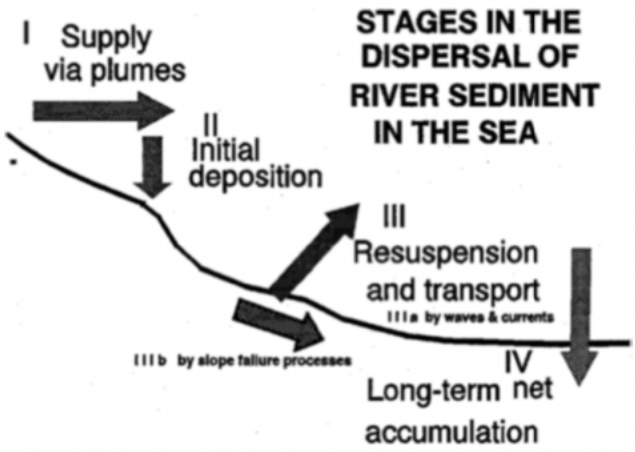

Figure 1.4 Schematic of the typical sediment transport pathway for marine dispersal dominated river systems. Figure is sourced from Wright and Nittrouer (2009).

The sediment settling velocity is a function of the grain diameter and density of the sediment. This is complicated by the aggregation of fine particles, termed flocculation, where smaller particles aggregate to form larger flocs. Flocs can have order of magnitude increases in settling velocity which can greatly influence how far sediment can be transported from river plumes (Geyer et al. 2000). The

flocculation process is thought to be dependent on sediment composition, turbulence intensity, the chemical interaction with salt water, and the organic compounds that aggregate particles together (Geyer et al. 2004). Coarser sediments such as sand will be deposited near the inlet mouth and would produce a delta offshore of the inlet in the absence of wave activity. Flocs have also been shown to be deposited in close proximity to the river inlet due to their high settling velocity (Milligan et al. 2007; Warrick et al 2008). Average plume trajectories have been shown to coincide with fine sediment depositional areas for marine dispersal dominated rivers (Wright and Nittrouer 1995).

For example, offshore of the Waipaoa River in Poverty Bay, aggregate and coarser particles were found to settle in the embayment and slightly offshore, while finer sediment is more dispersive along the continental shelf (Moriarity et al. 2015). Some sediment was found to be stored in long-term mud deposition areas located at bathymetric low points, but a majority would be resuspended by wave orbital currents in the thin wave boundary layer, which can reach concentrations high enough to form turbidity currents that transport sediment further offshore (Traykovski et al. 2000, Hale and Ogsten 2015). If river flood events co-occurred with significant waves, sediment was likely transported offshore immediately, but if they did not co-occur, sediment could be stored temporarily in Poverty Bay and on the continental shelf (Bever et al. 2011, Moriarity et al. 2015). In Poverty Bay, Kniskern et al. (2010) used isotopic dating to show that muddy sediments are stored ephemerally between 30-50 m, and that longer-term deposition was found offshore at 80-120 m. Due to the proximity to Hawke Bay and similar environment, similar aspects are expected to be found in Hawke Bay, although these processes have not yet been assessed for the region.

1.4 Ocean colour remote sensing

Satellites routinely image the surface of the coastal ocean, providing ocean colour data with sufficient spatial resolution to resolve features such as river plumes. Satellite ocean colour datasets now allow for long time scales (> 20 years) to be studied, and the observed ocean colour directly relates to the surface suspended sediment concentration (Kirk 1994), allowing estimates of the suspended sediment concentration in river plumes to be analysed over time. These snapshots of surface sediment characteristics have much higher spatial coverage than would be possible observationally, but lack vertical information and have time resolution of one day or greater.

Satellites measure the spectrum of the water leaving radiance $L_w(\lambda)$, which corresponds with the Inherent Optical Properties (IOPs) of the water, including non-algal particles (including sediment), chlorophyll, coloured dissolved organic matter, and water itself, which can scatter and absorb light, and together attenuate light through the water column (Kirk 1994). To account for changes in downwelling light, normalized reflectances such as the remote sensing reflectance $R_{rs}(\lambda) = L_w/E_d$, where E_d is the downwelling irradiance at the sea surface, are used to obtain information about the IOPs, as these are independent of the ambient light field (Kirk 1994).

Estimates of the Suspended Sediment Concentration (SSC) from R_{rs} measurements can be approximated analytically, or from empirical relations determined from global datasets or locally collected data (Basdurak et al. 2020). Many studies have estimated the sediment concentration in river plumes and coastal settings from satellite imagery (Many et al. 2018, Aurin et al. 2013, Constantin et al. 2018), where Total Suspended Solids (TSS) or SSC is commonly estimated from wavelengths in the red or near-infrared portion of the spectrum. These studies have determined seasonal SSC patterns and related spatial SSC variability to variations in river discharge and wind variability (Pawlowicz et al. 2017; Constantin et al. 2018), indicating that satellite ocean colour data provides a useful tool for investigating surface SSC variability in river plumes over long time scales.

1.5 Study site

1.5.1 Site description

Hawke Bay is a large southeast facing embayment on the east coast of the North Island of Aotearoa New Zealand, extending from the Mahia Peninsula southward to Cape Kidnappers (Fig. 1.2). The bay is ~80 km long, and has 9 significant rivers that discharge into the bay. The rivers have a relatively high combined average sediment flux of 11 million tonnes per year (Hicks et al. 2011). Limited oceanographic work has been conducted to understand the circulation, sediment transport and depositional patterns that occur in the Bay (Stevens et al. 2021). River plumes with elevated suspended sediment concentrations are common features of the Bay (Fig. 1.5), which have not been studied in detail for the entire Hawke Bay prior to in this thesis.

Figure 1.5 Satellite imagery of suspended sediment in Hawke Bay. The left image shows Hawke Bay and the right image shows the Wairoa River plume during a flood event. Image data is from Sentinel-2 (European Space Agency).

The continental shelf offshore of the Bay is broad and gently sloping, in comparison to the shelf to the north and south of the Bay, and extends to the Hikurangi subduction zone offshore. The

region is highly geologically active with complex uplift patterns (Komar 2010) and steep coastal mountains, including the Huiarau, Kaweka, and Ruahine Ranges. The coastal mountains are sedimentary with mainly sandstone and mudstone layers. The sediment delivered to the southern portion of the bay is generally mesozoic greywacke with other conglomerates, sandstones and mudstones, and the sediment delivered to the northern portion of the bay is primarily tertiary sandstone (Komar 2010). The issue of sedimentation in the Bay has likely been exacerbated since human settlement in the area, as the conversion from native forest to pasture land has been shown to increase the sediment yield by a factor of four in the region (Eyles and Fahey 2006).

1.5.2 Oceanographic description

The Hawkes Bay region is subject to predominantly southwest winds and is subject to highly variable and sporadic precipitation that can occur throughout the year (Chappell 2013). The rainfall patterns in the region are highly linked to the direction in which storms approach the region. Occasional cyclone events typically approach from the east to northeast and have the potential to transport significant amounts of precipitation to the region. The Bay is susceptible to strong wind and wave forcing at times. The average significant wave height recorded off Napier was 1.2 m, but high wave events can be from 2.5–3.5 m, and the largest events are greater than 8 m (Komar 2010). Waves on average approach from the east-southeast, are larger in winter, and wave heights in the bay can be variable for a given swell due to wave refraction. Waves create longshore currents that are important for sediment transport and beach erosion in the southern bay (Komar 2010). The spring tidal range is 1.9 m and during neap is 1.2 m as measured at the Napier Port.

There are two dominate currents that flow offshore of the Bay: the warmer and saltier East Cape current from the north and the cooler and fresher Wairarapa coastal current from the south (Fig. 1.6; Kerry et al. 2023; Stevens et al. 2021); the latter being a mixture of the Southland and D'Urville water masses that are generally mixed between the two islands (Chiswell 2002). Chiswell (2002) showed that water from the Wairarapa coastal current is commonly advected into Hawke Bay by studying the propagation of temperature signals northward into the Bay.

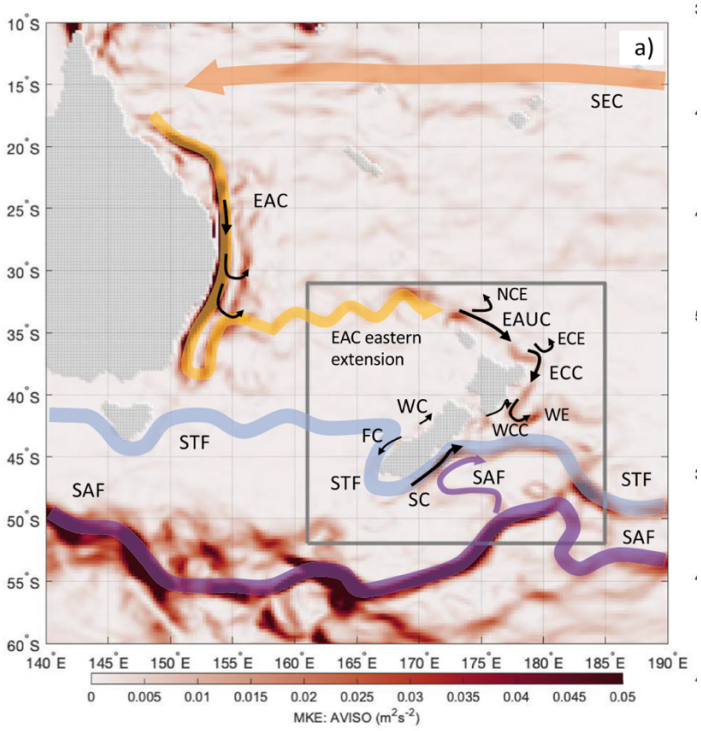

Figure 1.6 Boundary currents around Aotearoa New Zealand. Of particular interest is the East Cape Current (ECC), Wairarapa Coastal Current (WCC), and Wairarapa Eddy (WE). The colour scale refers to the mean kinetic energy ($m^2\ s^{-1}$). Figure is sourced from Kerry et al. (2023).

The circulation pattern in Hawke Bay has been sporadically studied in the past 60 years. Ridgeway (1960) used Lagrangian drift cards deployed from an airplane and documented where the cards ended up on local beaches. Vectors were then drawn between the drop location and the beach where the card was found, to conclude that the general circulation pattern in the bay is an inflow into the center of the bay and then a divergence toward the north and south from there. Ridgeway and Stanton (1969) drew a similar conclusion by measuring the density at an instance throughout the Bay and hypothesizing a potential circulation pattern from the density observations (Fig. 1.7).

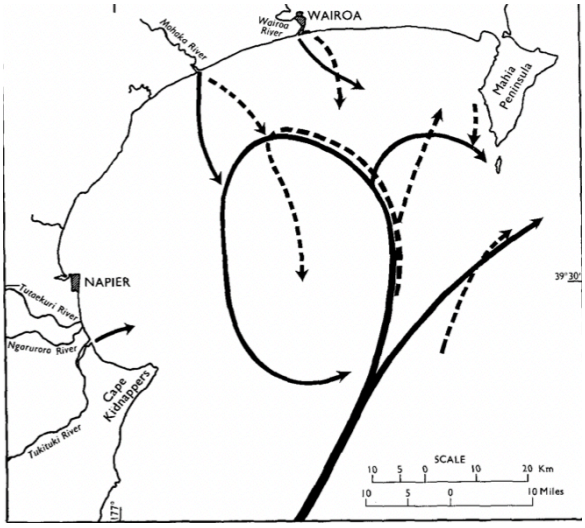

Figure 1.7 The estimated circulation of Hawke Bay from Ridgeway and Stanton (1969). Figure is sourced from Ridgeway and Stanton (1969).

White (1994) conducted a detailed study of suspended sediment and circulation patterns in the southern region of Hawke Bay, observing highly stratified river plumes, sediment resuspension from waves in non-riverine regions, and sharp salinity gradients in the rivers. General circulation patterns for the southern region of Hawke Bay were estimated (Fig. 1.8), showing nearshore flows commonly northward while outside of the nearshore the flow was commonly southward directed towards Cape Kidnappers. These past studies of the circulation may have characterized general patterns of the Hawke Bay circulation, but given the limited time periods of observations it is likely that key elements to the circulation and water column structure may vary from these generalisations.

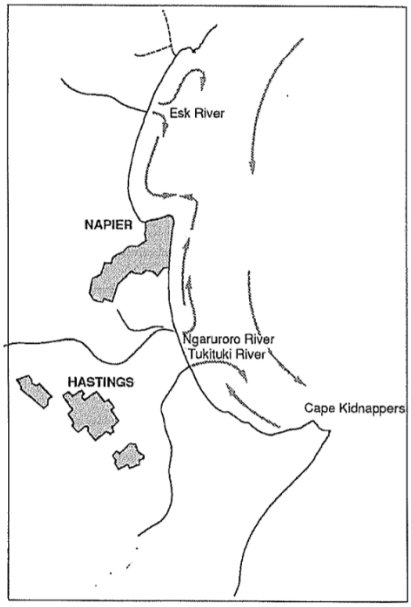

Figure 1.8 The estimated circulation in the southern Hawke Bay region from White (1994). Figure is sourced from White (1994).

1.5.3 Sediment characterisation

The sediment characteristics in the Bay follow common continental shelf sedimentary patterns, with coarse sand on beaches and muddy areas becoming progressively dominant with distance offshore. There are also several gravel zones and rock reefs in the Bay, as described below. Pantin (1966) comprehensively sampled and described the bed sediment characteristics in the Bay (Fig. 1.9), observing that coarse beach sand (with the median grain size (d_{50}) around 250 μm) persists for a relatively short distance offshore until fine sand becomes the dominant sand size in the Bay (in the range of 63–150 μm, and from 100–125 μm; Marshall 1929, Pantin 1966, Hume 1989, White 1994). Muddy regions offshore were recorded to have silt/clay to sand ratios of typically 70/30.

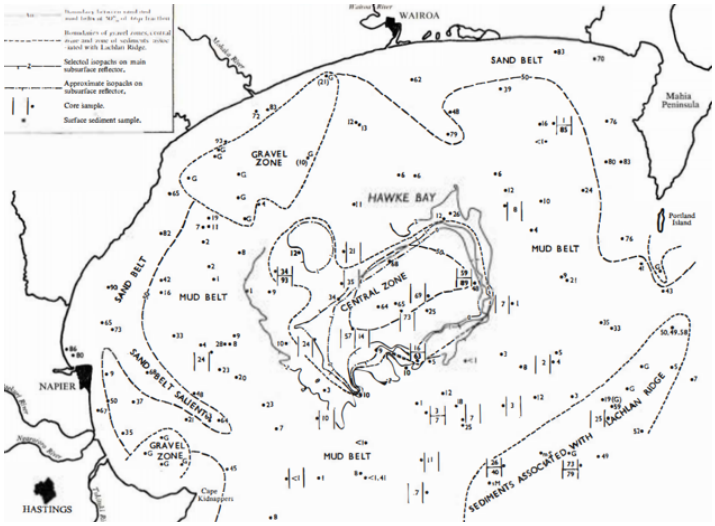

Figure 1.9 The locations of sediment samples and bed characteristics as measured by Pantin (1966). Figure is sourced from Pantin (1966).

Gravel is found along numerous beaches of the Bay, including at the inlets of the major rivers, and a few offshore regions such as offshore of the Mohaka River (Pantin 1966). Grain sizes at the bed of the Tukituki River near the inlet and up to 1.5 km upriver from the inlet range from 4–32 mm, with the average d_{50} 16 mm. Rocky reefs areas in the Bay include the Pania reefs, Wairoa Hard, Clive Hard, and offshore of the Mahia Peninsula. A region in the middle of the Bay contains coarse sediment mixed with little mud. Pantin (1966) hypothesized that stronger bed stress may be found at this location due to the inflow of offshore currents into this area. The compiled bed sediment datasets (data from Bostock et al. 2019 and Hawkes Bay Regional Council) show similar patterns to the description from Pantin (1966) with additional spatial variable variability resolved by more recent sediment samples. Sand is found in the nearshore region, with mud offshore of ~20–30 m depth, and gravel/reefs found at few locations throughout the Bay (Fig. 1.10).

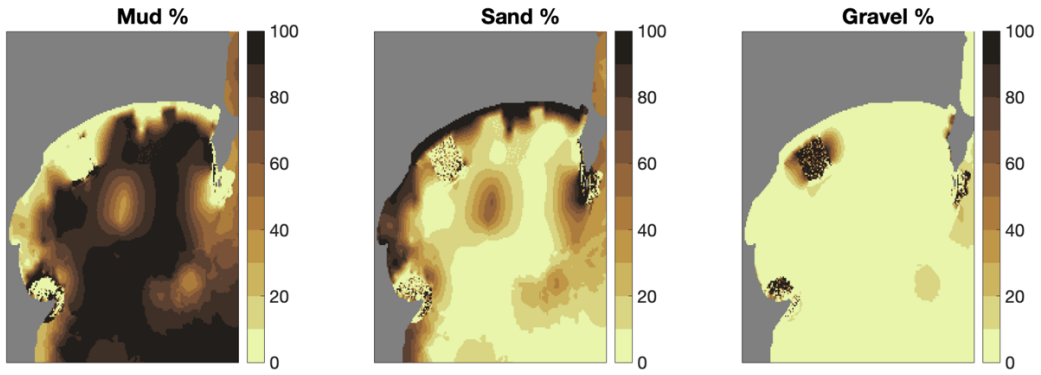

Figure 1.10 The merged and interpolated bed sediment characteristics in Hawke Bay. The data sets includes data from Pantin (1966), Bostock et al. (2019), and data from Hawkes Bay Regional Council. The gravel class includes rocky reef areas.

Estimates of sedimentation rates from carbon dating have been made from Pantin (1966) and sediment thicknesses have been mapped from seismic data (Paquet et al. 2009). Pantin (1966) measured a maximum depositional rate of 0.23 cm per year and more typically rates of ~0.07 cm per year in other muddy regions. From a geophysical analysis, Paquet et al. (2009) mapped estimates of geographic, depositional, and hypothesised sediment transport pathways for 20,000 and 7,200 years ago (Fig. 1.11a,b). The most recent period analysed by Paquet et al. (2009) displays depositional zones offshore of the Ngaruroro, Tūtaekurī, and Tukituki Rivers as well as offshore of the Wairoa River, with limited deposition occurring at Kidnappers and Lachlan Ridges (Fig. 1.11b). These studies provide a basic description of likely sedimentation in the Hawke Bay, but further detailed investigation is needed to determine the present day sedimentation regime in Hawke Bay.

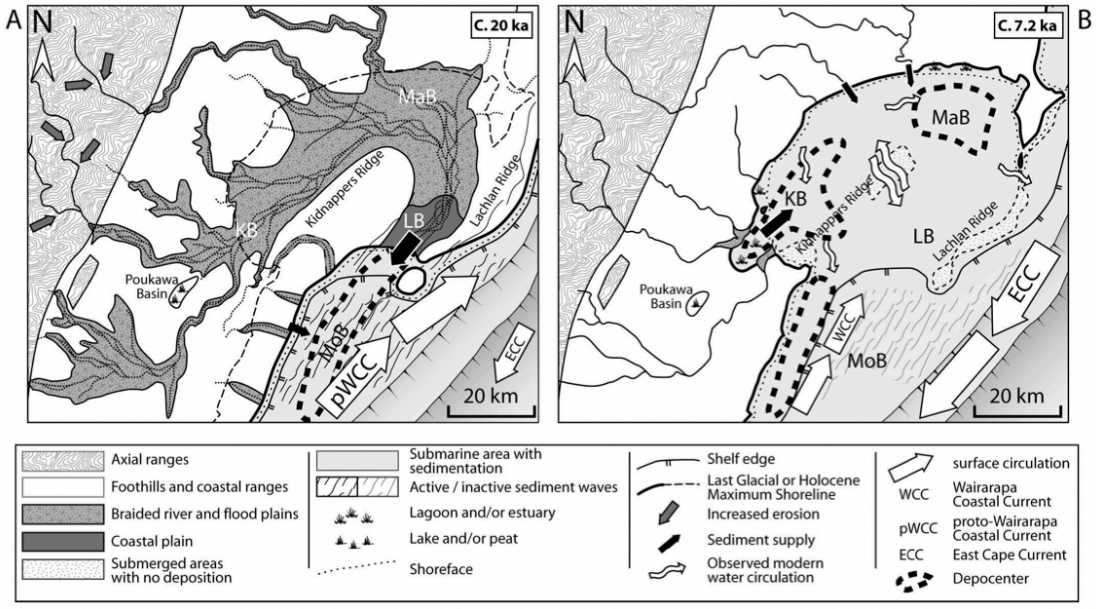

Figure 1.11 Summary reconstructions of past sediment deposition and transport pathways. Figure is sourced from Paquet et al. (2009).

1.6 Research objectives and approach

The overarching aim of this thesis is to detail the controls on the coastal dynamics of small mountainous river plumes and associated cross-shelf suspended sediment transport. Specifically, the characteristic scales of suspended sediment in river plumes over long time scales will be determined from satellite remote sensing, the fundamental drivers of variability will be assessed using a calibrated numerical model, and finally to document river plume dynamics in high temporal resolution through a mooring deployment offshore of a small mountainous river. This thesis sets out to determine the how environmental conditions impact river plume dynamics and sediment transport in an energetic coastal ocean, particularly for smaller rivers than have been mostly focused on in prior research.

The aims work together to cover a range of temporal and spatial scales and show how those scales interact to respond to varying environmental conditions. These aims were studied in the case study system of Hawke Bay, Aotearoa New Zealand, a semi-enclosed bay with four significant small mountainous rivers that discharge into the Bay. Together, the research presented in this thesis provides a comprehensive description of the circulation and sediment transport in Hawke Bay as well as insights pertaining to small mountainous river systems worldwide. Hawke Bay is a natural laboratory for studying small mountainous rivers.

This thesis is separated into three components that use different methods to investigate varying spatiotemporal scales and processes regarding circulation and sediment transport in Hawke Bay. Chapter 2 uses satellite ocean colour data to document the surface SSC variability in Hawke Bay for over 20 years. Chapter 3 utilises a realistic numerical ocean model developed for Hawke Bay that simulates the three dimensional circulation and sediment transport in Hawke Bay. Chapter 4 uses a mooring dataset that was collected offshore of one of the main rivers in Hawke Bay that recorded river plume circulation and the response to environmental forcing in high detail.

The following Chapters 2–4 are formatted as individual manuscripts that will be submitted to peer reviewed journals and Chapter 5 is a conclusion and summary of the thesis. The main chapters include:

- **Chapter 2**: Using ocean colour remote sensing to determine the length scales of sediment transport from small mountainous river plumes.
- **Chapter 3**: Circulation and cross-shelf sediment fluxes in an energetic bay with multiple small mountainous rivers
- **Chapter 4**: The variability of cross-shelf flows offshore of a small mountainous river

Chapter 2: Using ocean colour remote sensing to determine the length scales of sediment transport from small mountainous river plumes

Contribution of Authors

Chapter 2 presents the article "Using ocean colour remote sensing to determine the length scales of sediment transport from small mountainous river plumes" which will be submitted to the journal *Remote Sensing of Environment* for review. Ted Conroy conceptualized the study, performed all field work and data analysis, and wrote the article. Karin R. Bryan provided feedback, supervision, and editing of the article throughout the process. Cedric G. Fichot provided assistance with the conceptualization, interpretation, and editing of the article.

2.1 Introduction

Relative to the size of their watersheds, small mountainous rivers deliver disproportionally large amounts of sediment, nutrients, terrigenous organic matter, and pollutants to the coastal ocean (Milliman and Syvitski 1992). These systems are generally located on active margins with steep coastal mountain ranges and are driven by weather systems characterized by fast, episodic storm events (typically 1–3-day duration) that quickly deliver freshwater and sediment to the ocean. Suspended sediment transport within these river plumes is complex and has important implications for long-term sediment deposition (Geyer et al. 2004, Hetland and Hsu 2013). It also plays an important ecological and biogeochemical role through its effects on water column turbidity and its supply of particulate matter to the benthos (McKee et al. 2004).

Small mountainous rivers typically flow into an energetic coastal ocean influenced by wave-driven currents that can resuspend deposited sediment (Wright and Nittrouer 1995). Studies have shown that transport to long-term sediment depositional sites in these systems occurs in multiple deposition-resuspension steps following the initial gravitational settling from the river plume (Geyer et al. 2000, Hill et al. 2000, Milligan et al. 2007, Bever et al. 2011, Hale and Ogsten 2015). In these systems, which are classified as marine dispersal dominated (Walsh and Nittrouer 2009), the length scales of the primary sediment deposition are generally shorter than the length scale of the inner-shelf zone, where fine grain sediment can be resuspended. Wave-driven currents can then initiate gravity flows that transport sediment offshore to longer term depositional areas (Traykovski et al. 2000). Plume dynamics, which are characterized by a strong near-field jet and mediated by various factors influencing mid-field and far-field plume dispersal (Hetland and Hsu 2013, Horner-Devine et al. 2015), are critical because they determine where sediment initially falls from the plume.

Characterizing plume dynamics from marine dispersal dominated rivers is therefore critical to understand sediment deposition patterns. Previous studies have shown the initial depositional site is generally within a few kilometers to a few tens of kilometers from the river mouth, as is the case for the Eel River (Geyer et al. 2000), the Columbia River (Wright and Nittrouer 1995), and the Po River (Harris et al. 2008) These observations suggested that aggregation (flocculation) increases the effective settling velocity of particles, given that the length scale would be much longer (e.g., tens of kilometers) based on unaggregated-particle Stokes settling velocity and the observed horizontal transport. In-situ measurements of sediment transport in these systems are difficult to obtain due to the highly energetic environment and dynamic nature of the plumes, and often prevent long temporal observational records of sediment deposition from mountainous river plumes.

Satellite remote sensing of ocean colour is being increasingly used to estimate suspended sediment concentrations in surface coastal waters, using the strong relationship existing between the optical backscattering coefficient of particles and water remote-sensing reflectance in the red and

near-infrared spectral domains (Kirk 1994; Nechad et al. 2016). The long record of satellite ocean colour data (> 20 years) can now facilitate detailed studies of suspended sediment dynamics in nearshore systems. For instance, recent work using satellite ocean colour have documented suspended sediment variability in river plumes, including the characterization of spatial patterns, and the assessing variability with discharge and environmental conditions (Pawlowicz et al. 2017, Saldias et al. 2012, Gangloff et al. 2017, Many et al. 2018, Zhang et al., 2020). However, few studies have used these ocean colour records to provide more specific information about sediment transport and initial deposition patterns from rivers to the coastal ocean.

Here, using Hawke Bay in Aotearoa New Zealand as an ideal test site, we demonstrate how these >20-years records of ocean colour data can be used to document detailed spatiotemporal patterns of mountainous river plumes and determine the length scales of sediment deposition from these rivers in the coastal ocean. Ocean colour data from MODIS, in combination with an empirical relation for Total Suspended Solids (TSS), provided daily snapshots of river plume variability. We analysed the plumes of three mountainous rivers flowing into Hawke Bay, a large energetic coastal embayment in New Zealand. The temporal variability of TSS is investigated and compared with the environmental conditions, and the spatial gradient of the TSS in the plumes is used to gain new insights about the initial deposition sites of sediments from river plumes. The relative controls of river discharge, wave forcing, and wind forcing are compared and related to river plume length scales and their relative importance for river plume trajectories.

2.2 Regional setting: Hawke Bay

Hawke Bay is a 40-by-80-km embayment located on the North Island of Aotearoa New Zealand (Fig. 2.1). The Bay is on the eastern coast and faces south toward the Pacific Ocean and is exposed to significant swell from the Southern Ocean. Hawke Bay is located inshore of the Hikurangi margin, and is bordered by steep, highly erodible coastal mountain ranges, where median annual rainfall rates are around 2 m or higher (Chappell 2013). The four largest rivers discharging to the Bay are the 1) Wairoa River, 2) Mohaka River, 3) the combination of the Ngaruroro, Tūtaekurī, and Mokotūāraro Rivers which merge near the river inlet (here denoted as the Ngaruroro/Tūtaekurī as they are the main contributors), and 4) the Tukituki River (Fig. 2.1). The focus of this work is on these larger rivers, although other rivers such as the Esk and Nuhaka Rivers (Fig. 2.1) can create noticeable river plumes. The river inlet morphology is highly variable in time, as some of the river inlets close during the dry season while the larger river inlets generally remain open year-round. The inlet widths of the 4 rivers generally range from 50–200 m, and a submerged ebb-tidal delta will commonly form offshore of the inlets. These types of inlets are commonly found in micro-tidal regimes on wave-dominated coasts (McSweeney et al. 2017). The flow from the inlet to the coastal ocean is strongly modulated by both tidal currents and the river discharge, and the rivers have generally short (few km

to flood tide only) salinity intrusions, except for the Wairoa River, which can have a salinity intrusion exceeding 10 km in the dry season (K. Bryan, unpublished data).

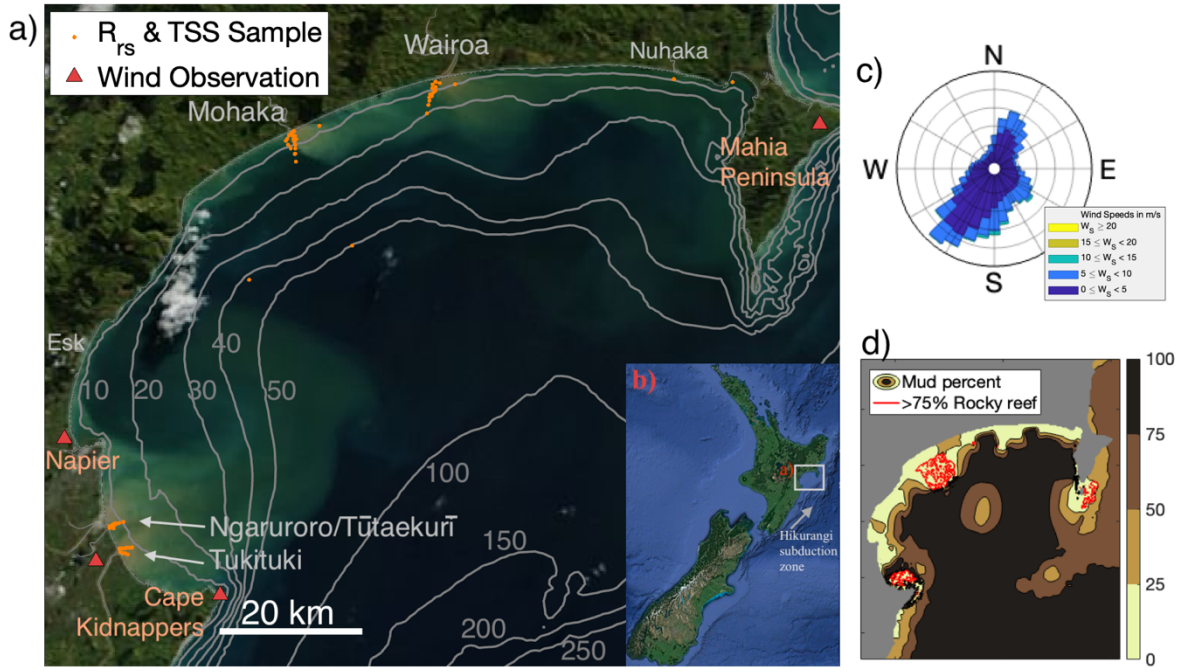

Figure 2.1 a) Map of Hawke Bay, Aotearoa New Zealand. The location of the Bay in Aotearoa is shown in b) in the red box (image from Google Earth). Sample locations are shown in orange and bathymetric contours (m) are plotted in grey. The true colour image is from NASA MODIS. Red triangles and text show meteorological stations where wind data is used. The main rivers flowing into the Bay are labelled in grey and places are labelled in orange. c) Wind rose from the Napier Airport meteorological station showing the frequency occurrences of wind magnitude (m s^{-1}) and direction over the period of this study from 2000-2021. d) The percent mud throughout the Bay and the areas of rocky reef (coloured red).

The bathymetry of the Bay is generally smooth with a gentle slope that extends to the continental slope and the Hikurangi subduction zone (Fig. 2.1). The seafloor composition in the Bay is muddy/fine-sand nearshore, and sandy/mud (ranging from 1–50% sand) offshore of the ~20 m isobath, but varies spatially (Pantin 1966, Bostock et al. 2019). Large sedimentary cliffs (> 100 m) line a significant portion of the coastline of the Bay, which are prone to landslides and erosion into the Bay. Estimates of sediment accumulation in the Bay range from 0.1 cm yr^{-1} in muddy areas of the Bay and up to 0.3 cm yr^{-1} in two main depositional areas (Pantin 1966, Paquet et al. 2009). The Bay is susceptible to strong wind and wave forcing. The average significant wave height recorded off Napier is 1.2 m, but although it typically reaches 2.5–3.5 m during high wave events, it can also reach > 8 m in extreme cases (Komar 2010). Waves approach on average from the east-southeast and are generally larger in the austral winter (Godoi et al. 2016). When rainfall events coincide with high-wave events, sediment is more likely to be transported to long-term depositional areas than when rainfall events

occur during calm conditions (Bever et al. 2011). The southern portion of the Bay experiences wind on average from the SW, as seen at the Napier airport weather station (Fig. 2.1), although winds from the NE, S, and SE are also common. In the northern portion of the Bay, SW winds are also common, but NE and E winds are more common than in the Southern Bay (Fig. 2.1; Chappell 2013).

Hawke Bay is microtidal, with a spring tidal range of 1.9 m, and neap tidal range of 1.2 m (as measured at the Napier Port). Current patterns in the Bay are not well studied. The prevailing notion of the mean currents is inflow at the center of the Bay from the South producing a pair of semi-persistent cyclonic and anticyclonic eddies from west to east (Stevens et al. 2021), which are likely influenced by the offshore boundary currents. The East Auckland Current predominately flows offshore of the Bay in the summer months, flowing from North to SE, carrying subtropical warmer, saltier water, while the Wairarapa Coastal Current, flowing from the South, carries cooler fresher water into the Bay (Stevens et al. 2021).

2.3 Methods

2.3.1 Satellite ocean colour data

Satellite ocean colour data from MODIS Aqua and Terra was used as the source of remote sensing reflectance (R_{rs}) data. Level 1A MODIS files were obtained from the NASA Ocean Colour website (https://oceancolour.gsfc.nasa.gov) and were atmospherically corrected and processed to level 3 with the SeaDas OCSSW multi-level processor. The atmospheric correction was modified from the default *l2gen* parameters to suit the commonly turbid water in the study area. Specifically, the dark-pixel atmospheric correction used the 748 and 859-nm bands, the iterative correction was turned off, the cloud detection method used the 2130-nm band with a threshold of 0.018 (following Aurin et al. 2013), the pixel saturation flag was turned off, and the straylight flag was turned off in order to retain pixels directly adjacent to the coast due to the small scale of the river plumes. These changes to the default *l2gen* settings allow for higher reflectance values to be processed, although it led to an increase in noise due to glint and a higher return of negative reflectance values in open-ocean waters (e.g. Feng et al. 2018). Pixels were processed at the nadir resolution of 250 m for the 645 nm band, and gaps in the data due to off-nadir image collection were filled by successive runs of the processing algorithm using larger interpolation stencils.

For each day, either an Aqua or Terra image was selected based on the number of cloud-free pixels in the Bay, given differences between the two sensors have been shown to be acceptable for this type of study (Dogglioti et al. 2016). Negative reflectance values were removed. All images were visually inspected for data quality, and where cloud remnants from the OCSSW processing were evident in pixels, these pixels were manually removed. Usable data existed for most of the Bay for about 40% of the entire MODIS record. The atmospherically corrected MODIS R_{rs} was compared

with in-situ R_{rs} (described below) for a limited number of matchups that occurred during two separate days of cloud-free sampling, collected within 3 hours of image collection.

2.3.2 In-situ data

Concurrent hyperspectral radiometry and water samples for TSS (n = 65) were taken at multiple locations in the Bay (Fig. 2.1) to facilitate the development of a local TSS algorithm applicable to MODIS. Typically, the data and samples were collected along cross-shelf transects off the major rivers' entrances following discharge events. A Seabird Scientific HyperOCR hyperspectral radiometer was deployed from a boat on a floating platform measuring downwelling irradiance ($E_d(0+)$), and water-leaving radiance (L_w) above the water surface using the skylight-blocked approach (Lee et al., 2013) over the spectral range of 350–800 nm at 3.3 nm resolution. For each sample, the boat was anchored to sample a consistent region of the river plume, and the HyperOCR sampled for two minutes at 3 Hz and then averaged over the sample duration. While data recorded, a 1 L bottle sample was taken at the sea surface for the TSS measurement. The remote-sensing reflectance was calculated as $R_{rs} = L_w/E_d(0)$ (Fig. 2.2a) and was corrected for self-shading using the method of Yu et al. (2021). The full data set can be accessed through the GLORIA database (Lehmann et al. 2023).

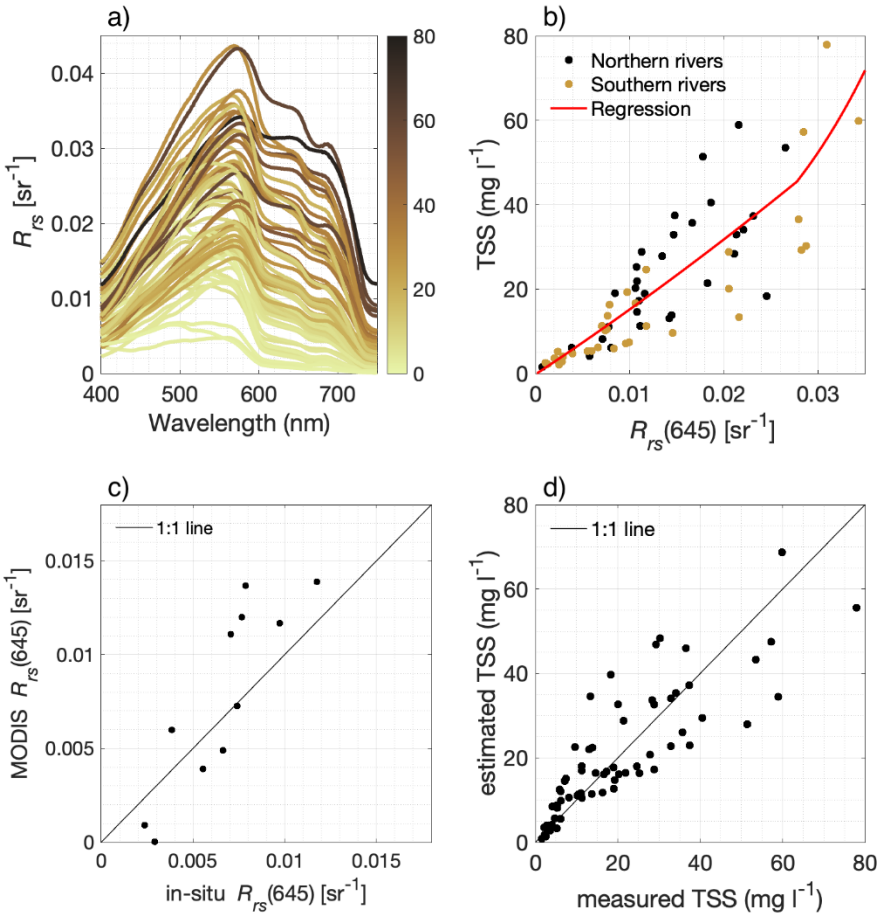

Figure 2.2 The measured remote sensing reflectance, TSS, and the empirical regression between remote sensing reflectance and TSS. a) R_{rs} (sr^{-1}) spectra coloured by co-located TSS (mg l^{-1}). Locations of samples are shown on the map in Fig. 1. b) Piecewise quadratic and exponential regression between in-situ R_{rs} (using MODIS 645 nm spectral response function, c) comparison of in-situ R_{rs} at 645 nm with co-located MODIS derived R_{rs} at 645 nm after the atmospheric correction, d) the evaluation of the regression compared with the observed values of TSS (mg l^{-1}).

The MODIS red band (centered on 645 nm) was used for an empirical relation to estimate TSS (Fig. 2.2b). The hyperspectral R_{rs} data were weight-averaged to match the MODIS 645 nm spectral response (denoted as $R_{rs}\,(645)$), then a piecewise quadratic and exponential regression was fit to the TSS data

$$TSS = 5984R_{rs}^2(645) + 1480R_{rs}(645) - 0.2438 \qquad \text{for } R_{rs}(645) < 0.0274\ sr^{-1}$$

$$TSS = 7.863exp(63.2R_{rs}(645)) \qquad \text{for } R_{rs}\,(645) \geq 0.0274\ sr^{-1} \quad (2.1).$$

2.3.3 Additional data sources

River flow data were collected by the Hawkes Bay Regional Council for the four rivers at 15-minute intervals (https://www.hbrc.govt.nz/environment/river-levels/). Concurrent river suspended sediment and river flow data for the Wairoa, Mohaka, and Tūtaekurī/Ngaruroro Rivers (but not the Tukituki River) were sourced from Hicks et al. (2011), where concurrent measurements of river flow and cross sectionally averaged suspended sediment concentration were made. The data were used to fit a power-law regression model between discharge and TSS for the Wairoa, Mohaka, and Tūtaekurī/Ngaruroro Rivers. Wind data were sourced from four stations positioned across the Bay (Fig. 2.1), where hourly wind speed and direction were recorded, maintained by NIWA and Hawkes Bay Regional Council.

Modelled wave height, period, and direction were sourced from a wave hindcast model of Aotearoa New Zealand (Albuquerque et al. 2021) which extends until the end of 2019. The wave model grid has a 9-km resolution in the study area which captures the Bay's geometry and wave shadowing effects from the headlands of the Bay. The wave model output was interpolated to the MODIS grid, using nearest values for the extrapolation to locations outside of the wave model grid. Wave bed shear stress was calculated as $\tau = 0.5\rho f_w u_b^2$, where ρ is the water density, and the wave friction factor f_w was calculated as $f_w = 1.39(A/z_0)^{-0.52}$ (Soulsby 1997). The wave orbital velocity was calculated as $u_b = \frac{\pi H}{t}\sinh(kh)$ and the wave orbital amplitude as $A = H/2\sinh(kh)$, where linear wave theory was used to compute the wavenumber k, and the bottom roughness was calculated as $z_0 = d_{50}/12$. The median grain size d_{50} was sourced from a compiled sediment bed data set from Bostock et al. (2019) merged with samples collected by Hawkes Bay Regional Council (293 in total)

as well as seafloor classification data obtained from sonar. The bed sediment percent mud (grain size less than 63 μm) and rocky reef data were interpolated to cover the Bay (Fig. 2.1).

2.3.4 Analysis methods

For the major rivers in the Bay, a time series of TSS was extracted by finding the maximum TSS value within a 1 km radius of the general region of the river mouth, which was to account for the change in river inlet position over time, and the lateral advection of the plume by waves and currents. Each value was manually checked to make sure an appropriate pixel was selected. Additionally, for each major river in the Bay, the plume centerline, defined as the path that would follow the dominant along-plume velocity (and create a local maximum of TSS), was computed to quantify the horizontal scale of each plume, given that the plumes can have complicated geometries. To calculate the plume centerline for each river, the TSS field was smoothed to reduce spatial noise. Next, starting at the maximum TSS value near the river mouth, the centerline was computed by following the local maximum in the TSS until either the 2 mg l^{-1} value was reached, or the sign of the gradient along the transect changed from negative to positive. Each plume centerline was quality-checked and manually drawn if necessary. A majority of the transects needed to be manually altered, typically due to noisy or missing data. Only transects displaying an unambiguous TSS plume were retained, which excluded days with small plumes comprised of few pixels (250–500 m) or which showed elevated TSS from wave resuspension or advection from other locations such as alongshore coastal currents.

2.4. Results and discussion

2.4.1 On the Rrs-TSS relationship in Hawke Bay

Although significant scatter remained, the empirical regression of TSS on $R_{rs}(645)$ captured the general relationship between the two variables and facilitated the retrieval of reasonably accurate TSS concentrations (r^2=0.71, RMSE=9.16 mg l^{-1}, MAPE=33.53%; Fig. 2.2b,d). A quadratic regression captured the TSS variability relatively well at low TSS, but an exponential fit captured it better at high TSS values. This exponential fit represented the relationship between these two variables for high *Rrs*(645) values (> 0.0274 sr^{-1}) because *Rrs*(645) becomes less sensitive to changes in TSS as TSS concentration increases. Here, the algorithm was developed using in-situ data covering a TSS concentration range of <1 to 78 mg l^{-1}.

Although the TSS concentrations in the Hawkes Bay rivers can reach > 1000 mg l^{-1} during high-discharge events (Hicks et al. 2011), almost all *Rrs*(645) values derived from the satellite ocean colour imagery were < 0.047 sr^{-1} (corresponding to estimated TSS concentration of ~150 mg l^{-1}), and the vast majority of them were < 0.037 sr^{-1} (corresponding to estimated TSS concentrations of < 80 mg l^{-1}). The comparison of the in-situ R_{rs} with MODIS derived R_{rs} at 645 nm (Fig. 2.3c) shows moderate ability in replicating the observed values (r^2=0.56, RMSE=0.0040 sr^{-1}).

The higher scatter observed in the *Rrs*(645)-TSS relationship at higher TSS values (Fig. 2.2b) was likely the result of several factors. The northern and southern rivers exhibited different relationships (Fig. 2.2b) likely in part because of differences in sediment characteristics (e.g., particle size, organic carbon content). Differences in sediment characteristics including particle size, shape, and mineral composition directly influences the specific backscattering coefficient of the sediment, which can directly impact the relation between R_{rs} and TSS (Kirk 1994). These differences among rivers are likely due to varying geological characteristics of source sediment from the Northern region of the Bay (Tertiary sandstone) compared to the Southern region (Mesozoic sandstones; Pantin 1966). Additionally, elevated and variables concentrations of phytoplankton and chromophoric dissolved organic matter (CDOM), which can vary independently from non-algal suspended particles, can also impact *Rrs*(645) and create scatter in the *Rrs*(645)-TSS relationship (Kirk 1994). Although differences in the *Rrs*(645)-TSS relationship exist between rivers, a single algorithm/relationship was derived here from the collated data set to avoid creating any artificial spatial gradients in the imagery caused by applying region-specific algorithms.

2.4.2 River discharge and TSS concentrations

The daily river discharge (interpolated to the MODIS image collection times) shows that the Wairoa and Mohaka Rivers have the largest median discharge events (Fig. 2.3a), compared with the Tukituki and Ngaruroro/Tūtaekurī Rivers. The mean and 99.9th percentile daily discharge ($m^3\ s^{-1}$) are 110 and 2183 (Wairoa River), 71 and 1015 (Mohaka River), 47 and 1241 (Ngaruroro/Tūtaekurī Rivers), and 41 and 1329 (Tukituki River). We note that daily values do not reflect the highest magnitude event discharge due to the typical short event durations.

The remotely sensed TSS offshore of these rivers was found to be of similar magnitude for the three rivers investigated (Fig. 2.3b), with mean values (in mg l^{-1}) of 21 (Wairoa), 24 (Mohaka), and 23 (Tukituki). The estimated mean TSS in the rivers from rating curves (in mg l^{-1}) yielded 214 (Wairoa) and 114 (Mohaka), while the 99th percentile values reach concentrations of 2518 and 1036 mg l^{-1} for the Wairoa and Mohaka Rivers respectively. The difference in magnitude between the estimated river TSS and remote sensing derived offshore TSS indicate that substantial dilution of the suspended sediment concentration occurs offshore of the river inlet or that the empirical relation for TSS used here underestimates the higher range of TSS.

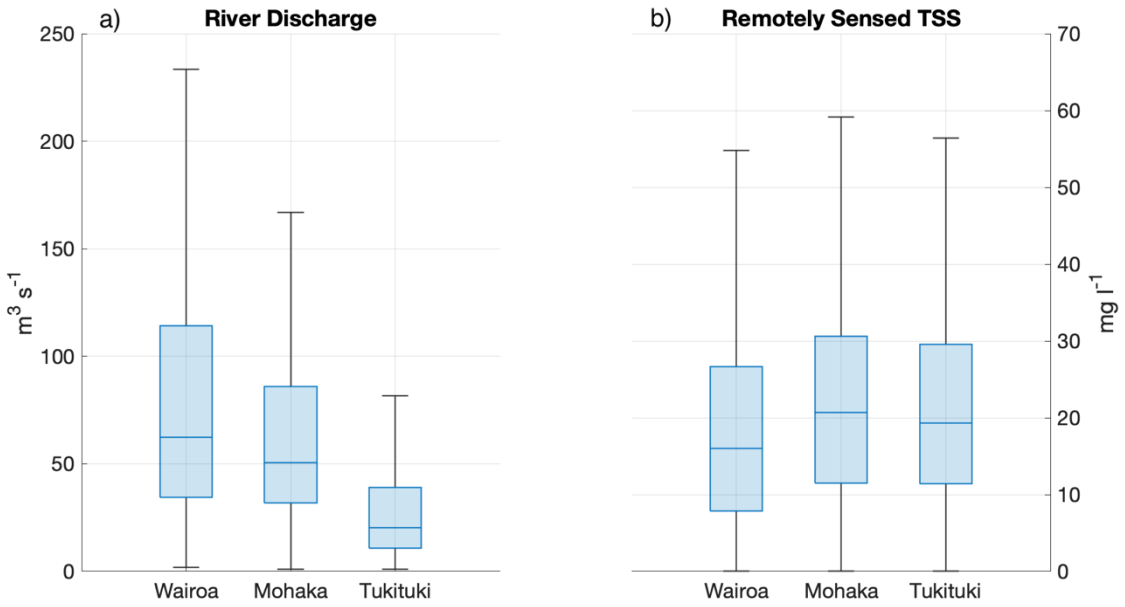

Figure 2.3 Box and whisker plot of the river discharge and remotely sensed TSS for each river. a) The daily river discharge (m^3 s^{-1}) for each river, and b) box and whisker plot of the TSS (mg l^{-1}) offshore of each river derived from MODIS.

2.4.2 Temporal variability of TSS

The TSS averaged over the nearshore coastal waters of Hawke Bay (0–10 m depth range, Fig. 2.4c) has a strong seasonal cycle with persistently elevated values (~15 mg l^{-1}) in the austral winter, when background total discharge into the Bay is around 300–400 m^3 s^{-1} (Fig. 2.4a), and during discharge events when the total discharge into the Bay is from 500 to >2000 m^3 s^{-1} and the nearshore averaged TSS can reach values from 15–30 mg l^{-1}. The significant wave height follows a similar seasonal pattern to the river discharge (Fig. 2.4b), commonly co-occurring with discharge events, with generally larger heights (1–3 m) during the winter, generally occurring predominately from the S as well as from the E/NE, and generally smaller heights in the summer (Fig. 2.4b). During the summer, the TSS generally drops to values in the 0–5 mg l^{-1} range when the discharge drops substantially, although sizeable rainfall events can occur during summer when storms and tropical cyclones impact the region (Chappell 2013), which can also produce large easterly swells.

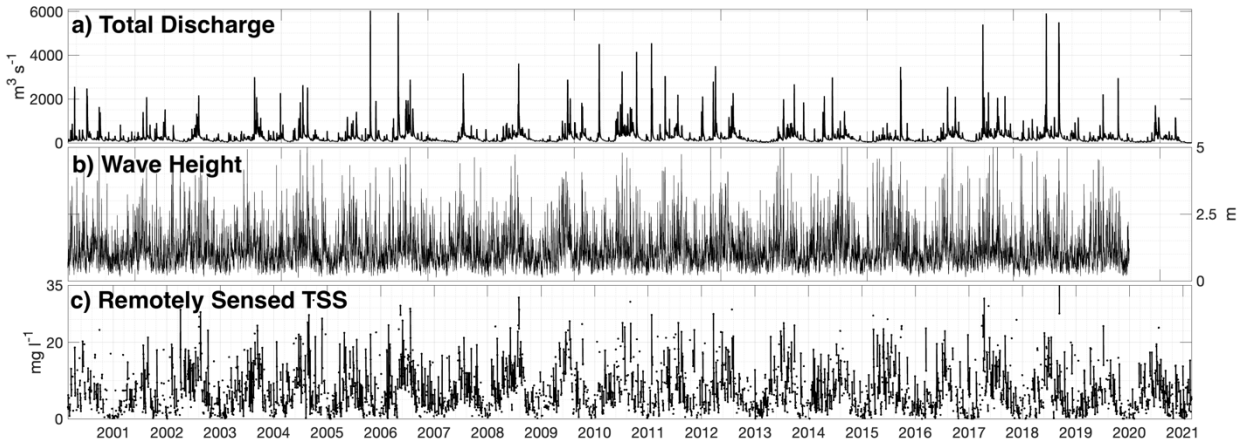

Figure 2.4 Time series of environmental conditions in Hawke Bay from 2000 to 2021. a) The summed river discharge from the four main rivers in Hawkes Bay, b) time series of the significant wave height (m) in the northern part of the Bay offshore of the Mohaka River, derived from the wave model hindcast of Alburqurque et al. (2021) which terminates in 2019, and c) time series of remote sensing derived TSS (mg l^{-1}) averaged between 0-10 m depth in the Bay. The TSS is plotted such that lines connect data points when there are consecutive data points, otherwise individual data points are shown.

Remotely sensed TSS concentrations near the outflow of major rivers is often elevated due to the riverine flux of sediment into the Bay. Near the river mouths TSS concentrations can reach ~150 mg l^{-1} (Fig. 2.5b, d, f). For the major rivers in the Bay, large discharge events are the main contributors to the total annual flux (Fig. 2.5a, c, e, g), as is common for small mountainous river systems (Milliman and Syvitski 1992). The Wairoa River has the largest flux, followed by the Mohaka River. The Ngaruroro/Tūtaekurī and Tukituki rivers export roughly similar amounts of sediment (not shown). Due to the proximity of the rivers, the sediment fluxes to the Bay from different rivers commonly co-occur. However, the fluxes for all rivers display strong interannual variability, which is driven by a small number of large discharge events as indicated by the stepwise nature of the fluxes. Discharge events for all rivers are generally short (1–3 day durations) and the corresponding TSS signal from remote sensing has short lag times (0–1 days).

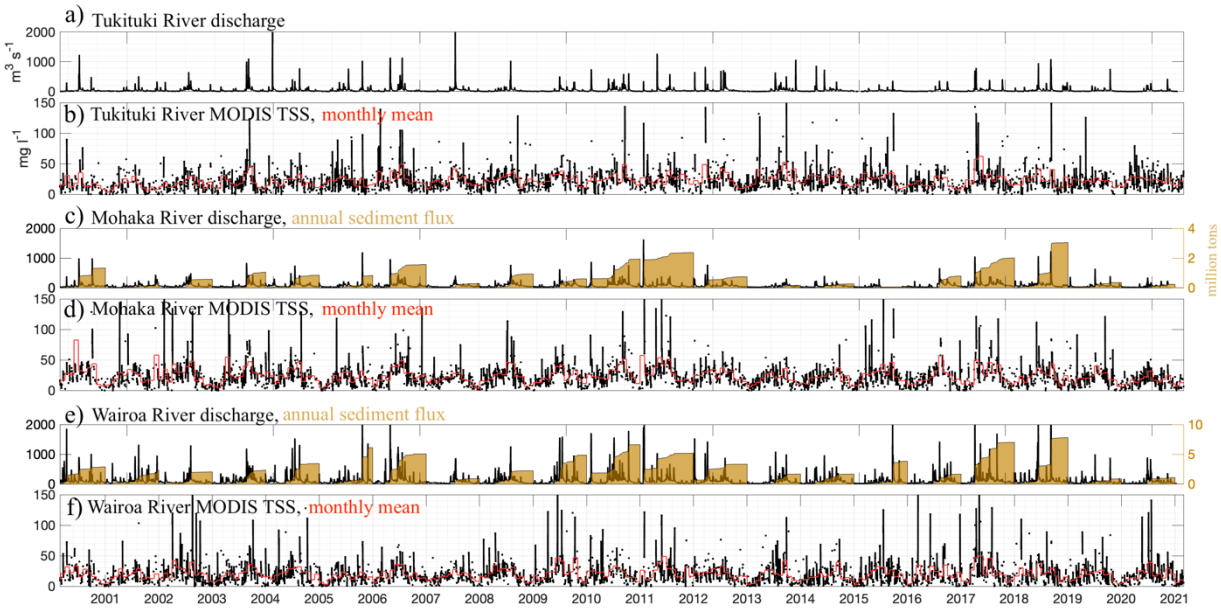

Figure 2.5 The timeseries of remotely sensed TSS for the major rivers in Hawke Bay. a) Timeseries of river discharge ($m^3\ s^{-1}$), river suspended sediment flux estimated from regressions for river TSS (right axis) in accumulated millions of tons annually (panels a, c, and e). The MODIS derived TSS ($mg\ l^{-1}$) is shown for each river in panels b, d, and f, along with monthly averages of TSS in red. The TSS is plotted such that lines connect data points when there are consecutive data points, otherwise individual data points are shown.

The monthly averaged values of TSS for each main river (red lines in Fig. 2.5) show a clear seasonal cycle, which is more apparent for the larger rivers (Mohaka and Wairoa). Interannual variability is present in all the signals, caused by a range of interannual variability in the river discharge and subsequently the sediment flux for all the rivers. Monthly averages of TSS (Fig. 2.6) show a clear seasonal signal in the intensity of TSS both around the main river areas and on the continental shelf. In the summer months, average TSS values around the river mouths are around 5–10 $mg\ l^{-1}$, as well as in the Southern part of the Bay near Cape Kidnappers. Persistent elevated TSS can be seen directly north of Cape Kidnappers, a region with large sedimentary cliffs adjacent to the shoreline that are prone to erosion. Some of the elevated values in the area may also be due to the river discharge from the Maraetotara River, which has a much smaller discharge regime than the Tukituki River. In the peak of the winter, average TSS values around river mouths are elevated to values between 20–25 $mg\ l^{-1}$, and the entire shelf inshore of 50 m has average values around 5 $mg\ l^{-1}$.

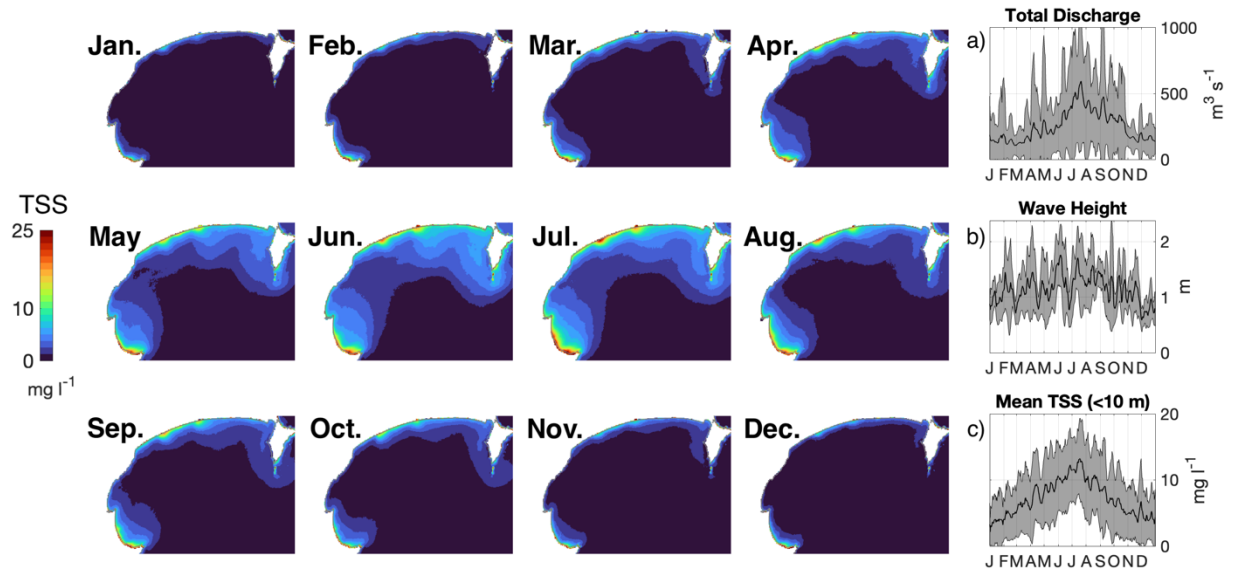

Figure 2.6 Monthly means of TSS (mg l^{-1}) over the entire MODIS record. The panels on the right show weekly moving means of annual variability (black line) and one standard deviation (shading) for a) total river discharge (m^3 s^{-1}), b) significant wave height offshore of the Mohaka River (m), and c) the spatially averaged TSS in 0–10 m depths in the Bay.

The time-series of TSS offshore of rivers (Fig. 2.5) shows that river discharge at seasonal and event timescales appear to be the dominant signal driving the TSS variability of the Bay. For each river, the TSS time series partitioned into the annual, monthly, and higher frequency components is used to determine the linear relationship with the total TSS time series. The annual component of the TSS, averaged over the four main rivers, comprises 2.8 % of the variance, the monthly component comprises 22 % of the variance, and the remainder (the total minus the annual and monthly—the event-driven component) comprises 70 % of the variance. Similarly, the cumulative sediment flux into the Bay generally occurs in a small number of discrete events every year (Fig. 2.5). Although the TSS from remote sensing also shows that most of the signal is from discrete events, the time scales of TSS in the Bay reflects other processes related to river plume dynamics, sediment resuspension, as well as clouds during large storm events causing missing data.

2.4.3 High-TSS events in the Bay

An example of a discharge and wave event is shown in Fig. 2.7 for June through August of 2017. The first snapshot (Fig. 2.7c) shows moderate TSS values in the nearshore of the Bay, where the TSS reaches 30–40 mg l^{-1} offshore of the major rivers, likely caused by a moderate discharge event the day prior. Wind of around 9 m s^{-1} from the E during this time likely caused northward deflection of the Mohaka and Wairoa River plumes, while transport in the Southern Bay is directed offshore and to the north. The TSS transects for each river plume (if distinct plumes are present) are

plotted as black lines on the map view plot, and the TSS values are shown in the plot below each map view plot, plotted as the distance in km from the river mouth. Panel d shows a slight increase in discharge from the Wairoa River, causing the initial TSS in the transect to reach above 50 mg l^{-1} then abruptly drop within 2 km of the river mouth. These days both show the plume from the Wairoa River traveling up the coast where the TSS transect extends much further than the other rivers. An elevated TSS region from the Wairoa River is also visible after a moderate discharge event with S to SW winds (Fig. 2.7d), again causing transport upcoast for all rivers.

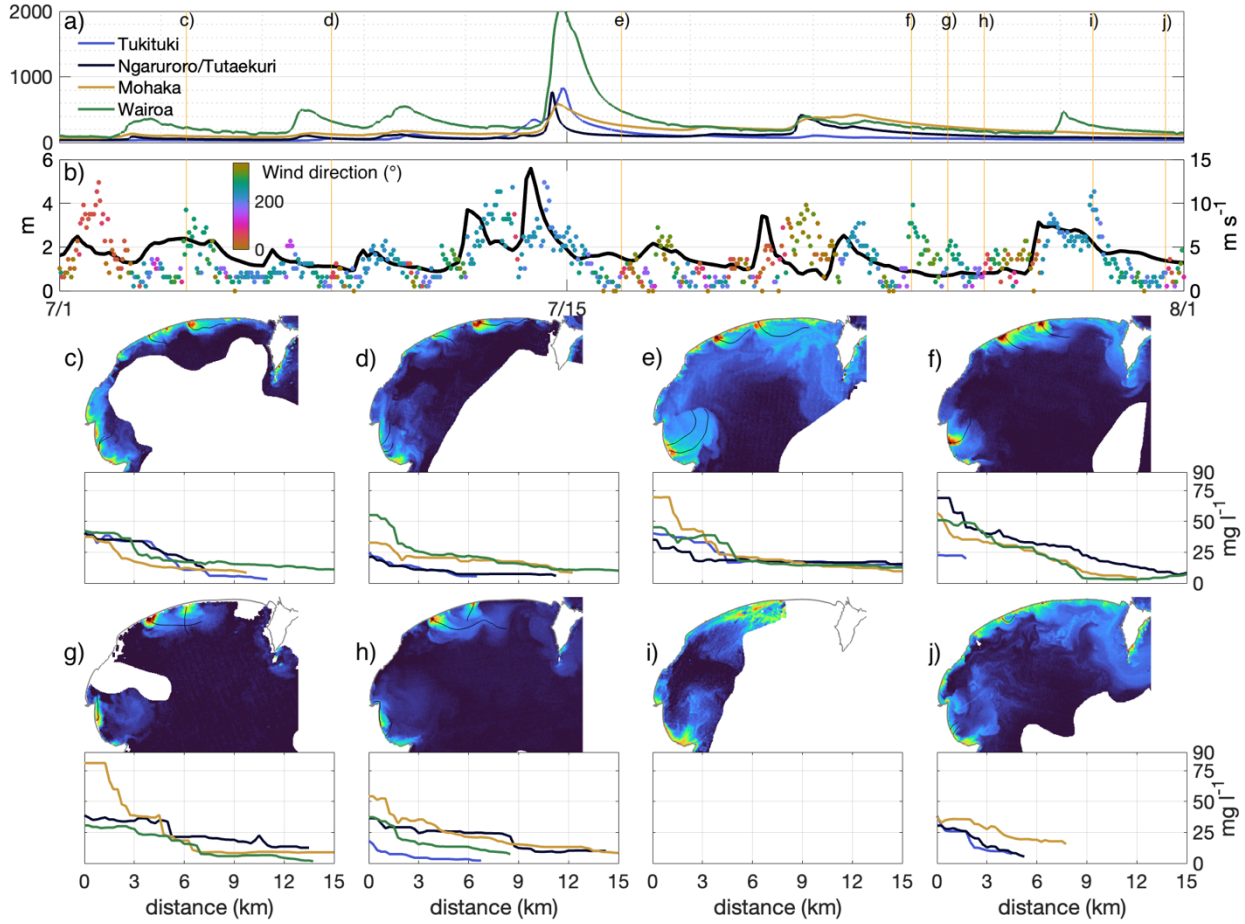

Figure 2.7 Example of a river discharge event in the winter of 2017 from June 15 to August 15. A time series of forcing variables is shown including a) river flow (m^3 s^{-1}) for the main rivers, b) significant wave height (m) in black on the left axis and the wind speed and direction (coloured) on the right axis. The gold lines marking the times of TSS (mg l^{-1}) panels numerically listed in a). Transects of TSS along plume centrelines are shown in the lower right for each corresponding day for each river plume, unless no clearly defined plume was observed for that river or day. The scale bar for the TSS map view plots is shown in the lower right (range 0–50 mg l^{-1}).

A large storm event occurred on July 15, and a MODIS image was acquired two days after (Fig. 2.7e). During the storm event, wind speeds exceeded 10 m s^{-1} from the SW, the significant wave height exceeded 5 m, the Wairoa River discharge reached 2100 m^3 s^{-1}, and the other rivers discharges exceeded 500 m^3 s^{-1}. The TSS offshore of the rivers were elevated until ~6 km from the river mouths

and large areas of the Bay showed increased TSS as compared with the other days during this period, potentially due to the large wave and high winds over the previous two days. Another discharge event occurred (~400 $m^3 s^{-1}$) on July 22, followed by a MODIS image collected on July 24 (Fig. 2.7f) with westerly winds causing plumes to be directed offshore and to the left. With the river discharge still elevated, the wind direction then shifted from N to NE to E, causing plume directions to shift accordingly. A southerly wind event (> 10 m s^{-1}; Fig. 2.7i) with a significant wave height of ~3 m occurred on July 28 which caused widespread increased TSS in the northern region of the Bay, and increased TSS advected northward from Cape Kidnappers. Likely remnant increased TSS from this wind event is then observed two days later (Fig. 2.7j).

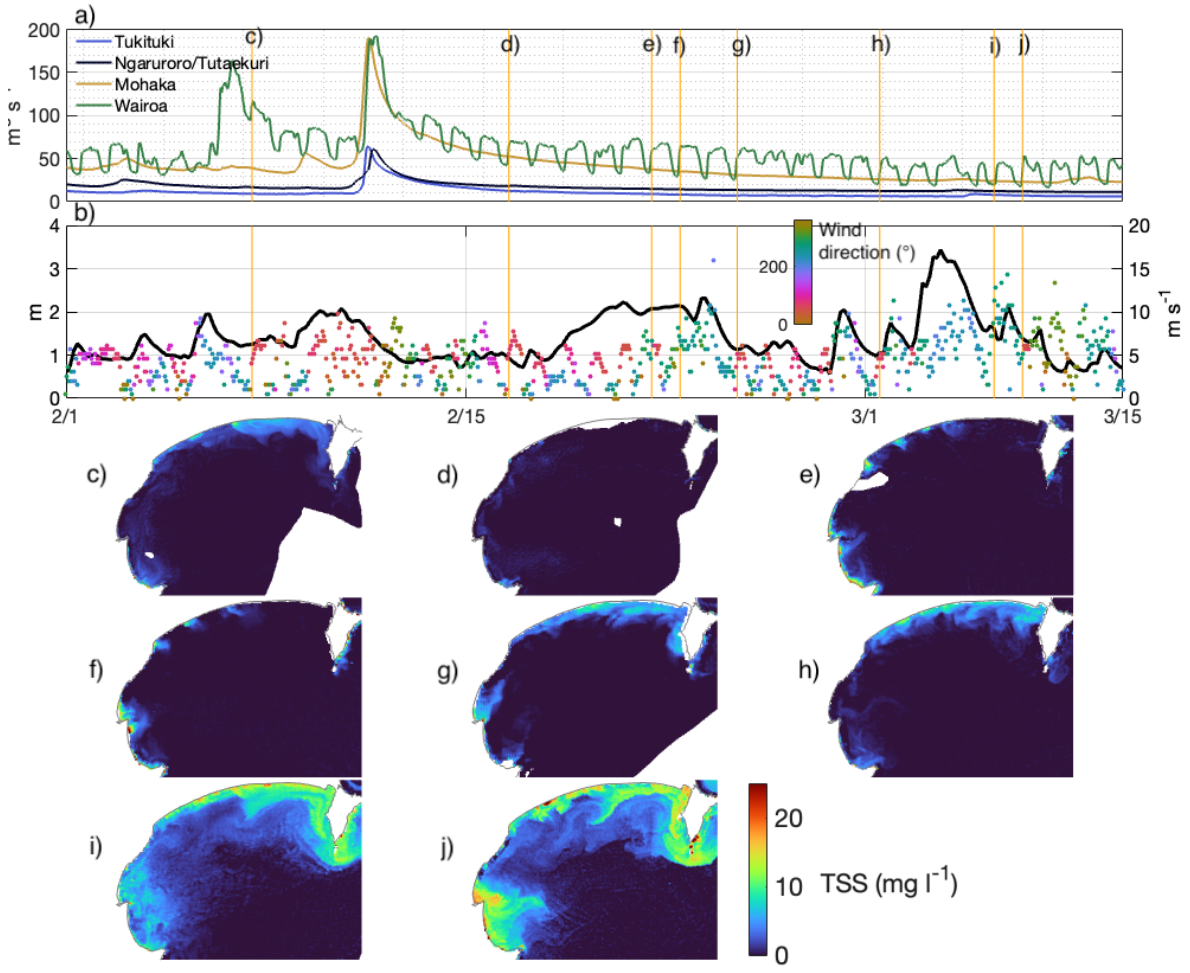

Figure 2.8 Example of elevated TSS due to wind and waves from February to March of 2006. A time series of forcing variables is shown including a) river flow ($m^3 s^{-1}$) for the main rivers, b) significant wave height (m) in black on the left axis and the wind speed and direction (coloured) on the right axis, with the panels showing TSS (mg l^{-1}) at the numeric labels plotted in a).

At other times, moderate to high TSS values are found after significant wave or wind events without substantial river discharge occurring, indicating resuspension of sediment from the inner

shelf. For example, Fig. 2.8 shows a period from February to March of 2006 with two small discharge events with moderate surface TSS expression, followed by periods of moderate to large waves (from 2 to 3.7 m significant wave height) and a wind event. Panel c shows the remnants of the discharge event from the Wairoa River (peaked at 170 m^3 s^{-1}) and SW wind which caused upcoast transport towards the Mahia Peninsula, while panel d shows a return to low magnitudes of TSS in the Bay, as river discharge magnitudes further drop. Panels e-h show a period with increased wave heights greater around 2 m and regions of increased TSS in depths less than 20 m. On March 4, a 3.7 m wave event occurred along with moderate SW winds, and on March 5 the TSS in the Bay is greatly increased compared to background conditions, with TSS of 5–15 mg l^{-1} throughout most of the Bay. The day after, the wind speed increased to around 15 m s^{-1} from the E, and the TSS substantially increased, particularly in the Southern region of the Bay, advecting material offshore in the Southern region of the Bay and northward around the Mahia Peninsula in the Northern region of the Bay.

2.4.4 Typical spatial variability of TSS

The average spatial variability of TSS in the Bay is revealed by the percentage of time that the remotely sensed TSS concentration was above a threshold value, relative to the number of observations available at each pixel. Here, these percentages were computed for the 5, 15, and 45 mg l^{-1} thresholds (Fig. 2.9). In all cases, the most frequent occurrences were near the inlets of the main rivers, with the Mohaka and Wairoa Rivers exhibiting prominent half-circular regions of higher occurrence for both the 5 and 15 mg l^{-1} intervals (Fig. 2.9a-b). The 50% occurrence for 5 mg l^{-1} for these two rivers extended roughly 2.5 km from the inlet. The same 50% occurrence contours for the Tukituki and Ngaruroro/Tūtaekurī Rivers merged to form a continuous band roughly 2.5 km wide. The contours widen at Cape Kidnappers to 3.75 km from the shoreline, potentially due to enhanced sediment supply to the nearshore from cliff erosion and wave resuspension.

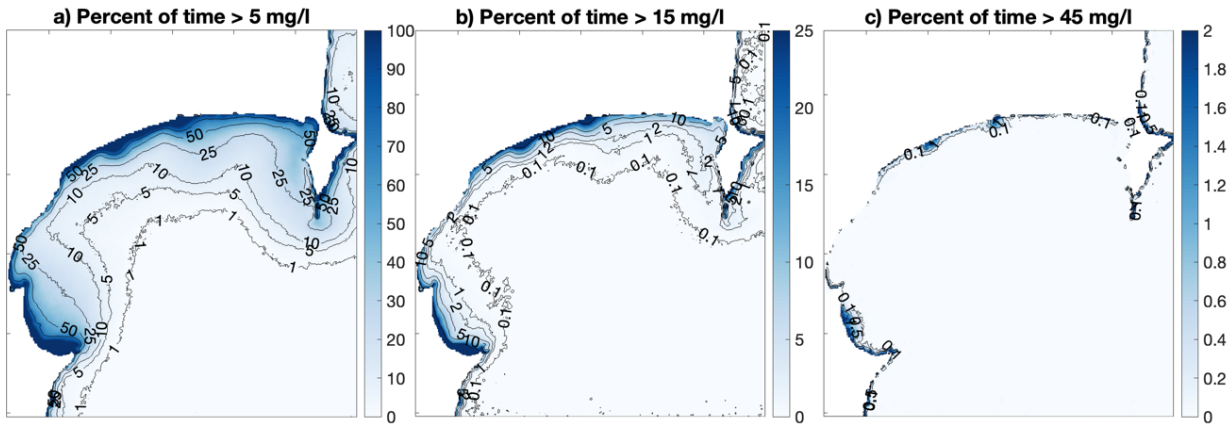

Figure 2.9 The percentages of occurrence for a range of TSS values. a) 5, b) 15, and c) 45 mg l^{-1} is shown for each pixel in the bay. The percentage was computed using the number of days that each pixel had available data.

The contours for the 15 mg l^{-1} threshold (Fig. 2.9b) follow similar spatial patterns as the 5 mg l^{-1} threshold. However, they are greatly reduced in areal extent for the 45 mg l^{-1} threshold (Fig. 2.9c), where high values are restricted to areas directly adjacent to the river inlets. For example, the 1% occurrence of the greater than 45 mg l^{-1} contour was located 2, 0.9, 2.5, and 1.5 km from the shoreline for the Wairoa, Mohaka, Ngaruroro/Tūtaekurī, and Tukituki rivers. For the rest of the coastline, the contours are typically 250 m offshore or not present.

2.4.5 Length scales of TSS concentrations in river plumes

The remotely sensed TSS can be used to infer the extent of the offshore transport in the surface layer. This can be altered by ambient subsurface currents and bed stresses which can prevent bed deposition. However, determining the length scales of the initial step of offshore transport is a key step for understanding the sediment transport to long-term depositional areas, determining regions of increased turbidity in the water column, and for assessing the health of benthic communities. Length scales of cross-shelf transport are dependent on the plume velocity to advect sediment, the plume thickness, and the sediment setting velocity. For example, Geyer et al. (2004) defined a general length scale of sediment deposition from a river plume as $L = uh/w_s$, where u is a characteristic along plume velocity (neglecting lateral advection), h is the plume thickness, and w_s is the settling velocity.

To quantify the length scales of initial deposition, the daily TSS transects for three of the rivers are used and two different length scale metrics are defined, including the e–folding distance (the distance following the transect until 37% of the initial TSS) and the distance to the 5 mg l^{-1} value. We note that not every TSS transect may reach the thresholds for an e–folding value or reach 5 mg l^{-1}. The e–folding distance is dependent on the gradient of TSS along the plume, which is controlled by

sediment advection and fallout from the plume. The 5 mg l^{-1} length scale is additionally used as a general outer boundary value of the river plume.

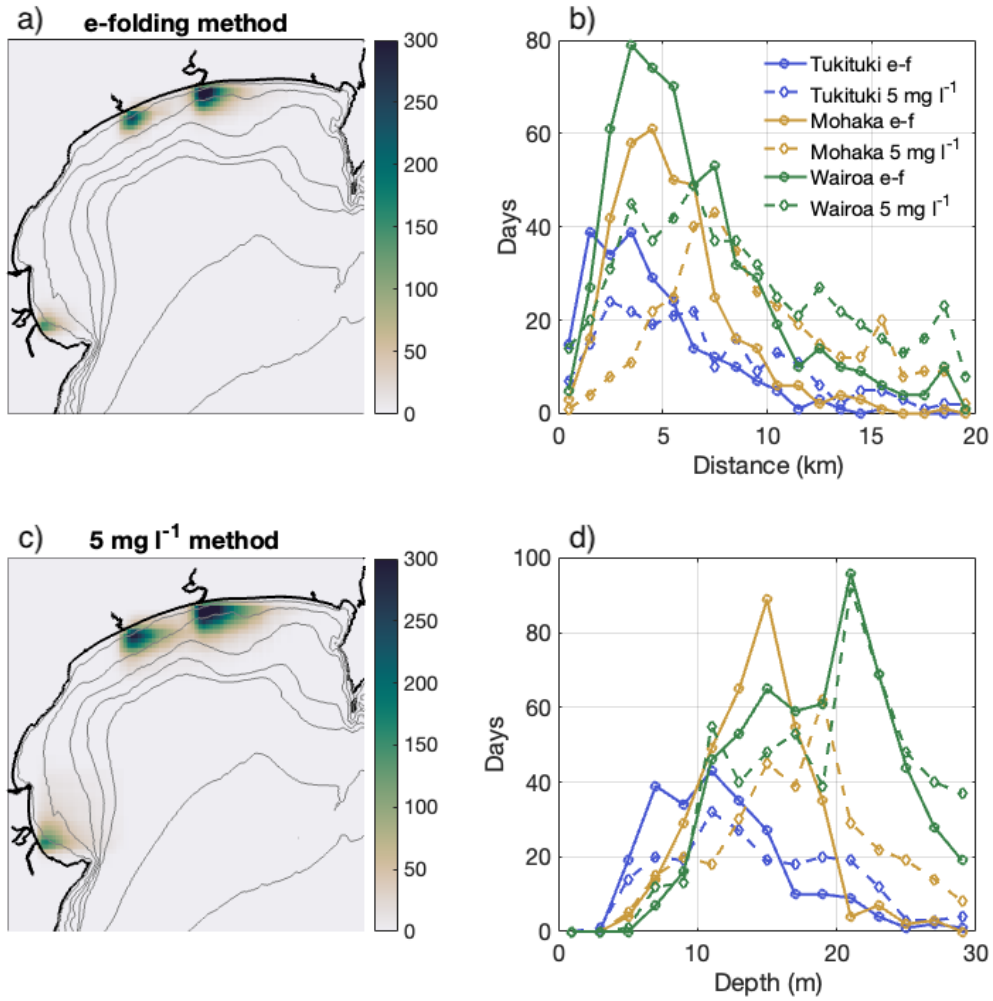

Figure 2.10 The estimated locations, transit distances, and depths of likely initial sediment deposition from two methods. a) The number of occurrences on a 1 km grid on e–folding locations computed for the Tukituki, Mohaka, and Wairoa Rivers. b) Histogram counts of the e–folding distance of TSS for along plume centerline transects for each river. The solid lines are the e–folding metric (named e-f), and the dashed lines are the distance of the 5 mg l^{-1} TSS value. c) The number of occurrences on a 1 km grid on 5 mg l^{-1} locations computed for the Tukituki, Mohaka, and Wairoa Rivers. d) Histogram counts of the depth corresponding to each location for each river. The solid lines are the e–folding metric, and the dashed lines are the distance of the 5 mg l^{-1} TSS value.

For each major river where a TSS plume was clearly identified, the distance from the edge of the river mouth inlet to the e–folding location and depth at that location, as well as the distances and depths to the 5 mg l^{-1} value (dashed lines), are shown in Fig. 2.10b,e. In general, the larger rivers have greater distances that extend further offshore to deeper depths, and the 5 mg l^{-1} metric is generally further offshore and deeper than the e–folding metric. Spatially, the southern rivers e–folding

locations are mostly inshore of the 10 m isobath clustered around the rivers (Fig. 2.10a). In contrast, the locations are inshore of the 20 m isobath for the Mohaka River, and even further offshore for the Wairoa River (Fig. 2.10a). The e–folding locations for the Tukituki River is well distributed in all directions from the river mouth while the northern rivers are mostly distributed directly offshore and down coast (in the direction of Kelvin wave propagation) from the river mouths. In comparison to the e–folding locations, the locations of the 5 mg l^{-1} value (Fig. 2.10d) show similar patterns but with more instances found, and generally exacerbated patterns that reflect the ending location of the transect.

The e–folding distance for all rivers has broad distributions with most transects having distances from 2–6 km, with a peak for the Wairoa and Mohaka Rivers around 3–4 km and 2–3 km for the Tukituki River (Fig. 2.10b). The histogram for all rivers shows a tail with distances greater than 10 km extending to 20 km, with more instances found for the Wairoa and Mohaka Rivers. The distances to the 5 mg l^{-1} value are slightly shifted to further distances but follow similar patterns. The similarities between the two metrics likely reflect commonly occurring TSS values offshore of the river mouths (10–15 mg l^{-1}) that would give e–folding values around 5 mg l^{-1}. The peak depths of the e–folding locations are deepest for the Wairoa River (21 m), followed by the Mohaka River (15 m) and the Tukituki River (11 m), which reflect a combination of the traversed distance offshore and the bathymetry offshore of the river. The initial transect TSS value shows weak linear relations with daily river discharge (r^2 from 0.1–0.2), and the e–folding distance displays higher scatter (r^2~0.025) than the distance to the 5 mg l^{-1} value (r^2~0.21) when related to daily river discharge. This likely signifies that the e–folding distance metric and TSS gradients are also controlled by other hydrodynamic and sediment processes, while the distance to the 5 mg l^{-1} is more related to advection related to river discharge.

Using general settling velocities for clay (0.01 mm s^{-1}), fine silt (0.1 mm s^{-1}), and aggregated particles or coarse silt (1 mm s^{-1}), along with plume velocities ranging 0.2–1 m s^{-1} and plume thicknesses ranging 0.5–4 m (Geyer et al. 2004), we can estimate the distances over which different sediment sizes are advected offshore before exiting the plume layer. Clay particles can be advected over tens to >100 km because of their low settling velocity, whereas fine silt particles travel anywhere between a few to a few tens of km. Particles with settling velocities of 1 mm s^{-1} likely travel a few km at the most. Aggregated particles have been shown to be deposited proximity to the river inlet due to their high settling velocity (Milligan et al. 2007, Warrick et al 2008). These results imply that the bulk of suspended sediment falls out of plumes within roughly 5 km from the river inlet and that the bulk settling velocities are 0.1 mm s^{-1} or higher. The furthest distances found here (>10 km) are likely dominated by particles with low settling velocities (~0.01 mm s^{-1}). However, without additional data to constrain the hydrodynamics of the river plumes, it is not possible to further constrain estimates of settling velocities.

2.4.6 Plume directionality

The direction of the river plume has important implications for determining which processes are most important for sediment dispersal in Hawke Bay. The main processes important for directing river plume transport in addition to the river momentum and buoyancy forcing are the Coriolis force (steering the plume down coast and northward in the direction of Kelvin wave propagation), wind driven currents, including upwelling and downwelling processes that can modify the plume structure (Horner–Devine et al. 2015), the inlet configuration (Geyer et al. 2000), and tidal modulation (Basdurak et al. 2020). If the length of the plume is greater than the baroclinic Rossby radius of deformation, which is on the order of 10 km for typical conditions, the Coriolis force is more likely to steer the plume towards the left and create a buoyancy-driven coastal current, and in the absence of other forcing with steady discharge, a recirculating bulge can form (Horner–Devine et al. 2015).

The river plume directionality was classified as spreading either down coast (northward), up coast (southward), or offshore, by classifying the location of the end location of the TSS transect in three 60° windows extending from each river mouth (Fig. 2.11a). Both the Mohaka and Wairoa Rivers plumes were predominately directed down coast ~65% of the recorded times, with less occurrences directly offshore (29%), and a small percentage of times the plumes directed up coast (<10%). In contrast, the plumes from the Tukituki and Ngaruroro/Tūtaekurī (not shown) Rivers predominately were directed offshore (52%), with comparable instances (~25%) directed either up or down coast. The dominant plume directions can also be seen in the locations of the TSS transect points (Fig. 2.10c).

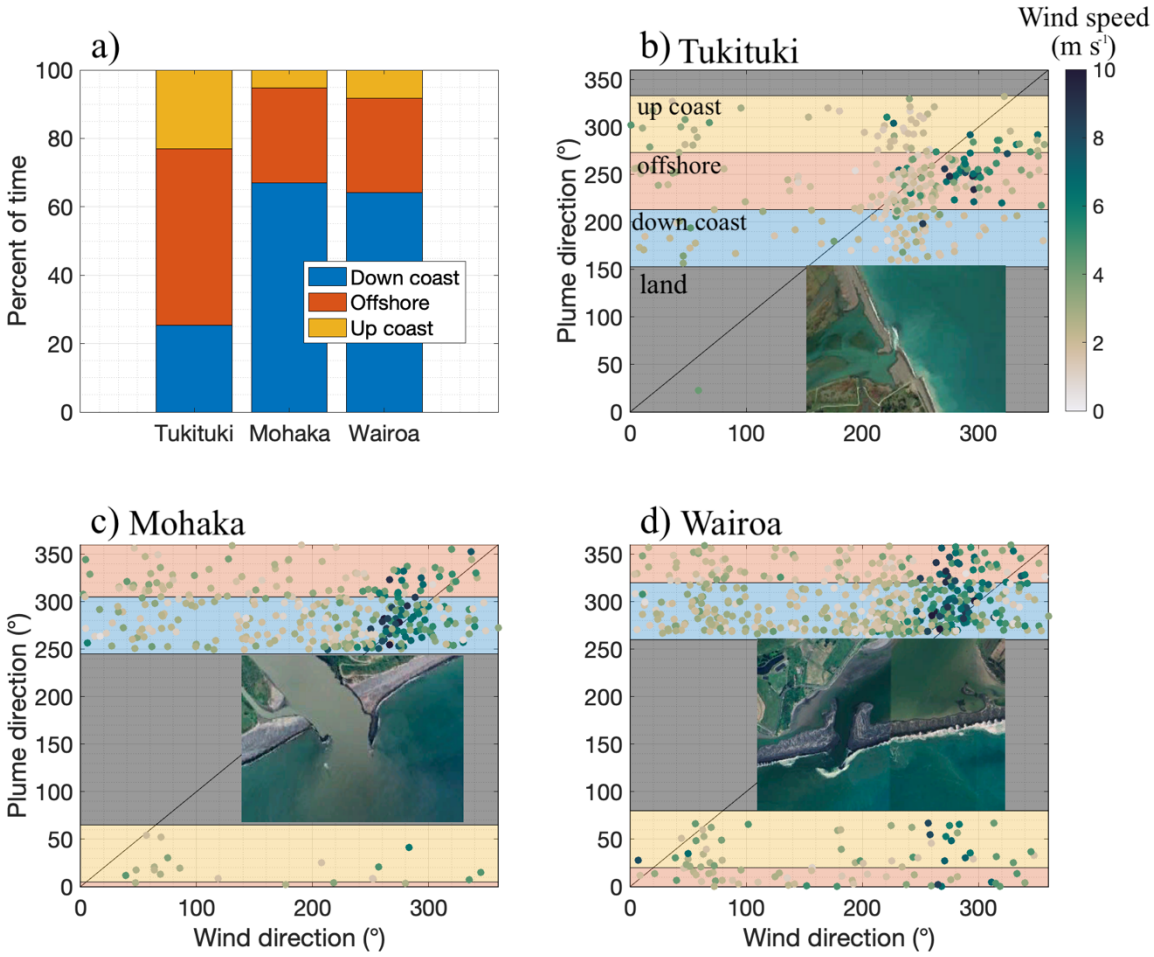

Figure 2.11 The river plume directionality and relation with wind direction. a) Plume directionality of each TSS transect for each river, in 60-degree sections offshore of the coastline at each river, computed using the location of the end point of the TSS transect. Down coast is oriented northward and up coast southward. b–d) Wind direction and speed (m s^{-1}) from the nearest wind station, averaged over the previous six hours to satellite image collection compared with plume direction for the Tukituki, Mohaka, and Wairoa Rivers. The grey shading represents the land boundary for each river, and the coloured shading corresponds to the colours from a). The coastline orientation is shown by Google Earth images at each of the river mouths.

Using the plume directions for each river, the angle of the river plume from the river mouth to the end of the TSS transect was computed and compared with the wind speed and direction (Fig. 2.11b–d) from the nearest weather station, where the wind speed and direction was averaged over the 6-hour period prior to satellite image collection. Downwelling winds from the SE to W (for the southern and northern regions of the Bay respectively) would be expected to vertically thicken and horizontally compress the plume along the coastline, while upwelling winds (NW to E) would be expected to thin and expand the plume in the cross-shore direction (Fong and Geyer 2001).

In general, the plume directions show weak linear relations with wind direction, with lighter winds showing more scatter than higher wind speeds. For the Tukituki River when wind speed is >5

m s^{-1}, a linear response is shifted such that the river plume is typically directed ~30° to the left of the wind direction, predominately during W–SW winds where the plume is directed offshore. For the Mohaka and Wairoa Rivers, the strongest winds came from the W–SW, where most of the correlation between wind direction and plume direction is found, with lighter winds from other directions showing higher scatter. Relatively few instances of higher wind speeds for wind directions other than W–SW were observed for the available plume transects.

These results indicate that the river-plume directionalities are sensitive to the predominant W–SW winds, which typically exhibited greater wind speeds. High scatter and low wind speeds for other wind directions limit the understanding of the plume response for those conditions. In the Merrimack River plume, Kakoulaki et al. (2014) found that the plume responded to wind speeds greater than 4 m s^{-1}, comparable to the speed threshold observed here. However, Kakoulaki et al. (2014) shows that the plume direction was typically offset from the wind direction by 45° due to Coriolis deflection. The Tukituki River displays a leftward shift related to wind direction but there is too much scatter for the Mohaka and Wairoa River plumes to discern any relation.

Other processes not considered here that likely influence plume trajectories include the inlet configuration, which for the Eel River was found to be important for setting the initial direction of the near–field plume (Geyer et al. 2000). The inlets in Hawke Bay can form complex morphologies which direct the near–field plume either up or down coast (e.g. Fig. 2.11b–d). Tidal motions have been shown to influence small discharge plume direction to either down coast or up coast depending on the tidal stage (Basdurak et al. 2020).

2.4.7 Relation between TSS and forcing mechanisms

Although the river forcing is likely the dominant driver of TSS variability, other processes including resuspension from wave bed shear stress and wind driven currents are likely important for resuspending sediment, potentially mixing to the surface layer, and advecting sediment throughout the Bay (e.g., Fig. 2.8).To illustrate this, the average TSS values are computed for varying forcing conditions (Fig. 2.12), including wind speed (averaged over the previous six hours), total river discharge into the Bay (the maximum value over the previous two days) and the significant wave height (averaged over the previous day). Additionally, for the wave height averages, days were selected on whether the total river discharge was greater than 500 m^3s over the previous 7 days.

The averaged composites show that river discharge is a key factor in the magnitude of TSS variability adjacent to the rivers and the inner shelf in general. Roughly half of the wave events greater than 2.5 m co–occur with elevated river discharge, leading to higher TSS during times of a past discharge event than without. However, wave events during low discharge also show elevated TSS in the northern nearshore region of the Bay as well as the Cape Kidnappers region, indicating

that wave resuspension alone is an important driver of TSS variability. Additionally, broad regions of the Bay show elevated mean TSS concentrations (~15 mg l^{-1}). For more moderate wave events (1–2.5 m), there is noticeably lower TSS away from river mouths, although elevated values are still seen around Cape Kidnappers. The TSS shows a slight increase in relation to increased wind speeds, but no clear pattern is apparent.

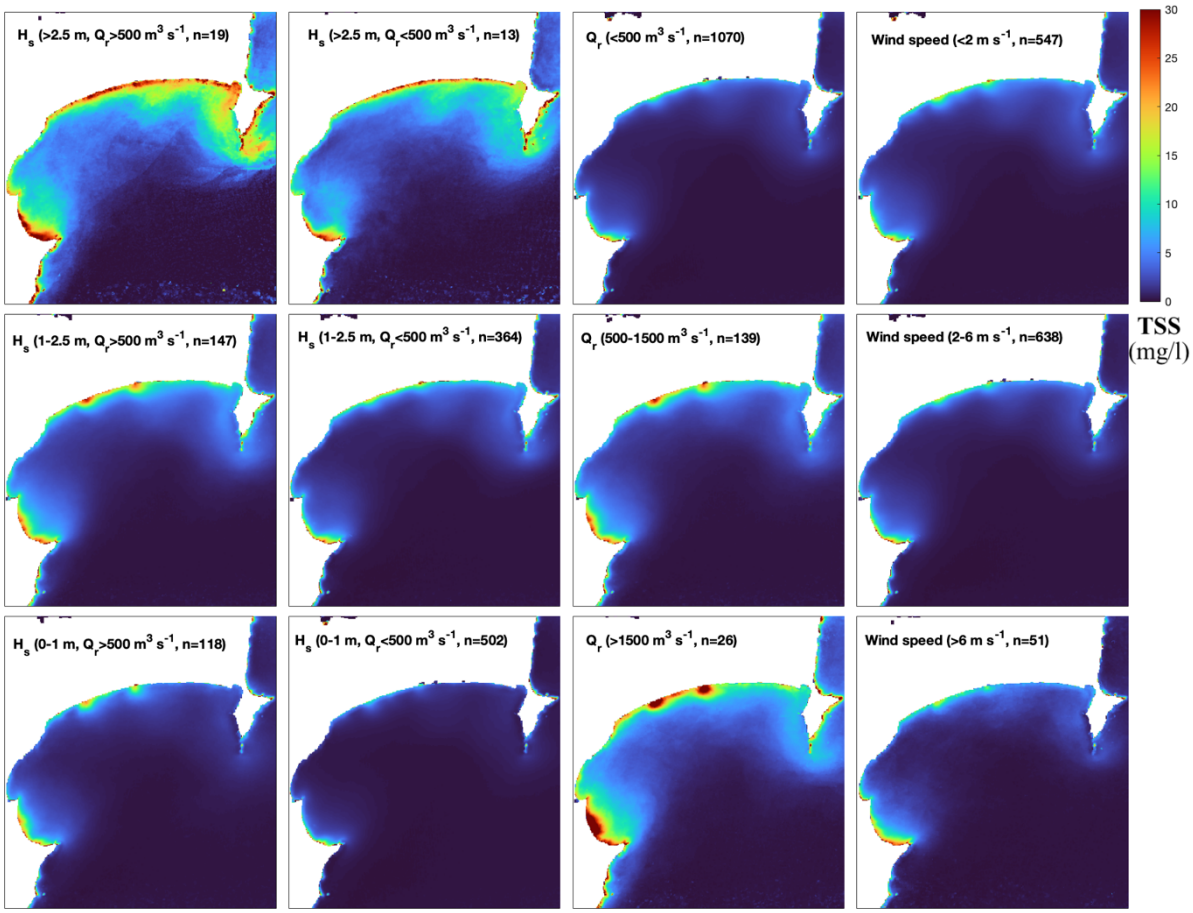

Figure 2.12 Average composites of remotely sensed TSS (mg l^{-1}) for various environmental conditions. The number of days averaged is shown for each plot. The left column averages wave conditions (using the 24-hour average significant wave height prior to image collection) when a greater than 500 m^3 s peak total discharge flowed into the Bay over the previous 7 days, and the middle–left column shows the same wave height ranges but when the total discharge did not reach a 500 m^3 s peak over the previous 7 days. The middle right column shows averaged days in total river discharge ranges (using the maximum value over the previous two days). The right column shows the averaged days under varying wind speed values (using averages over the previous 6 hours) measured from Napier Airport.

To estimate the relative contributions of forcing mechanisms with the surface TSS for each location on the MODIS grid, we use linear regression against three primary drivers (Fig. 2.13) including: 1) combined freshwater discharge into the Bay, 2) wind speed from the nearest wind

station averaged over six hours prior to image capture, and 3) bed stress due to waves. The linear regression (where significance levels are greater than 0.05) shows the river discharge is the dominant driver of TSS variability (Fig. 2.13a), particularly offshore of the Tukituki and Ngaruroro/Tūtaekurī rivers where the r^2 value is around 0.5 extending about 10 km offshore of the river inlet. Offshore of the Mohaka and Wairoa Rivers, high coefficients of determination of around 0.4 are found, and a broad portion of the Bay inshore of the 50 m isobath has elevated r^2 values of around 0.25. The linear correlation with the wave bed stress (Fig. 2.13b) has a broad region of moderate correlation with r^2 values greater than 0.2 for areas less than 50 m deep, and with higher correlations outside of regions of high correlation with the river forcing. The correlation with the wind speed is low throughout the entire Bay (Fig. 2.13c). However, the linear regression does not account for the temporal history of the TSS, as well as the expected nonlinearity in the relation between the bed shear stress and sediment resuspension.

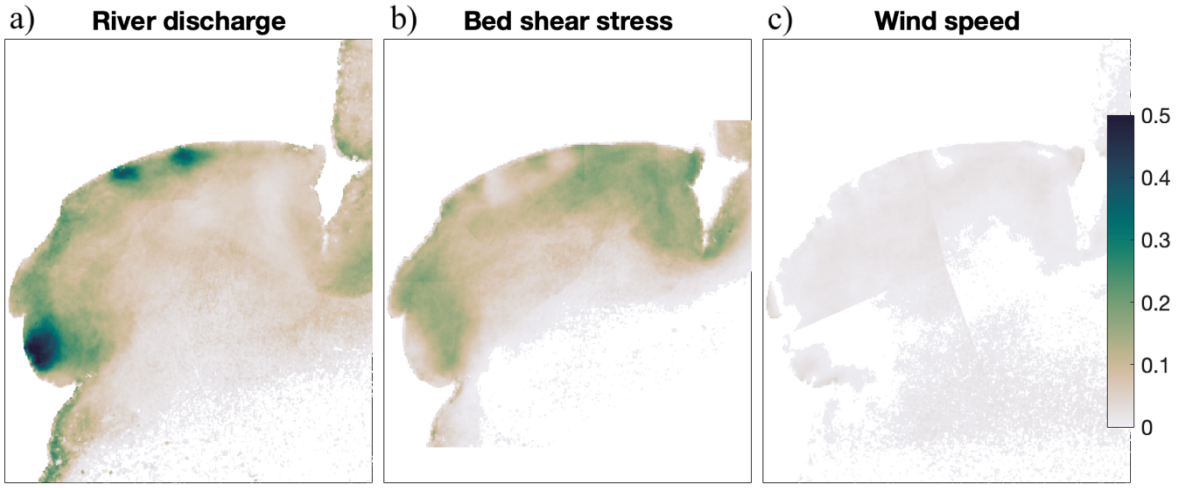

Figure 2.13 The coefficient of determination (r^2) between remotely sensed TSS and forcing mechanisms. The r^2 value for each pixel is based on the linear regression of TSS with a) the combined river discharge into the Bay, b) the wave bed shear stress, and c) the wind speed from the nearest wind station. The scale bar corresponds to all plots and only r^2 values where significance levels are greater than 0.05 are shown.

The bed stress due to waves, computed from modelled wave statistics, shows the wave climate of the Bay is often large enough to resuspend fine sediment that is deposited from the rivers (Fig. 2.14). The rivers predominately transport suspended sediment from clay to coarse silt sizes. Therefore, general critical erosion thresholds of 0.05 N m^{-2} for a fine silt sized particle (Fig. 2.14a) and 0.1 N m^{-2} for a coarse silt (Fig. 2.14b) are used here to gauge the frequency of exceedance (as the percentage of time) of the critical shear stresses for sediment deposited from the rivers. The bed stress exceedances show spatial variability associated with variable bottom roughness, as there are multiple rocky zones within the Bay (Fig. 2.1), as well as due to wave shadowing from the geometry of the Bay. The rocky zones within the Bay have persistently high enough shear stress values to resuspend

any material that was deposited there. Inshore of 30 m depth, roughly half of the time fine silt will be able to be resuspended. Coarse silt can be resuspended approximately a quarter of the time. Offshore of 50 m depth, fine sediment is likely resuspended for the largest wave events.

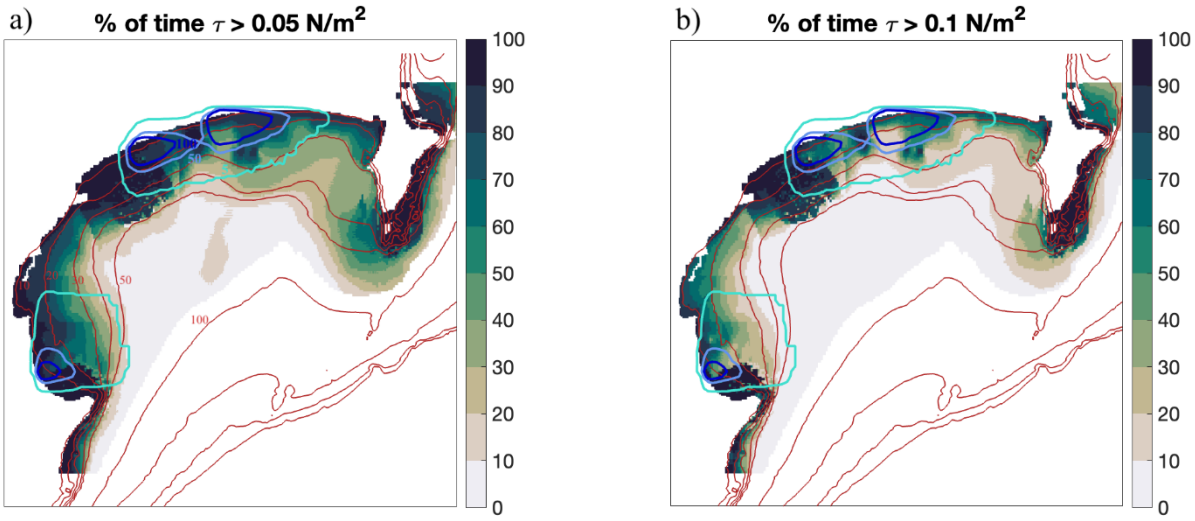

Figure 2.14 The spatial relationship between bed stress and surface transport regions. a) The percentage of time (evaluated at the time of image collection) of exceeding 0.05 N m^{-2} and b) 0.1 N m^{-1}. Bathymetry contours are shown in red and labelled on a). The blue to turquoise lines represents the contours of 100, 50, and 5 occurrences of the 5 mg l^{-1} TSS value (as seen in Fig. 10c) which was computed on a 1 km grid.

In the regions of likely initial deposition, here using the locations of the 5 mg l^{-1} TSS (Fig. 2.10c) transect points for occurrence values of 5, 50, and 100 (Fig. 2.14), shear stress exceedances for the fine and coarse silts are frequent, particularly for the higher occurrences (blue lines). However, this simple comparison does not consider the complexities of sediment erosion, including sediment consolidation, cohesion, and aggregation (Grabowski et al. 2011), and only provides a speculation into subsurface processes.

2.4.8 Length scales of plume transport

The derived length scales of likely sediment deposition found in this work largely corroborate prior studies of marine dispersal dominated river systems (Walsh and Nittrouer 2009), with relatively short length scales of surface transport that are typically further transported subsurface by processes that are not captured by satellite remote sensing. We found that the depths of the e–folding locations are typically shallow enough for material to be suspended upon common wave events, but more work is needed in Hawke Bay to further document these processes. For example, in the Waipaoa River (just north of Hawke Bay), the aggregate and coarser particles settle in the bay and slightly offshore (<7 km offshore), while finer sediment is more dispersive (Moriarity et al. 2015). Some sediment was found to be stored in long-term mud deposition areas located at bathymetric low points, but a majority

would be resuspended by wave orbital currents in the thin wave boundary layer, which can reach concentrations high enough to form hyperpycnal currents transporting sediment offshore (Hale and Ogsten 2015). If river flood events co–occurred with significant waves, sediment was likely transported offshore immediately, but if they did not co–occur, sediment would be stored temporarily in the bay and on the shelf (Bever et al. 2011, Moriarity et al. 2015). Kniskern et al. (2010) used isotopic dating to show that muddy sediments are stored ephemerally between 30–50 m, and that longer term deposition was found offshore at 80–120 m. Similar subsurface processes likely occur in Hawke Bay, and more detailed measurements are needed to investigate how initial surface transport relates to long term sediment transport and deposition in Hawke Bay.

2.5. Conclusion

Using a twenty-year record of satellite ocean colour data, we assessed the spatial and temporal variability of suspended sediment concentration offshore of several small mountainous rivers. The use of satellite remote sensing, here combined with an empirical regression for TSS based on in-situ data, allowed for an unprecedented number of discharge events to be captured for multiple rivers as compared with traditional in-situ measurements of river plume sediment transport. Longer temporal records enabled a full range of discharge events, wave, and wind conditions to be captured. TSS offshore of the main rivers in the Bay showed strong seasonal cycles related to seasonal changes in river discharge, but that the majority of the TSS variance offshore of rivers occurred at timescales shorter than seasonal. Although there were interannual differences in sediment flux into the Bay, typical of small mountainous river systems due to the importance of individual events, the interannual TSS variations from remote sensing were small in comparison. This is likely due to the short time scale of the events, which may not be captured due to cloudiness from remote sensing. The empirical algorithm used here was well suited for general conditions (0–80 mg l^{-1}) but may not accurately estimate the higher range of TSS values possible during the largest discharge events.

The use of remote sensing allowed detailed spatial information of three separate river plumes to be tracked over time. We found that river plumes spatial extents are highly related to the river discharge magnitude, which sets the outflow velocity, buoyancy, and sediment concentration of the river plume. Rivers with larger freshwater fluxes have a larger corresponding inner-shelf footprint of persistent TSS conditions. Plume length scales were defined using the distance to the 5 mg l^{-1} TSS value as well as a metric based on the TSS gradient (e–folding distance of TSS) along the plume centerline. Length scales of the TSS plume extent (to the 5 mg l^{-1} value) were most commonly between 2–8 km offshore, with the larger rivers (Wairoa and Mohaka Rivers) having further distances. The e–folding distance was shorter, with peak values ranging 2–6 km. The transport distances and depths were consistent with the previously established notion that coarser particles settle from the plume in the range of a few km from the river mouth, with the bulk of sediment typically

falling from the plume within ~6 km, while finer particles can be transported further offshore greater than 10 km. The prevailing wind direction relative coastline orientation were important for the observed river plume transport directions.

In Hawke Bay, the dominant contributor of the TSS signal was river discharge followed by waves. Waves were shown to cause elevated surface TSS even during low river discharge. Wind was not as important of a driver for TSS signals at the surface of the Bay but was important for advecting river plumes. Further work in Hawke Bay should address subsurface processes to better understand how surface sediment transport in river plumes, and the patterns that can be detected from satellite remote sensing, is related to long-term sediment deposition. Future satellite remote sensing work of small mountainous river plumes will benefit from using datasets with higher accuracy TSS retrievals at high TSS, higher resolution imagery particularly in the near-field plume and coupling with in–situ data of plume circulation can lead to new insights about sediment deposition and settling from river plumes.

Chapter 3: Circulation and cross-shelf sediment fluxes in an energetic bay with multiple small mountainous rivers

Contribution of Authors

Chapter 3 presents the article “Circulation and cross-shelf sediment fluxes in an energetic bay with multiple small mountainous rivers” which will be submitted to the journal *Continental Shelf Research* for review. Ted Conroy conceptualized the study, performed all numerical modelling, data analysis, and wrote the article. Karin R. Bryan provided feedback, supervision, and editing of the article throughout the process. Joe O’Callaghan provided assistance with the interpretation, and editing of the article.

3.1 Introduction

The delivery of terrestrial sediment into the coastal ocean can cause impacts on the shelf and nearshore ecosystem, such as limiting light penetration and blanketing the benthic environment with fine sediments, ultimately changing the structure and function of these areas (Thrush et al. 2004). Sediment stressors are particularly relevant for coastal oceans that receive river discharge from small mountainous river systems, where high levels of sediment can be transited quickly to the coastal ocean (Walsh and Nittrouer 2009). In such cases, the longer-term fate of the material is dependent on inner shelf processes which can redistribute sediment across the shelf (Geyer et al. 2000).

In this study, we characterize the inner shelf circulation and cross-shelf sediment transport response of an embayment with multiple small mountainous rivers that is exposed to an energetic coastal ocean using a numerical model. The study is focused on Hawke Bay, Aotearoa New Zealand, where little oceanographic information is available, and the region is highly susceptible to devastating storm events, such as Cyclone Gabrielle in 2023 and Cyclone Bola in 1978. The region has steep deforested catchments and erodible soils that have the potential to cause widespread ecological damage to the near shore and shelf seabed during such events. A three-dimensional hydrodynamic sediment transport model is verified against observational data and used to explore the relative importance of environmental drivers in determining sediment fluxes throughout the Bay. This study sets out to describe the circulation patterns in Hawke Bay comprehensively for the first time, as well as investigating how environmental conditions impact small mountainous river plumes and cross-shelf sediment transport.

3.2 Background

3.2.1. Regional setting: Hawke Bay

Hawke Bay is a large southeast facing embayment, roughly 40 by 80 km, on the east coast of the North Island, extending from the Mahia Peninsula in the North to Cape Kidnappers (Fig. 3.1). The continental shelf offshore of the bay is relatively broad and gently sloping compared with the narrower shelf north and south of the Bay. Steep coastal mountains combined with high rainfall rates produce significant episodic river discharge events that transport on average 11 million tons (MT) of suspended sediment to the Bay each year (Hicks et al. 2011).

The Bay is susceptible to strong wind and wave forcing at times. The average significant wave height recorded off Napier was 1.2 m, but high wave events can be from 2.5 – 3.5 m, and the largest events are greater than 8 m (Komar 2010). Waves on average approach from the east-southeast, are larger in winter, and wave heights in the bay can be spatially variable for a given swell due to wave refraction. Waves create longshore currents that are important for sediment transport and beach erosion in the southern Bay (Komar 2010). The spring tidal range is ~1.9 m and neap are ~1.2

m as measured at the Napier Port. Current patterns in the Bay have received limited investigation, but early work suggests general current patterns of inflow at the Bay center and outflow at each headland (Ridgeway and Stanton 1969) as well as the presence of expansive freshwater plumes (Bradford et al. 1976).

There are two dominate currents that flow offshore of the Bay: the warmer and saltier East Cape Current (ECC) that flows from the north and the cooler and fresher Wairarapa Coastal Current (WCC) from the south (Stevens et al. 2021). Chiswell (2002) showed that water from the WCC can be advected into Hawke Bay. Kerry et al. (2023) studied the offshore circulation in much higher detail than has been done previously and showed that for mean conditions the WCC flows northward on shelf slope offshore of the Bay until roughly 1 km depth about 100 km from shore, where then the ECC predominately takes over with southward transport. The transport displays seasonal variability with larger southward ECC transport in summer (Kerry et al. 2023).

3.2.2. River plume and inner shelf flows

Transport of sediment within a river plume is dependent on the sediment characteristics, which determine the downward settling velocity, as well as the lateral advection which transports sediment particles horizontally (Geyer et al. 2000). The plume dynamics are dependent on the river velocity at the inlet mouth, the density contrast between the outflowing water and ambient ocean water, the barotropic pressure gradient, and ambient currents created by the wind or offshore currents (Horner-Devine et al. 2015; Hetland 2005). In the near-field region, the transport is dictated by the outflow momentum at the river mouth and behaves as a jet, being slowed down by shear mixing at the base of the plume. During discharge events, the freshwater will generally detach from the bottom at the mouth of the river inlet.

In the mid-field region, other processes become important. The density contrast between the fresh and ocean water produces lateral spreading at the rate of the internal wave speed (Horner-Devine et al. 2015). Local winds can create surface currents which transport the freshwater, as well as provide vertical mixing if the Ekman layer depth is greater than the plume depth. Upwelling winds have been shown to elongate the plume offshore, while downwelling winds tend to trap fresh water near the coast (Fong and Geyer 2001). If the length of the plume is greater than the baroclinic Rossby radius of deformation, the Coriolis force can steer the plume towards the left and create a buoyant coastal current, and if other processes are absent, a recirculating bulge can form (Horner-Devine et al. 2015). The ambient currents on the inner shelf are influenced by waves (surface and internal), wind, tidal forcing, and offshore flows such as boundary currents and submesoscale flows (Lentz and Fewings 2012; Kumar et al. 2016; Wu et al. 2020). Wind driven upwelling and downwelling flows can initiate cross-shelf and vertical velocities, and wave induced currents can drive cross-shelf, vertical and alongshore currents in the nearshore (Lentz and Fewings, 2012).

Wave current interaction offshore of the inlet and wave breaking near the inlet mouth can significantly alter the plume structure and currents (Wright et al. 1980) and create strong vertical velocities in the inlet region. Wright et al. (1980) documented enhanced deposition near the river inlet due to wave breaking. The geometry of the inlet and existence of a shoal or submerged delta also play key roles in the momentum structure of the inlet region (Olabarrieta et al. 2011). However, the influence of these processes on sediment transport has not been studied in detail, and understanding the role of these complexities in controlling zones of sediment deposition is essential to successful management of these stressors.

3.3 Methods

3.3.1 Numerical model

To simulate hydrodynamics and sediment transport in Hawke Bay, the Coupled Ocean-Atmosphere-Wave-Sediment Transport (COAWST) modelling system (Warner et al. 2008) was used. From the COAWST system, we utilized the coupling of the Regional Ocean Modelling System (ROMS), with Simulating WAves Nearshore (SWAN) and the community sediment transport model. ROMS is a three-dimensional, hydrostatic, finite difference numerical model that approximates the Reynolds averaged Navier-Stokes equations on a structured grid (Haidvogel et al. 2008). ROMS is commonly used in inner shelf settings (e.g. Suanda et al. 2018, Kumar et al. 2016). SWAN is a spectral wave model that solves the spectral density evolution equation (Booij et al. 1999) and includes refraction, shoaling, and dissipation. Atmospheric forcing to the ROMS is configured using the bulk fluxes formulation with atmospheric model data from the ERA-5 interim hindcast dataset (Hersbach et al. 2020).

The Hawke Bay SWAN model is forced by a wave hindcast of Aotearoa New Zealand waters by Alberqurque et al. (2022), which showed good skill at replicating wave height and period at the local wave buoy located in Napier (Alberqurque et al. 2022). At the model boundaries, spectrally averaged values were used to force SWAN at 2 km increments. SWAN was set up to compute the wave action balance equation in the frequency range of 0.04 to 1 Hz with a resolution of 24 bins in 36 directional bins. Exchange of information between ROMS and SWAN was set to occur every 10 minutes. The vortex force formulation was used to model the effect of waves on current and currents on waves (Kumar et al. 2012), and additionally modelled processes included wave driven mixing and bottom streaming.

At the outer boundary of the coarse domain, ROMS is forced by the momentum and density fields of a realistic hindcast simulation of Aotearoa New Zealand waters (De Souza et al. 2022, Kerry et al. 2023), termed the MOANA hindcast model. The MOANA hindcast model is a 5 km resolution ROMS model that performed well when compared to available sea surface temperature, and showed high skill for water level variability, including sea level set up and set down. The boundary condition

for the coarse grid for the density, velocity, and sea surface height fields use a radiation-nudging condition, allowing information to propagate out the domain, with a strong inflowing nudging time scale and a weak outflowing time scale (1 and 365 days respectively). At the open boundary, the Chapman condition is used for the free surface, the Flather condition for barotropic velocities, and gradient condition for the turbulent kinetic energy.

The MPDATA advection scheme is used horizontally and vertically for all tracers, as it is well-suited for the modelling of areas of large tracer gradients and preserving positive values of salinity and sediment concentration (Smolarkiewicz and Margolin 1998). Bottom roughness was computed as a time dependent function of the sediment grain size. The horizontal diffusivity and viscosity constants were set to 0.01 m^2/s to reduce numerical instability. The k-e turbulence closure model was used with default parameters, and mixing was formulated to occur along geopotential surfaces for tracers and along constant sigma surfaces for momentum.

Freshwater fluxes for most of the rivers that drain into the Bay are measured by the Hawkes Bay Regional Council and recorded at 15-minute intervals (https://www.hbrc.govt.nz/environment/river-levels/). For smaller ungauged rivers, including the Nuhaka, Waihua, and Waikere Rivers, linear scalings based on watershed areas with nearby rivers were used to estimate the discharge. The river freshwater flux entered the domain as a horizontal momentum flux as a point source for all rivers, which was vertically evenly distributed for the upper 20 layers of the water column. The temperature of the river flux for all rivers was set to the measured river temperature from data collected in the Tukituki River at Red bridge (Fig. 3.1). Two model runs were performed from the period of March 2017 to December 2019, one with only ROMS and with two-way ROMS and SWAN coupling. The coupled model is used for all analysis presented, and the ROMS only run is used for comparison to assess how waves impact river plume circulation in Hawke Bay.

3.3.2. Grids and bathymetry

Bathymetry used for the ROMS and SWAN grids are sourced from several datasets, including a 250 m gridded dataset from NIWA, lidar and multi-beam sonar datasets sourced from the Hawkes Bay Regional Council, where multi-beam datasets were focused on hard structure areas in the Bay. All datasets were vertically referenced to mean sea level in the time-period of 2006-2016, then merged and interpolated to the grid. The bathymetry was smoothed to meet the criteria of a maximum stiffness value of 0.2, and the minimum depth was set to -2 m (where positive is downwards). Wetting and drying was used with a minimum critical depth of 40 cm. The model used 22 vertical sigma layers with greater vertical resolution at the surface and bed.

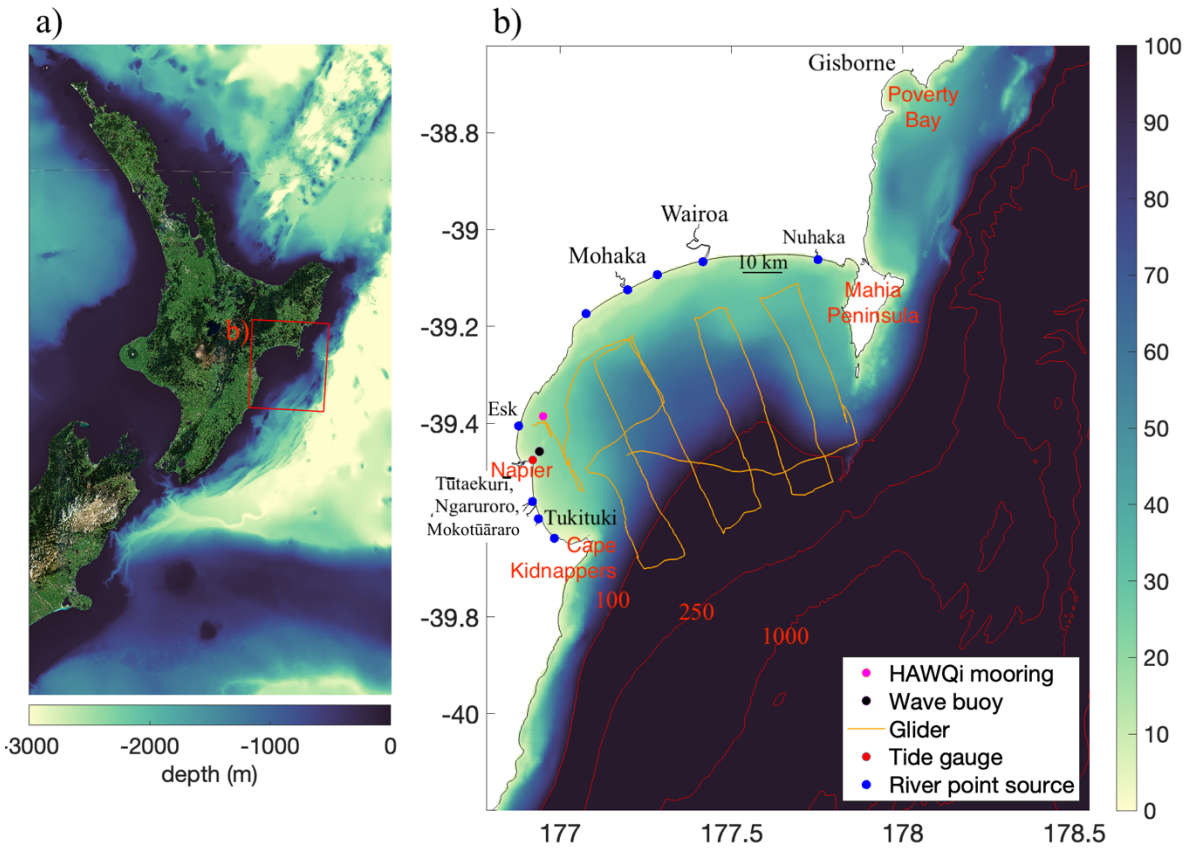

Figure 3.1 Overview of the Hawke Bay region, data sources, and COAWST model grid. a) The bathymetry of the north island of Aotearoa New Zealand (m), with the COAWST model domain shown in red. b) The ROMS and SWAN model domain and bathymetry (m), where the red contour lines show the bathymetry deeper than 100 m. Major rivers are labelled, as well as the data locations used, including the HAWQi mooring, wave buoy, tide gauge, and glider tracks. The blue dots represent freshwater and suspended sediment point sources. A 10 km scale bar is shown in the northern region of the Bay for reference.

The grid expands beyond the continental shelf and tens of kilometers north and south from Hawke Bay to reduce impacts from the boundary on the flow in the Bay (Fig. 3.1). The grid resolution is 500 m. The rivers and river inlets are not resolved by the grid and are implemented as point sources. This approach does not accurately simulate the near field plume, which is dependent on the inlet width, which is typically much narrower than 500 m, as well as estuarine processes which can impact the outflow density and momentum.

3.3.3. Sediment characteristics

Suspended sediment transport is modelled in the Bay by using a fixed number of grain sizes that represent the sediment characteristics in the Bay. The model options used in this work include allowing morphological bed changes, the sediment in the water column contributes to the water

column density, and only suspended transport considered. We use static sediment classes with no cohesive processes such as flocculation or bed consolidation.

The bed sediment grain size is initialized with data sourced from a compilation dataset from NIWA, with samples mainly collected in the 1960s, along with data collected by Hawkes Bay Regional Council in the 2010s, and grain size data collected in the Tukituki River and inlet in 2022 (Atkin, 2022). The sediment characteristics in the Bay follow common continental shelf sedimentary patterns, with coarse sand on beaches and muddy areas becoming progressively dominant with distance offshore. There are also several gravel zones and rock reefs in the Bay, as described below. Pantin (1966) comprehensively sampled and described the bed sediment characteristics in the Bay, observing that coarse beach sand (with the median grain size (d_{50}) around 250 mm) persists for a relatively short distance offshore until fine sand becomes the dominant sand size in the Bay (in the range of 63-150 mm, and around 100-125 mm in general; Marshall 1929, Pantin 1966, Hume 1989, White 1994). Muddy regions offshore were recorded to have silt/clay to sand ratios of typically 70/30.

Gravel is found along the beaches of the southern Bay, including at the inlets of the Ngaruroro/Tūtaekurī and Tukituki Rivers, as well as a few offshore regions such as offshore of the Mohaka River (Pantin 1966, Atkin 2022). Grain sizes at the bed of the Tukituki River near the inlet and up to 1.5 km upriver from the inlet range from 4-32 mm, with the average d_{50} 16 mm. The Mohaka and Wairoa River inlets also have coarse grain beaches with gravel sizes. Hard structure rocky reefs areas in the Bay include the Pania reefs, Wairoa Hard, Clive Hard, and offshore of the Mahia Peninsula. Seafloor classification for these areas has been done using sidescan sonar, which classified sediment types (data from Hawkes Bay Regional Council). We use the derived maps from these surveys to prescribe the sediment bed sediment class for these areas.

Bed grain size distributions have been measured in the Tūtaekurī/Ngaruroro River (average 4% clay, 19% silt, 77% fine sand; Atkin 2022), and the Wairoa River (50% fine sand, 45% silt, and 5% clay; data from Hawkes Bay Regional Council). White (1994) reported suspended d_{50}values from the Tukituki and Ngaruroro/Tūtaekurī rivers with clay sized values around 4 μm for the Tukituki and Ngaruroro/Tūtaekurī Rivers. More recent measurements collected by Hawkes Bay Regional Council in the Tukituki River report bimodal peaks of suspended d_{50} by volume of 15 and 45 μm. Additional measurements for suspended d_{50} taken in 2021 had bimodal peaks of 7 and 34 μm for the Wairoa River, 6 and 25 μm for the Mohaka River, and 13.6 μm for the Tukituki River. A small number (11) of grain size samples were taken in the four main river plumes at various distances offshore had a range of d_{50} values from 3–15 μm.

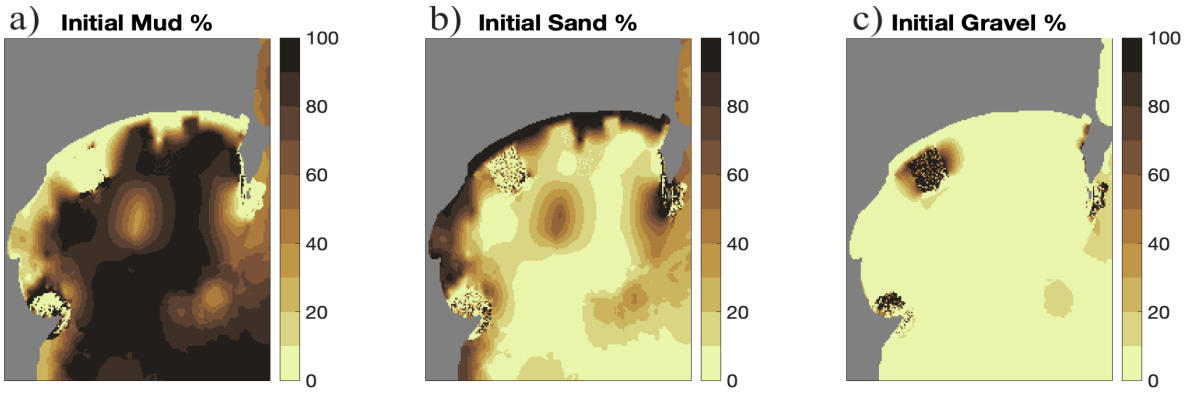

Figure 3.2 Bed sediment grain size percentages interpolated to the model grid. a) Mud, b) sand, and c) gravel sized sediments. These distributions were used to initialize the bed sediment model.

The initial bed composition was based on a spatial interpolation of the bed data to the model grid (Fig. 3.2). For rock areas, we use the gravel class, which will remain immobile for these simulations as only suspended transport is considered. Due to the ubiquitous presence of aggregated particles that have been documented in other river plume studies (Geyer et al. 2004), the lack of measurements that have been made in the region, and the significant influence that the effective settling velocity has on sediment dispersal (e.g. Geyer et al. 2004), we assume that a fraction of the river flux of suspended particles are aggregated and use commonly reported values for the diameter and settling velocity. For the bed sediment fractions, all gravel and rock areas use the gravel class with values measured from the Tukituki River ($d_{50} \sim 16000$ µm), and all sand in waters deeper than 5 m was set to fine sand while shallower than 5 m was set to the medium sand class. In muddy areas the mud percent was distributed as 50% coarse silt, 40% silt, and 10% clay.

Table 3.1 Sediment classes and characteristics used in the sediment transport model. The settling velocity was computed from the Stokes settling velocity and the critical shear stress from the Shields critical stress. The critical shear stress for erosion and deposition were set to the same value.

Sediment class	d_{50} (µm)	Settling velocity (mm/s)	River fraction (%)	Critical shear stress (N/m^2)
Clay	4	0.014	30	0.03
Silt	10	0.1	30	0.05
Flocculated silt and clay	10	1	20	0.05
Coarse silt	50	2	20	0.1
Fine sand	125	10	0	0.145

Medium sand	250	30	0	0.194
Medium pebbles	16000	800	0	12.2

Given the range of observed suspended sediment sizes observed in the Bay, general size values were chosen that were best thought to represent the observed variability in in-situ samples. Sediment settling velocities were calculated based on Stokes settling velocities, and critical Shields shear stress was used for each sediment type. Here the critical shear stress for deposition was set equal to the value for erosion. All sediment densities are set corresponding to the density of greywacke, 2650 kg m^{-3}, and the sediment porosity was set to 0.6 for all classes. The erosion rate for all classes was set to 5×10^{-4} kg/m^2, as was used for a ROMS modelling study directly north of Hawke Bay in Poverty Bay (Bever and Harris 2014). Other options used include that sediment concentration is included in the water column density calculation, and that morphology is active. Cohesive sediment processes such as flocculation and bed consolidation were not modelled. The bed was modelled with 5 bed layers, where a new layer was created upon 10 cm of sediment deposition.

The suspended sediment fluxes from all rivers were estimated based on power-law relationships between SSC and discharge, fit to data measured by Hicks et al. (2011). This data measured discharge and point-values of SSC at a wide range of discharge conditions for the Wairoa, Mohaka, Ngaruroro, Esk, Nuhaka, and Tūtaekurī Rivers.

3.3.4. Observational data

To validate the model performance, we use several different observational data sets that encompass the different aspects of the hydrodynamics in the Bay, including the inner shelf flow and vertical structure, tides, wave propagation, and surface sediment concentration. Water level is measured at the Napier Port, and wave height is measured from a Triaxis wave buoy located directly offshore of the Port (Fig. 3.1). A long-term mooring HAWQi has been deployed by Hawkes Bay Regional Council directly north of the Port in 18 m depth, with three CTDs in the water column and a downward looking ADCP at the surface. For one month in 2019, a Slocum 200 m electric glider was deployed in the Bay and collected 8506 profiles (Fig. 3.1; O'Callaghan 2020). The glider was equipped with a Seabird CTD and additional water quality sensors (additional details described in O'Callaghan 2020). We utilize a derived surface Total Suspended Solids (TSS) dataset sourced from daily MODIS satellite remote sensing imagery that used an empirical algorithm to estimate the TSS (Chapter 2). This dataset gives a 250 m resolution surface TSS snapshot each cloud free day for the entire period considered here.

3.3.5 Model skill metrics

To assess the performance of the COAWST model of Hawke Bay, we compare observed data with the numerical model output and use comparison metrics including the linear regression coefficient, root mean square error, and a skill score. The skill score is defined as

$$SS = 1 - \frac{1}{\sigma_{obs}^2 N}\sum_{i=1}^{N}(x_{obs} - x_{model})^2 \quad (3.1)$$

(Murphy 1988), where s is the standard deviation.

3.3.6 River plume analysis methods

Due to the episodic nature of river discharge events and the varying spatial positioning of river plumes, a set of analysis methods are described that allow for the systematic analysis of river plume properties. River discharge events are identified based on a 50 m^3s^{-1} prominence threshold and the duration of the event is defined as the width of the event at half of the prominence magnitude of the event. This metric generally encompasses the rapid beginning of the event but does not cover the tapering nature of the event, such that the duration metric does not fully account for the nonlinearity of event signals. To identify the time-varying spatial patterns of river plumes, salinity contours are computed and associated with each river through time. At each model output time, each major river plume is characterized spatially based on the surface salinity contoured at the values of 33, 30, and 20 psu which are assigned to a river if present for a given time.

Several metrics are defined to quantify the importance of different processes on plume vertical structure, mixing, and transport direction. As most mixing occurs vertically rather than at plume horizontal boundaries (Horner-Devine et al. 2015), and we are generally interested in mixing processes at the plume interface. The pycnocline depth is defined as the location of the maximum vertical density gradient ($\partial\rho/\partial z$). We designate this location in the water column as the plume interface and calculate stratification and mixing processes at that vertical location. The turbulence production is defined as $P = k_m\left(\frac{\partial u^2}{\partial z} + \frac{\partial v^2}{\partial z}\right)$, where k_m is eddy viscosity. The buoyancy flux is defined as $B = g\beta k_z\frac{\partial s}{\partial z}$, where β is the coefficient of saline contraction and k_z is the salinity diffusivity from the model, is used to determine the intensity of plume mixing.

3.4. Results

3.4.1. Model evaluation and overview

Over the period from 2017–2019, multiple discharge events occurred typically during the winter with event magnitudes surpassing 500 $m^3\ s^{-1}$ (Fig. 3.3a). The model shows high skill at reproducing the sea surface height at Napier Port (Fig. 3.3b) as well as the subtidal component of the

sea surface height (Fig. 3.3c). Note that due to the model output frequency of 3-hour intervals, the amplitude as shown in the comparison plot appears smaller than the hourly observed tidal data.

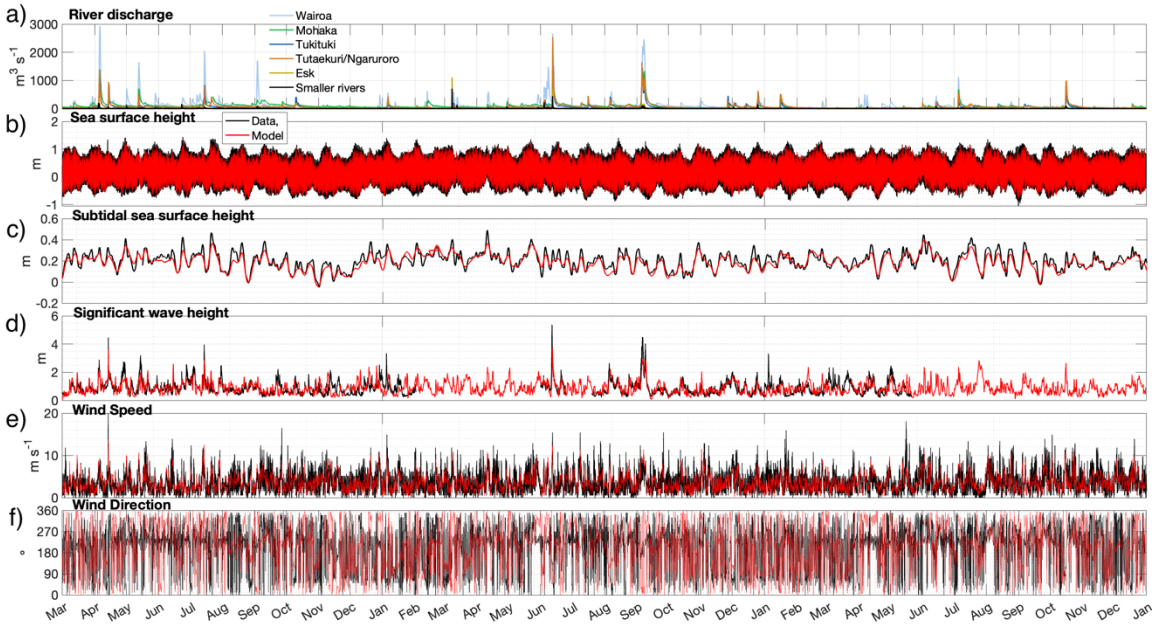

Figure 3.3 Timeseries of environmental conditions and modelled parameters. a) River discharge for main rivers in Hawkes Bay ($m^3 s^{-1}$). b) Sea level (m) measured at Napier Port (black) and modelled (red). c) Tidally filtered sea level (m). d) Significant wave height (m). e) Wind speed comparison ($m s^{-1}$), and f) Wind direction comparison (degrees).

The model simulates the variability of significant wave height (Fig. 3.3d), period, and direction (Fig. 3.4), and captures most events, although with discrepancies for some wave events. In general there is a slight overestimation of wave period in the model, and a slightly broader range of typical wave directions than observed (Fig. 3.4). The location of the wave measurement is affected by substantial shadowing from the headlands at either side of the Bay, resulting in a narrow range of measured swell directions from both the model and observations. The discrepancies of the wave modelling, including not simulating several smaller wave events with heights less than 2.5 m, is likely due to the boundary forcing of the wave model which used spectrally averaged values rather than the full directional spectrum. The wind surface forcing, sourced from the ERA-5 hindcast, reproduces the observed directionality and magnitude of the wind recorded at the Napier Airport (Fig. 3.3e-f) and shows moderate ability to replicate the east/west and north/south wind magnitudes (Table 3.2). Wind roses from Napier Airport show that the model reproduces the dominant wind direction from the SW (Fig. 3.6), but does not simulate a number of NNE wind events that are present in the observed record.

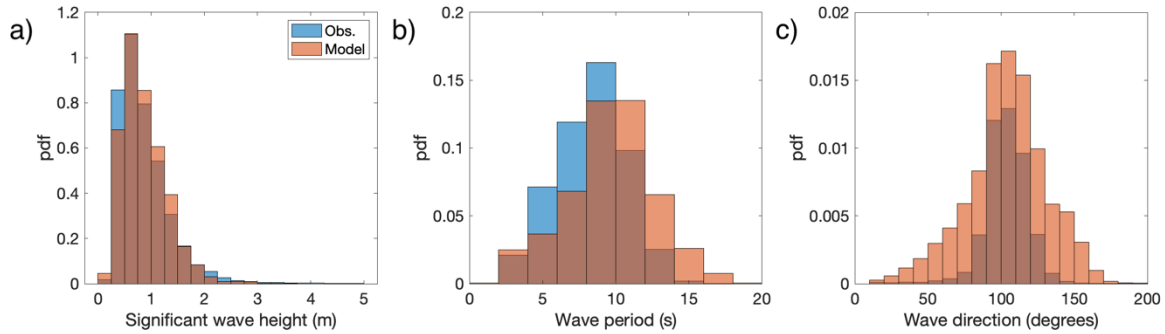

Figure 3.4 The comparison of wave statistics with modelled and observed values. The histograms compare probability density functions of the observed (blue) and modelled (orange) a) significant wave height (m), b) mean wave period (seconds), and c) mean wave direction (degrees) over the three-year model run period.

Table 3.2 Statistics from model/data comparisons. The table includes the linear correlation coefficient (R^2), Skill Score (SS), and Root Mean Squared Error (RMSE).

Data	Location	R^2	SS	RMSE
Sea surface height	Napier Port	0.99	0.98	0.07 m
Subtidal sea surface height	Napier Port	0.89	0.76	0.04 m
Salinity	HAWQi	0.56	0.02	1.4 psu
Temperature 0.5 m depth	HAWQi	0.98	0.95	0.7 degrees
U velocity 2 m depth	HAWQi	0.13	-0.85	0.07 m s^{-1}
V velocity 2 m depth	HAWQi	0.45	-0.03	0.09 m s^{-1}
Significant wave height	Offshore Napier Port	0.53	-0.1	0.44 m
Mean wave period	Offshore Napier Port	0.30	-0.4	3.5 seconds
Wind U velocity	Napier Airport	0.73	0.53	2.3 m s^{-1}
Wind V velocity	Napier Airport	0.75	0.44	2.0 m s^{-1}

At the inner shelf mooring HAWQi, located in 18 m depth, the model reproduces the seasonal and event time scale variations in water column temperature and salinity. Sea surface temperature displays a strong seasonal cycle varying from 10–25° (Fig. 3.5a), also well simulated by the model.

Sharp variations that interrupt seasonal patterns in the model are strongly related to variations in solar forcing, offshore boundary current transport, and wind forcing. Vertical temperature stratification also follows seasonal patterns (Fig. 3.5b), with warmer water overlying cooler water in the summer, punctuated by warming events, and during the winter cooler water typically overlying warmer water in both observations and the model. In contrast, salinity does not show a clear seasonal cycle but shows salinity generally around 35 psu interrupted by periodic changes and discrete events that quickly reduce the salinity (Fig. 3.5c). The model captures most of the drops in salinity, often capturing the general magnitude of the decrease in salinity. Only limited subsurface salinity measurements were recorded during the study period, but comparison with the available data suggests that the model salinity stratification is the correct magnitude (Fig. 3.5d), with background stratification of generally 1 psu or less and maximum difference values around 10 psu.

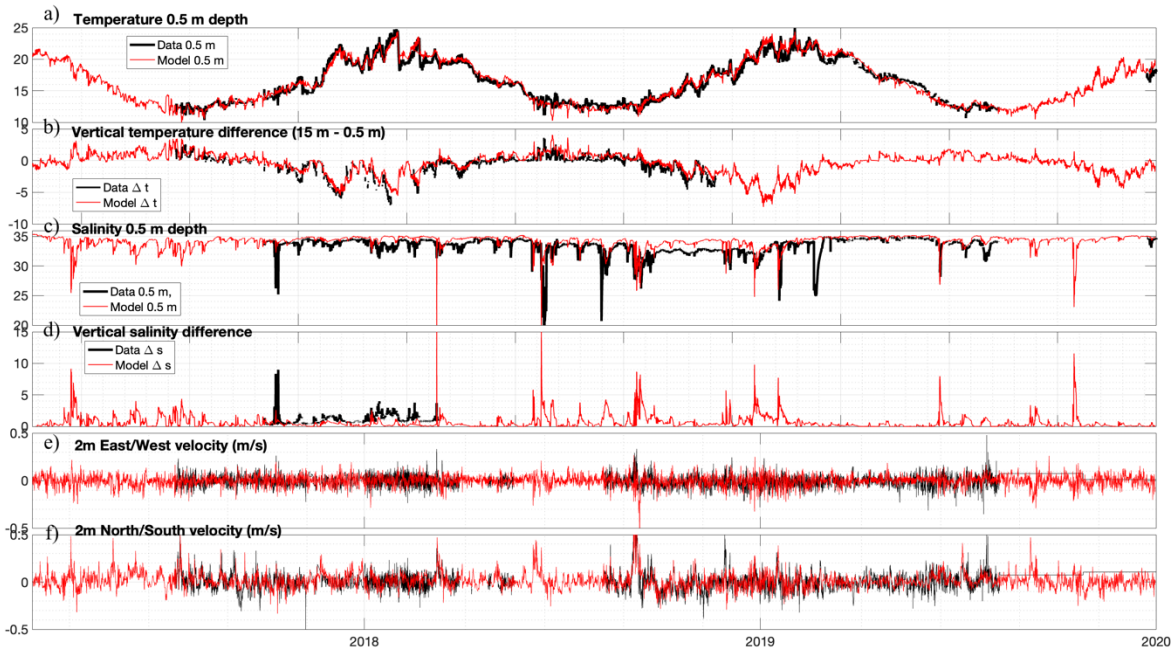

Figure 3.5 Model/data comparisons from inner shelf mooring HAWQi. a) Temperature at 0.5 m below the surface. Observed data is in black and modelled in red. b) Vertical temperature difference (between 15 and 0.5 m below the surface). c) Salinity at 0.5 m below the surface. d) Vertical salinity difference (between 15 and 0.5 m below the surface). e) East/west velocity at 2 m below the surface. f) North/south velocity at 2 m below the surface.

The surface velocity at 2 m from the surface at HAWQi is strongest along-shore (up to 0.5 m s^{-1}) with smaller cross-shore velocity (typically ~0.1 m s^{-1}) in both observations and the model (Fig. 3.5e-f). River discharge events cause the largest fluctuations in alongshore velocity (likely from the nearby Esk River), which causes northward surface flow. Tidal velocities oscillate in a counterclockwise orientation throughout the Bay associated with tidal propagation to the north along the coastline, with flow out of the Bay during ebb and into the Bay during flood. Tidal oscillations are

observed in the cross-shore flow while the along-shore flow is more dependent on river discharge and wind variability, both in observations and in the model.

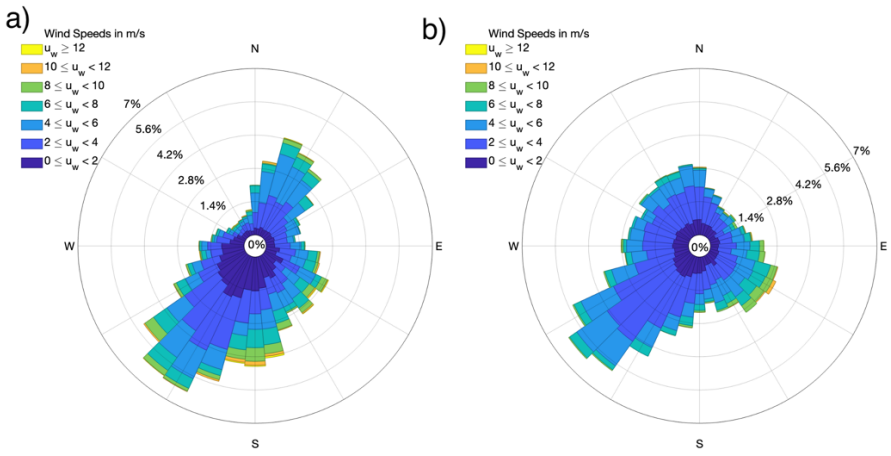

Figure 3.6 Comparisons of wind roses with observed and modelled values. Wind rose from observed data from a) Napier Airport during simulation period, and b) modelled wind at the nearest model location to Napier Airport.

The month-long glider deployment in March 2019 transited the entire inner shelf of the Bay from south to north, extending from ~40 to 150 m water depth (Fig. 3.7f). The glider showed that the upper 50 m of the water column is much warmer and saltier than the underlying water deeper than 50 m. Modelled vertical profiles of temperature generally show similar patterns to the observed structure (Fig. 3.7g), with the model correctly simulating bottom and surface temperature magnitude, but observations show sharper vertical gradients than the model. This can additionally be seen in the comparison of temperature and salinity space (Fig. 3.7e), where the model simulates the correct bounds of temperature and salinity at the highest temperatures near the surface, but at the lower mid and lower water column levels with temperatures below 19° the model shows a narrow band of salinity variability in contrast to the observed values. Importantly however, the model correctly simulates the regions of lower salinity water associated with the glider going shallower towards riverine influenced waters (e.g., times 2 and 4).

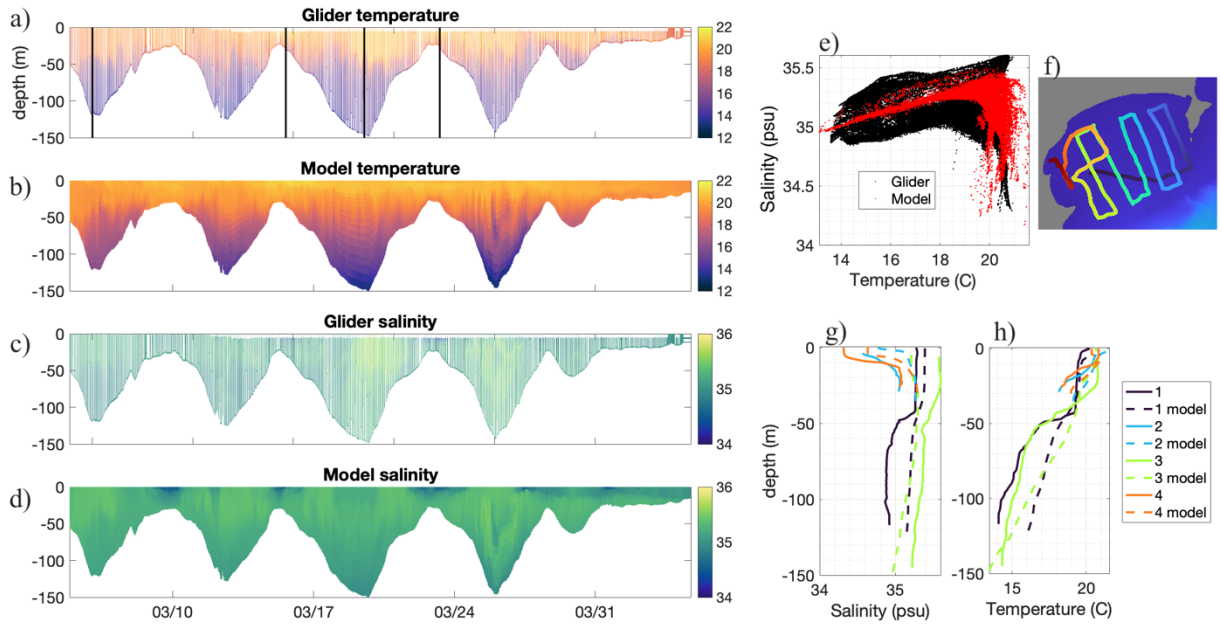

Figure 3.7 Model/data comparison of glider data, collected in April 2019. f) Shows the path of the glider data throughout the Bay (going from blue to red). a-b) show temperature profiles, c-d) show salinity profiles, and e) shows the comparison of observed and modelled temperature/salinity space. g-h) show vertical profiles at select times (shown in a), where the solid line is observed, and the dashed line is modelled.

Satellite derived TSS (from here noted as SSC) is compared with modelled SSC during cloud-free days (Figs. 3.8 and 3.9). The satellite derived SSC dataset shows spatial patterns and gradients of SSC; however, the model likely estimates SSC values below ~70 mg l^{-1} better due to the limited empirical data above this threshold used in the local algorithm (Chapter 2). The SSC from the model was obtained at similar times of MODIS imagery collection (either at 11 AM or 1 PM) for each day, and the model SSC was interpolated to the MODIS grid and no-data locations from MODIS were applied to the model to allow for comparison. The average daily model SSC shows elevated nearshore SSC in the range of 35–50 mg l^{-1} (Fig. 3.8a, while the MODIS derived dataset shows nearshore average SSC values in the range of 10–20 mg l^{-1} (Fig. 3.8b), with the mean daily bias showing the greatest offset near the coast (inshore of 20 m) with values up to 20 mg l^{-1} (Fig. 3.8c), and lower

values (~5 mg l^{-1} throughout the deeper regions of the Bay). The standard deviation of the mean daily bias similarly shows higher offsets near the coast, with highest values around 60 mg l^{-1}.

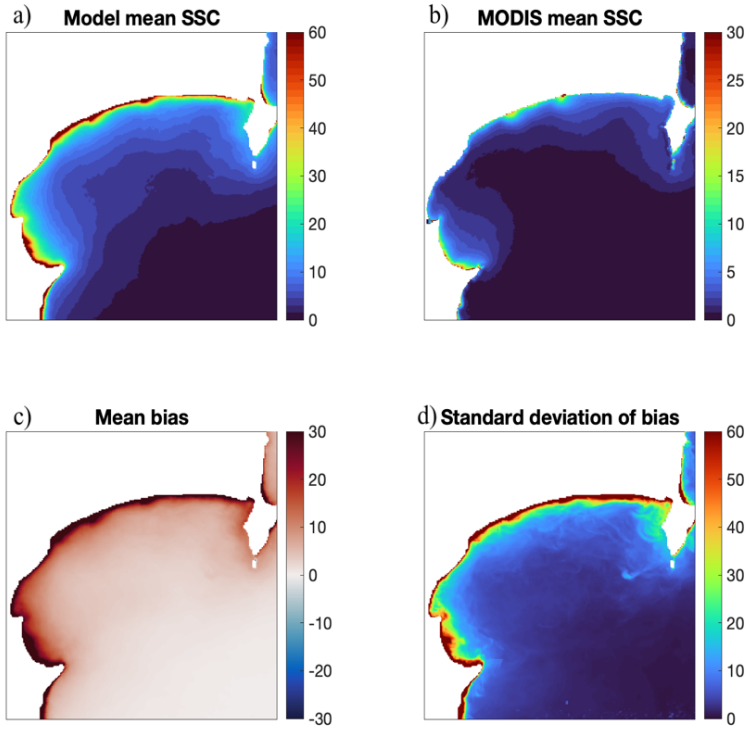

Figure 3.8 Comparison between model surface sediment concentration (SSC) and SSC derived from MODIS. a) daily model averaged SSC (mg l^{-1}). b) daily MODIS averaged SSC (note the change of colour range from a) (mg l^{-1}). c) Average daily bias between MODIS and the model (mg l^{-1}). d) The standard deviation of the daily SSC bias between the model and MODIS (mg l^{-1}).

Daily comparisons are made between MODIS SSC (Fig. 3.9 top rows) and the model SSC (Fig. 3.9 bottom rows) for a selected range of conditions spanning varying magnitudes of discharge events and wave conditions. In general, the model simulates the spatial patterns of SSC and the directionality of river plumes and frontal features that are commonly associated with wind forcing in the Bay. However, the model SSC is much higher than the MODIS SSC, such that the colour range is doubled for all model instances (Fig. 3.9). Qualitatively, spatial patterns for river plumes are similar between the two at each day, with similar directionalities occurring. Exact comparison is difficult due to the differing magnitude of the two, but the model displays circulation-related features found in the remote sensing data, including northward coastal currents (17-Oct-2019), transport associated with Cape Kidnappers (27-Feb-2019), eddying motion of suspended sediment (22-May-2019), and the formation of radial plumes (18-Jul-2018). The SSC estimated from MODIS is likely underestimated (Chapter 2), but the modelled SSC has additional uncertainty associated with the estimation of sediment flux, not well-resolving river inlets or the surfzone, as well as the ratio of sediment sizes that

are present in the rivers, which have a large impact on advection distances of sediment transport within plumes.

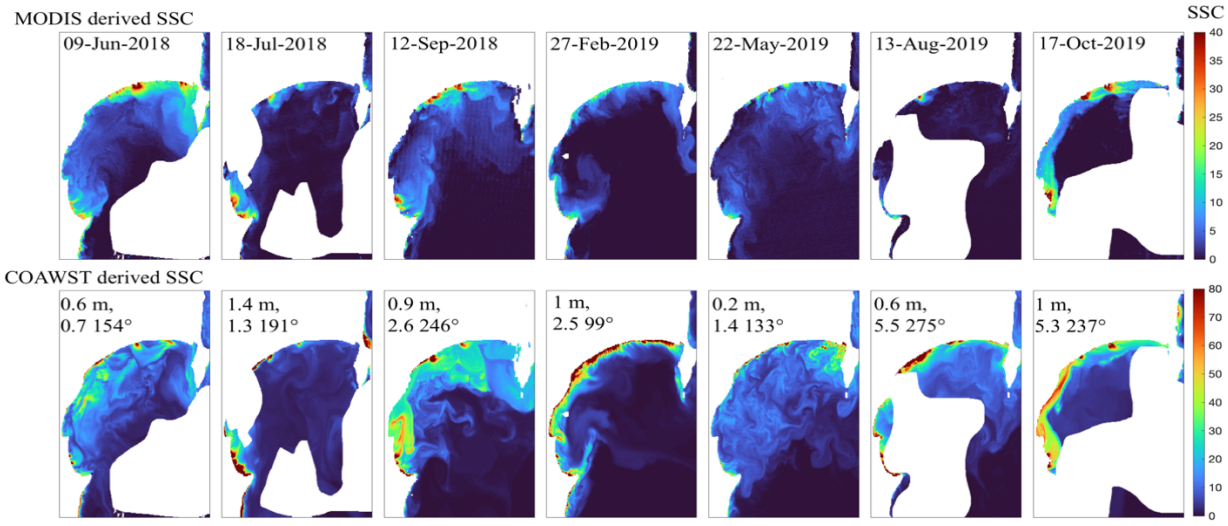

Figure 3.9 Select days of MODIS SSC (top row) and model SSC (bottom row) for a range of conditions (mg l^{-1}). The MODIS SSC colour range goes from 0 to 40, while the model SSC colour range goes from 0 to 80 mg l^{-1}. On the modelled SSC plots, the wave height (m), wind speed (m s^{-1}) and direction averaged in the 6-hour period before image collection are labelled. The gaps in the data correspond to clouds and regions of poor data.

3.4.2. Density and circulation patterns in Hawke Bay

Seasonal averages of key water mass and circulation features are shown over the duration of the 3-year run averaged over 3-month periods (Fig. 3.10, 3.11). Large seasonal changes are associated with varying solar radiation as well as river discharge, the latter results in wintertime low salinity waters (less than 32 psu) over much of the inner shelf in depths less than 30 m and enhanced vertical salinity stratification (greater than 3 psu). These patterns are greatest offshore of the rivers, with average surface salinity less than 30 psu and salinity stratification reaching 8 psu. The inner shelf less in than ~30 m displays pronounced seasonal variations in temperature, with higher warming than offshore in summer and higher cooling than offshore waters in winter. The wintertime cooling nearshore leads to cooler water overlying warmer water. Although the density structure resulting from river plumes, particularly from salinity variability, is a persistent feature of the Bay all year, it is strongest in winter.

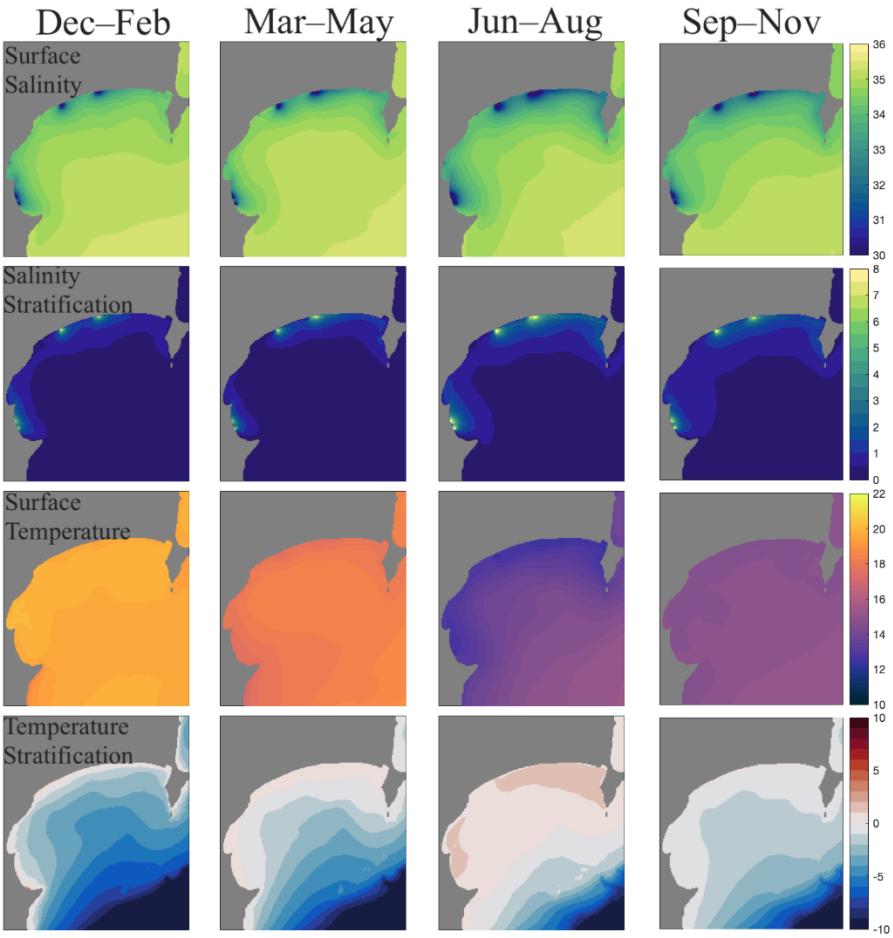

Figure 3.10 Seasonal averages of surface salinity (top row), the surface to bed salinity vertical stratification (second from top row), surface temperature (third row), and the surface to bed vertical temperature stratification (fourth row). Averages are computed over the three-year run time using ROMS average files that were output at monthly intervals.

The average wind direction is most commonly from the SW year-round, which appears to influence surface velocity patterns (Fig. 3.11). The strongest and most persistent surface velocity features are located in regions influenced by river plumes, with outward flow from the river inlets, with average velocity values greater than 0.2 m s^{-1} (Fig. 3.11). The river plumes from the Mohaka and Wairoa Rivers typically flow offshore and to the left, while the Tukituki River typically flows offshore and the Tūtaekurī/Ngaruroro River flows offshore and to the right. Other persistent patterns include flow out of the Northern Bay around the Mahia Peninsula, which during the winter months flows continuously in a coastal current from the Wairoa River along the coast out of the Bay. At the southern end of the Bay, flow also goes out of the Bay, either around Cape Kidnappers or directly offshore of the Bay, with stronger flow in the winter originating from the southern rivers. The middle of the Bay shows much slower surface average velocities (on the order of a few cm s^{-1}), with spatial variability showing eddying motions and recirculation regions with flow into the Bay.

Near bed average velocities are much weaker, with stronger landward flow (~0.025 m s^{-1}) in the winter in depths less than 30 m likely associated with buoyancy driven return currents. Average bed stress values are much larger in winter than summer, associated with seasonal variability in wave height, and are highest in shallower areas and areas with larger bed roughness such as rocky reef areas.

Offshore of the Bay, the Wairarapa Coastal Current (WCC) is a persistent current that flows Northward along the shelf break of the Bay throughout all seasons (Fig. 3.11). The WCC diverges towards the east roughly around Cape Kidnappers. The bottom currents in the region are the strongest offshore of the Bay in the WCC (>0.2 m s^{-1}) which is present year-round. The ECC flows generally southward offshore of the Mahia Peninsula but does not directly flow into Hawke Bay (not shown).

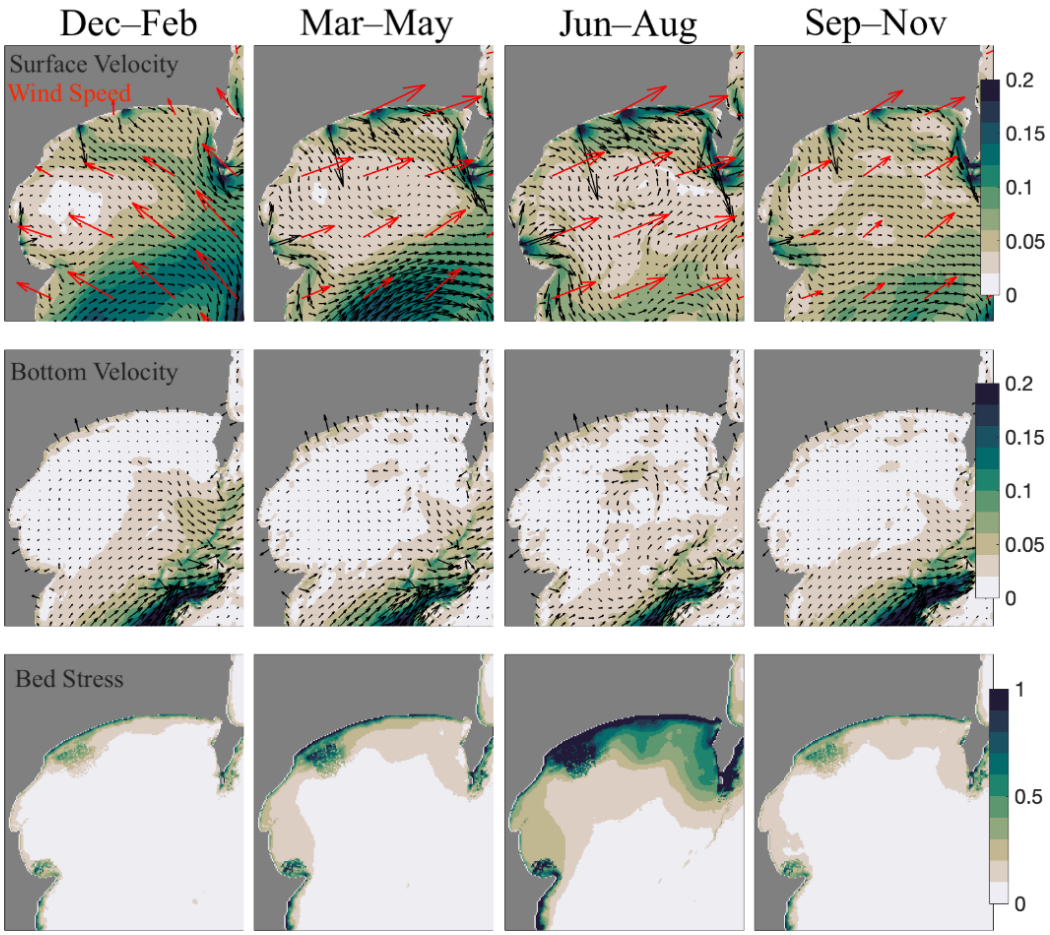

Figure 3.11 Seasonal averages of circulation in Hawke Bay. The plots show the seasonal averages of surface velocity and wind speed (m s^{-1}; top panels), bottom velocity (m s^{-1}; middle panels), and bed stress (N m^{-2}; bottom panels). Averages are computed over the three-year run using ROMS average files that were output at monthly intervals.

To highlight the temporal variability throughout the Bay associated with river plumes, tide, wind, and other inner shelf processes, timeseries of circulation features are shown at 6 locations for the year of 2019 (Fig. 3.12a) at 2 and 10 km from the shoreline, located offshore of the Tūtaekurī/Ngaruroro River (points 1-2), Wairoa River (points 3-4), and a location with no direct river influence (points 5-6). At 2 km offshore of the Wairoa River, the highest stratification occurs within 2 m of the surface, but during discharge events lower density water extends to the bed. At the locations offshore of the rivers, impacts of discharge are noticeable in the surface density and stratification (Fig. 3.12e-f), with similar magnitudes of surface density and stratification occurring offshore of the northern and southern rivers during discharge events. At the locations not directly offshore of a river, impacts from other rivers are seen in the density structure with reduced magnitude and a time lag. In all locations, the seasonal variability of inner shelf water masses is evident, with denser water more common in winter than summer (e.g. Fig. 3.12d).

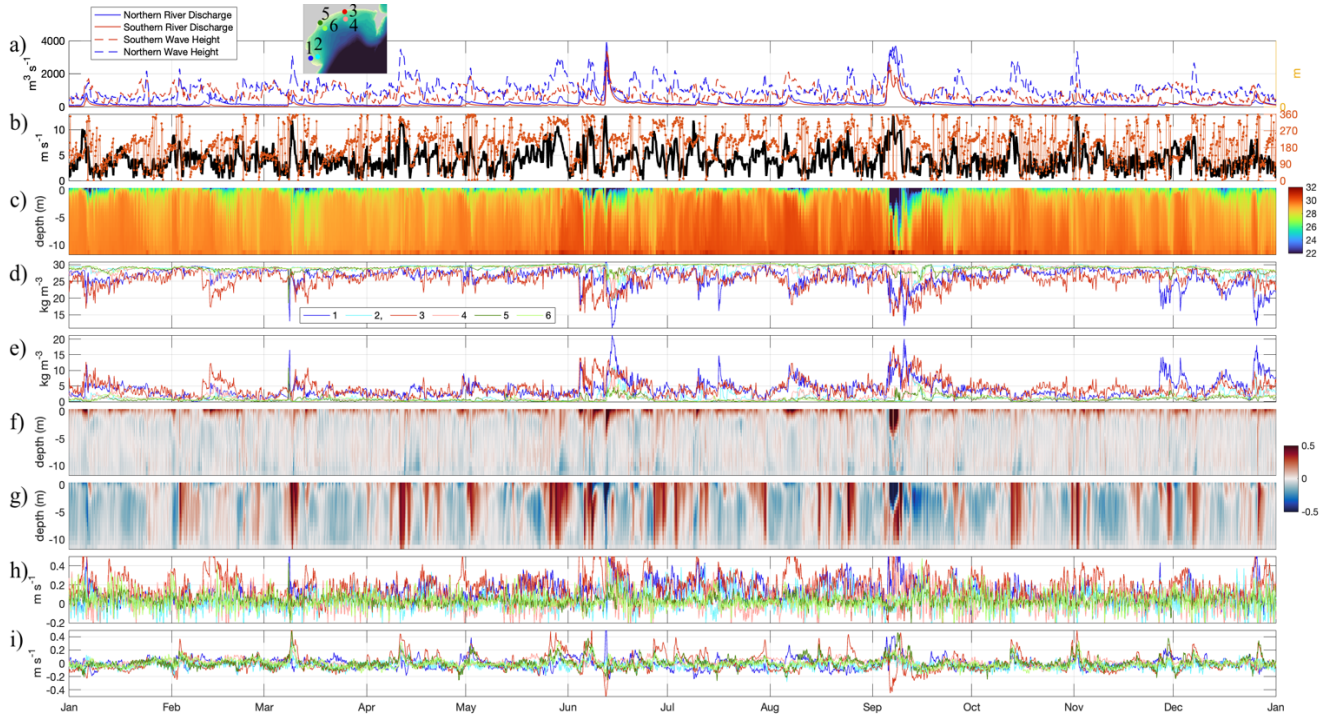

Figure 3.12 Inner shelf circulation timeseries for the year of 2018. The locations are shown in a), which are located 2 and 10 km offshore of the coastline for each region. b) Total river discharge from the southern rivers (red), northern rivers (blue), and northern wave height (dashed blue), and southern wave height (dashed red). c) wind speed and direction near the HAWQi mooring. d) Density of water (values added to 1000, in kg m^3) at point 3, 2 km offshore of the Wairoa River. e) Surface density (kg m^3). f) Density stratification (kg m^3). g) Cross-shore velocity at point 3 (m s^{-1}). h) Cross-shore velocity at point 3 (positive offshore; m s^{-1}). i) Surface cross-shore velocity (m s^{-1}). j) Depth averaged alongshore velocity (positive northward; m s^{-1}).

The cross-shore flow structure 2 km offshore of the Wairoa River (Fig. 3.12g) is predominately baroclinic and shows upper layer seaward flow associated with buoyancy and spreading of the river

plume, and landward flow at depth. At other locations, the surface cross-shore velocity typically flows offshore (Fig. 3.12i), with variation associated with discharge events as well as wind and other forcings. This is in contrast with the alongshore flow structure, which is predominately barotropic and varies with periodic wind events (Fig. 3.12h), except for discharge events which can show alongshore baroclinic structure. The depth averaged alongshore velocity (Fig. 3.12j) generally shows similar responses between locations, with locations 2 km from the coastline showing higher velocities than 10 km offshore. The alongshore directionality shows differences from the northern and southern locations for easterly wind directions due to the orientation of the Bay.

3.4.3. River plume variability

The modelling results show that the density structure and circulation patterns in Hawke Bay are largely influenced by the presence of buoyancy from rivers (Fig. 3.10, 3.11), and modulated by wind and other forcing conditions (Fig. 3.12). The river plumes have been shown to predominately flow northward, likely corresponding to the predominate SW wind direction but are periodically affected by reversals in wind direction. However, the way in which the rivers influence the plume, and consequently the distribution of sediment, depends on the detailed characteristics of the river and event characteristics (Fig. 3.13).

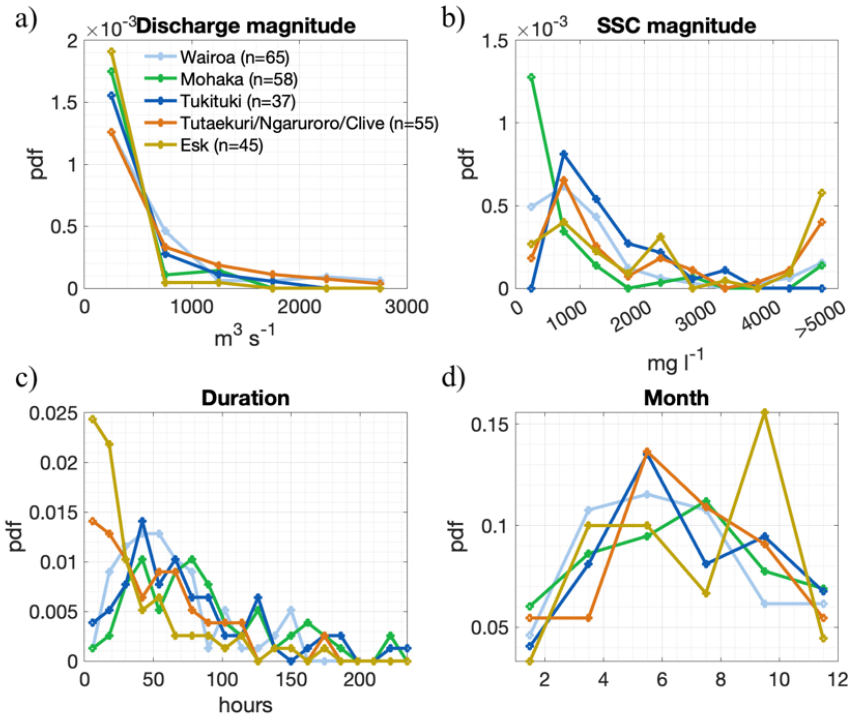

Figure 3.13 Description of river discharge events in the period of 2017-2019 for the largest rivers that enter Hawke Bay. a) The magnitude of each event, b) the magnitude of SSC during the peak discharge, c) the duration in hours, and d) the month of the year that the discharge event occurred in.

In general, larger river discharges were associated with short duration intense events, with the Wairoa and Mohaka rivers experiencing the largest events in terms of discharge while the smaller rivers (Esk and Tūtaekurī/Ngaruroro Rivers) events were associated with the highest SSC values. To demonstrate this, the main rivers discharge events are identified and compared with environmental conditions. Over the three-year period, for the five largest rivers that discharge into the Bay, generally around 50 events were found each, with a higher probability of smaller magnitude discharge events (Fig. 3.13). Most durations were between 0.5–3 days with a number of extended events greater than 100 hours. The SSC during events, in the range of 500 to > 4000 mg l^{-1}, and event durations followed similar patterns between rivers, with a greater number of shorter events with lower SSC (Fig. 3.13c).

The typical spatial patterns of river plumes were assessed through salinity contours compiled through time (Fig. 3.14). These patterns show that the Mohaka and Wairoa Rivers have radial patterns that extend to the left towards the Mahia Peninsula. The Tukituki and Tūtaekurī/Ngaruroro Rivers show expanses that stretch from Cape Kidnappers to north of Napier.

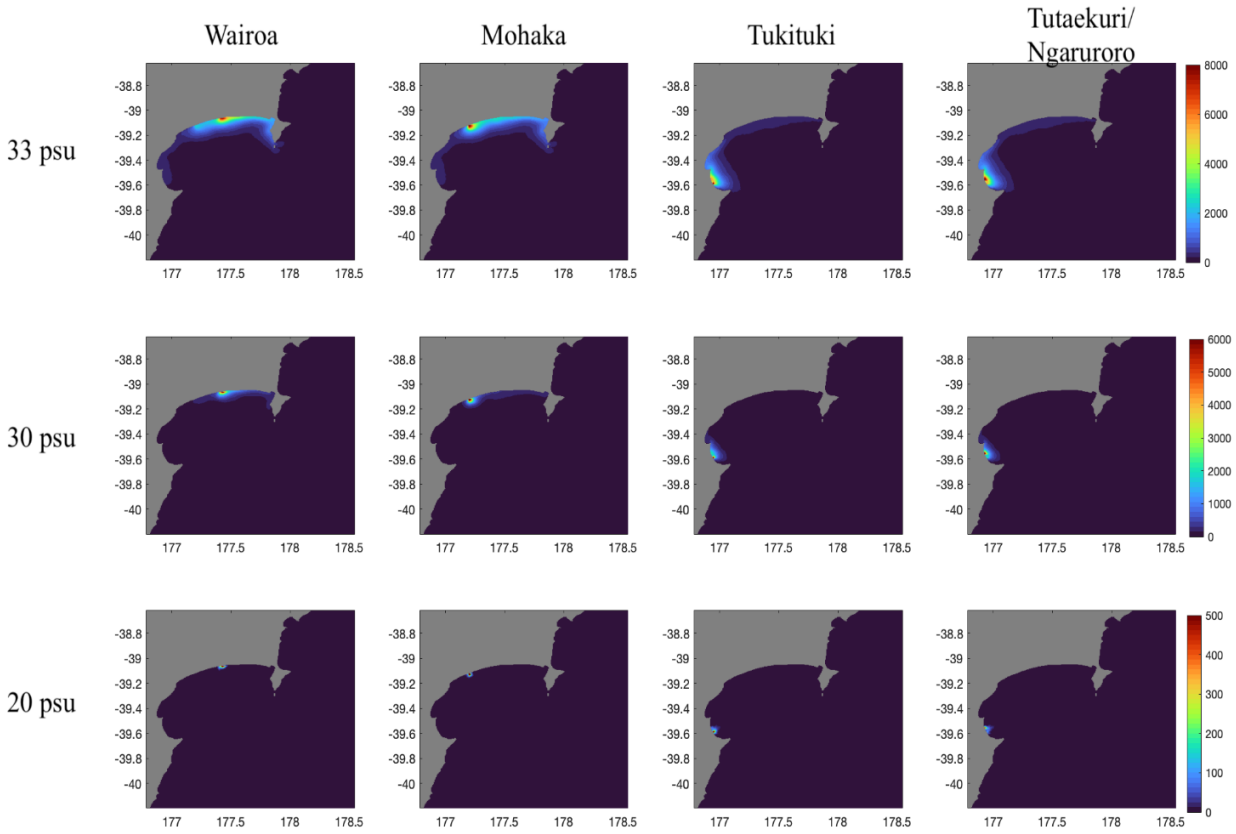

Figure 3.14 River plume salinity contour boundary heat maps for each river. Each column represents a river for 33, 30, and 20 psu contours (rows). The colour scale represents the number of occurrences from 2017-2019 (from the 3-hour model output).

For each discharge event for each river, the river plume characteristics show variability primarily associated with the magnitude of discharge and wind. The river plume characteristics were

computed for each discharge event by averaging the values from the beginning to end of the event, using spatial coordinates from the 30 psu salinity contour (e.g. Fig. 3.14). This value was chosen as it was often present and includes varying regions of the river plume without extending to far-field plume regions such as the 33 psu contours (Fig. 3.14). The plume velocity was averaged between the depth of the pycnocline and the surface. The plume directions were most directed offshore and to the left (traveling northward) for all rivers. The Wairoa River has the highest tendency of leftward directions, which is expected due to the change in coastline orientation with respect to the predominate wind direction. Plume directions show linear relations with wind along and cross-shelf velocity (Fig. 3.15b-c), except for onshore wind, which shows no relation, likely due to the broad area that encompasses the analysis region. Density stratification displays a nonlinear relation with maximal stratification values reached for each river above a threshold discharge (ranging from 300-500 m^3s^{-1}).

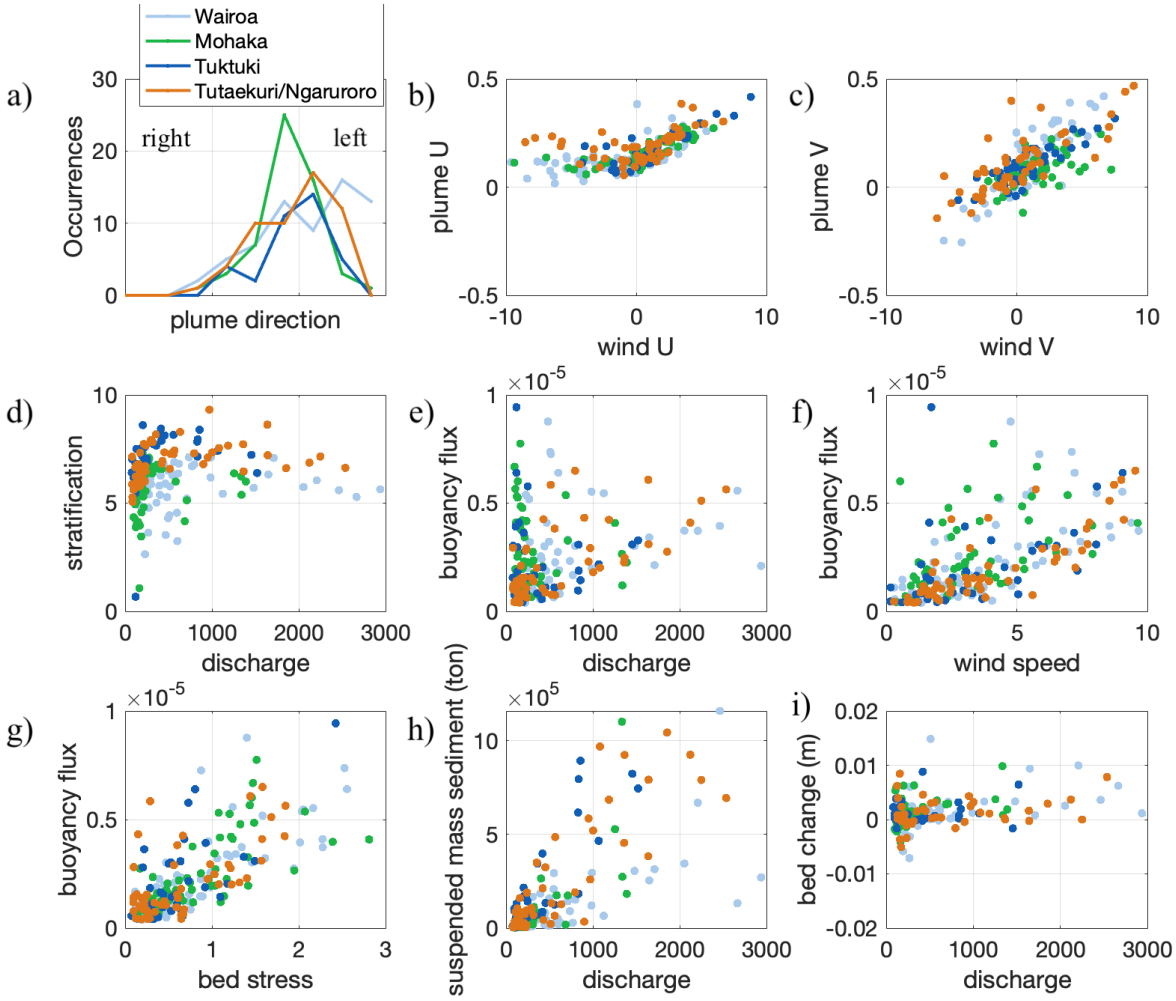

Figure 3.15 River discharge event plume statistical descriptions. Plume values were calculated using spatial averages over the 30 psu salinity contour. a) plume direction (in relation to the shoreline) during discharge event, b) wind and plume cross-shore velocity averaged during discharge event, c) wind and plume alongshore velocity averaged during event, d) surface to bottom density stratification and river discharge averaged over

discharge event, e) the buoyancy flux ($m^2\ s^{-3}$) at the pycnocline and river discharge averaged over discharge event, f) the buoyancy flux ($m^2\ s^{-3}$) at the pycnocline and wind speed averaged over discharge event, g) the bed stress (N m^2) and buoyancy flux ($m^2\ s^{-3}$) averaged over discharge events h) the suspended sediment mass (tons) and river discharge averaged over discharge event, and i) the spatial average of bed vertical change (m) and river discharge over discharge event. The spatial bounds of the bed change were determined by the surface locations of the 30 psu contour during the times of the discharge event.

The mixing intensity, shown here by the buoyancy flux at the pycnocline, varies with river discharge (Fig. 3.15f), wind speed (Fig. 3.15g), and bed stress (Fig. 3.15g). Generally, higher discharge initiates higher plume momentum which causes increased shear driven mixing, while wind predominately acts on the mid-field and far-field plume (Horner-Devine et al. 2015). Higher bed stress is typically not associated with increased mixing at the plume base and the correlation could be due to other processes associated with storms. However, tidal mixing originating at the bed has been shown to impact plume interface mixing (Spicer et al. 2021). Further investigation that separates the plumes into different regions would likely show the spatial differences in mixing patterns related to inertial and wind forcing. For discharge events greater than ~200 m^3s^{-1} a positive (accumulated) bed sediment change occurred within the bounds of the 30 psu plume, with average values over the plume area increasing with discharge in the range of roughly 1-10 cm. For discharge events less than ~200 m^3s^{-1}, both erosion and deposition occurred, likely signifying greater wave driven bed changes rather than from fluvial input.

The four rivers showed overall similar responses to conditions with generally similar ranges of velocity, stratification, and buoyancy flux values. Differences between the rivers include slightly higher observed stratification offshore of the Tukituki and Tūtaekurī/Ngaruroro Rivers (~1–2 kg m^{-3} higher) . While the relationship between wind and plume directionalities are linear for all rivers (Fig. 3.15b,c), the coastline orientation varies across the Bay, resulting in differing cross-shore plume directionalities, with the northern river plumes most commonly directed northward and the southern rivers most commonly directed offshore.

3.4.4. Sediment flux

Fluvial sediment is transported seaward by river plumes and can be resuspended by waves and advected to other parts of the Bay. The fluvial sediment flux consists of four size classes (Table 3.1) where the settling velocity is a key factor in determining the horizontal distance of transport from the rivers. Averaged SSC values over the month of July 2019 for each size sediment class show the general patterns of the size class distribution in the Bay (Fig. 3.16). The clay size class with settling velocity of 0.014 mm s^{-1} is broadly dispersed, with low SSC values (~5 mg l^{-1}) extending throughout the entire Bay. The silt size, floc, and coarse silt size classes are concentrated in nearshore waters with the highest values found in waters less than 20 m deep, indicating short transport distances from rivers

(generally less than 2 km). The total surface sediment concentration (Fig. 3.16c) is roughly a magnitude smaller than the bed sediment concentration (Fig. 3.16f) averaged over the period. The bed sediment concentration shows elevated values dispersed offshore of the coastline in comparison to the surface concentration, which is concentrated nearshore, and shows regions of concentrated elevated values in the southern Bay and offshore of the Wairoa and Nuhaka Rivers.

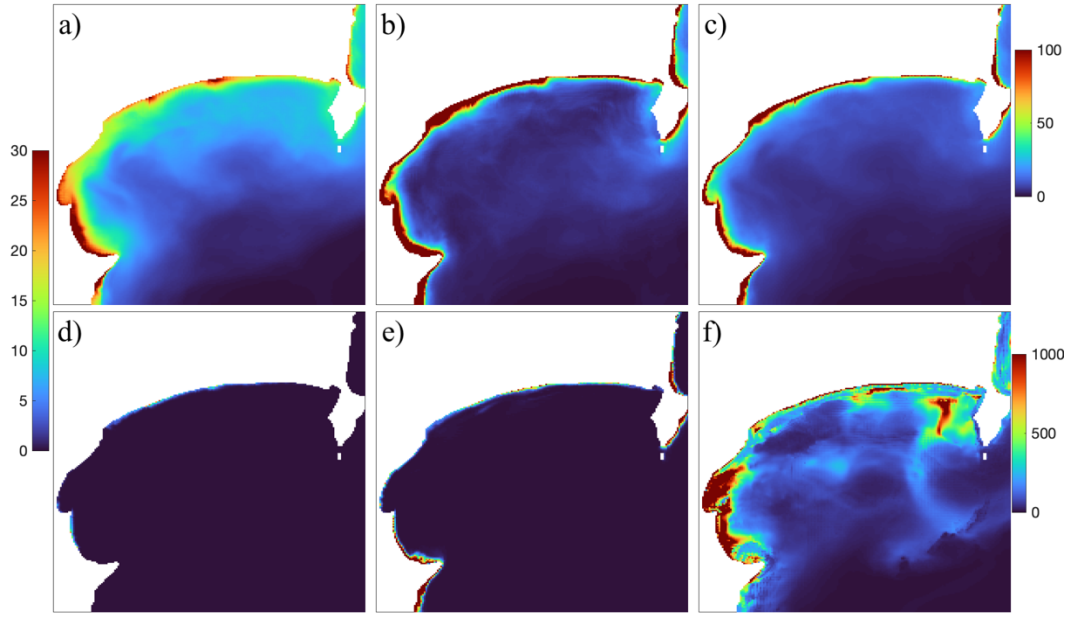

Figure 3.16 Modelled SSC concentrations for differing sediment sizes and locations in the water column. Average SSC concentrations (mg l^{-1}) for the mud sediment size classes (a,b,d,e), and the c) total surface sediment concentration and f) bed sediment concentration, averaged over the month of July 2019. The mud size classes include a) clay, b) silt, d) flocculated, and e) coarse silt. Note that the bed and surface sediment concentration plots have different colour scales.

To further describe sediment transport throughout the Bay, the sediment fluxes are decomposed into change of mass of suspended and bed sediment (Fig. 3.17b), and the mass of the suspended sediment in the Bay is divided into different depth intervals (Fig 3.17c). The estimated sediment fluxes from each of the main rivers ranged between 1–3 million tons of sediment input to the ocean over the three-year period, with the Wairoa River having the largest flux and the other main rivers having similar flux magnitudes between 1–1.5 million tons. Smaller rivers such as the Esk River contribute a relatively small amount to the total flux into the Bay.

The initial model bed displayed continuous erosion for ~5 months, which we classify as an adjustment time for the initial interpolated sediment bed into a state more equilibrated with typical bed stresses. Over the three-year period, about 8 million tons of sediment were input to the Bay from rivers, which is well below the annual average of 11 million tons per year (Hicks et al. 2011). During

normal wave conditions (1-2 m swell), 1–2 million tons of sediment can be in suspension in the Bay (Fig. 3.17b), and during wave and/or river events, >10 million tons can be in suspension in the Bay. The bed mass change is anti-correlated with suspended sediment mass, indicating that most of sediment suspended is sourced from the bed, which is then redistributed throughout the Bay. The flux of sediment mass out of the Bay occurs during periods of bed mass erosion, which is predominately transported northward around the Mahia Peninsula (not shown).

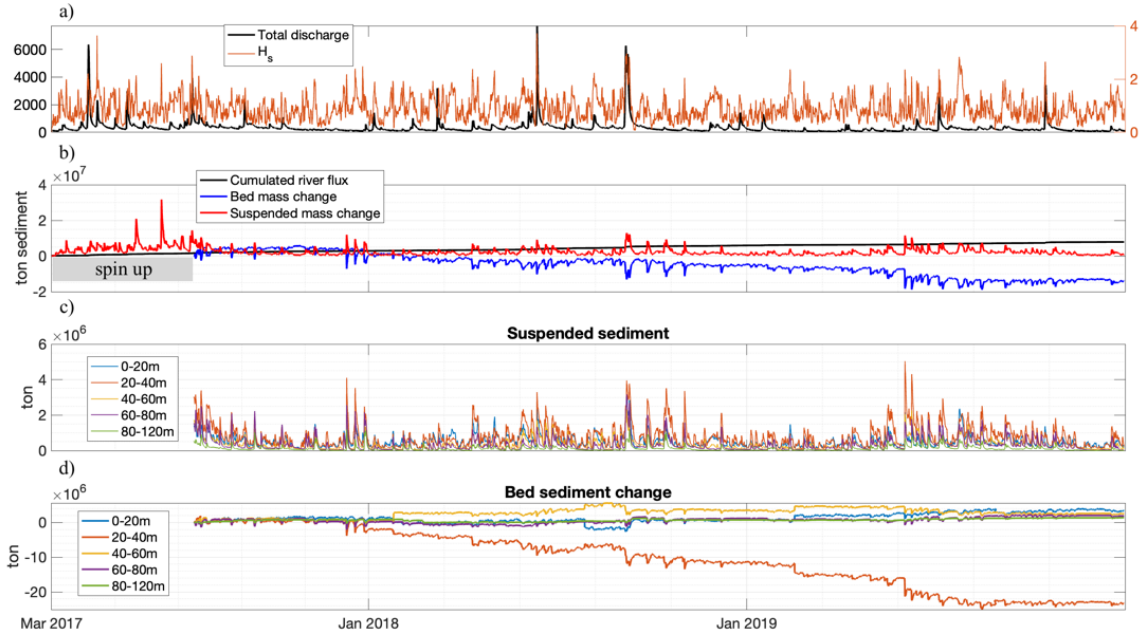

Figure 3.17 Timeseries of sediment fluxes in Bay. a) The significant wave height (orange; m) and total river discharge (black; m^3 s^{-1}). b) Tons of sediment separated into the cumulative river flux (black), bed mass change (blue), and suspended sediment mass change (red). d) The integrated bed sediment mass change (tons) at 20 m depth intervals in the Bay.

The largest changes to the bed mass throughout the study period occur in the 20-40 m depth range, with accumulation occurring offshore of 40 m depth, with little change occurring deeper than 80 m (Fig. 3.17d). Most of the suspended mass is found in depths less than 40 m (Fig. 3.17c), and the suspended mass throughout the depths of the Bay vary similarly in time. The relatively high and consistent suspended mass is associated with suspended sediment concentrations on the order of 500-5000 mg l^{-1} when bed stress is elevated, with maximum values around 20,000 mg l^{-1}.

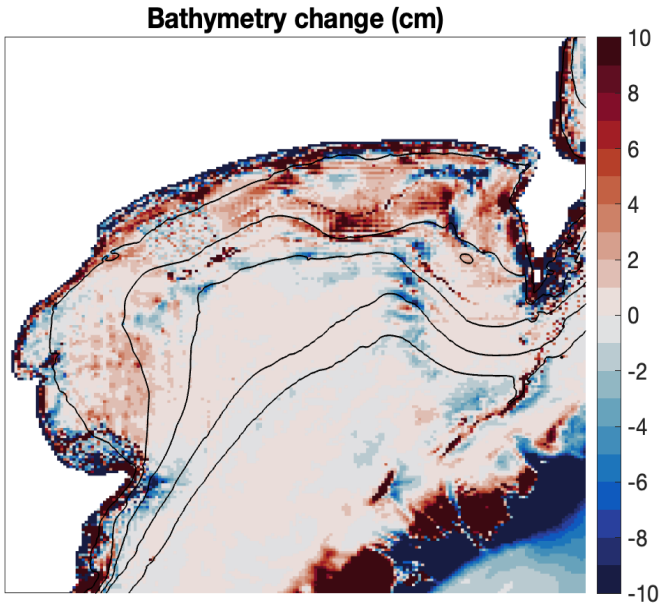

Figure 3.18 Long term bathymetry change (cm) at the end of the model run. The bathymetric contours (black lines) are shown for the 20, 40, 60, 80 and 100 m depths.

Over the three-year period, two general bed change patterns occurred, including 1) an adjustment of bed elevation adjacent to the coastline, and 2) accumulation offshore of 20 m. Erosion occurred adjacent to the coastline with deposition directly offshore on the order of 5-10 cm, and larger changes occurred in the regions of rocky reefs which experience higher bed stress (Fig. 3.18). Accumulation areas are typically between 20-60 m, with the largest region occurring offshore of the Wairoa and Nuhaka Rivers. Changes in bed muddy grain sizes show that all the clay sized material eroded from the shelf (Fig. 3.19i), fine silt eroded from the nearshore except offshore of the Esk River (Fig. 3.19j), which was accumulated in the middle of the Bay. The aggregated material, which did not have initial distribution and was only input from the rivers, shows depositional zones with ~6 km from rivers, generally directly offshore of the Mohaka and Wairoa Rivers, and transported northwards from the southern rivers towards the Esk River (Fig. 3.19k). Coarse silt was removed from the nearshore (Fig. 3.19l) and transported to the middle of the Bay. The model shows that the bed stress in the Bay can consistently suspend bed material, from which the transport is then dependent on the near bed circulation, which was not thoroughly investigated here.

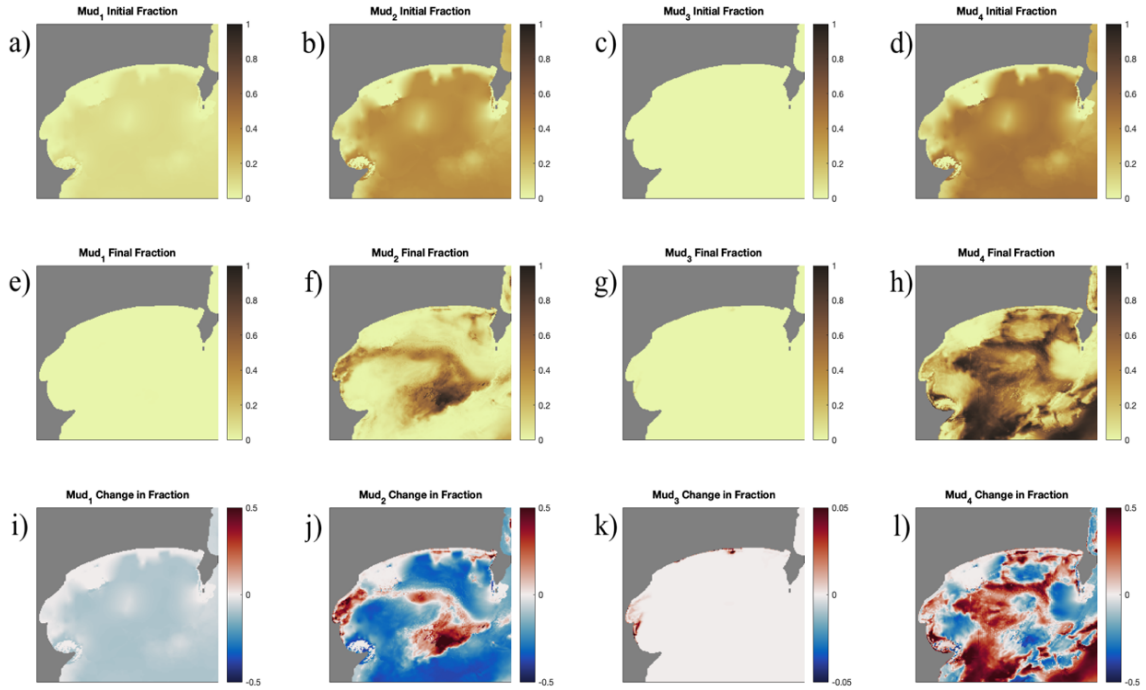

Figure 3.19 Grain size changes for the mud size classes. The plots show the initial fraction (top row), final fraction (middle row), and changes in fraction (bottom row). The grain sizes are found in Table 3.1.

3.4.2. Influence of waves on hydrodynamics

The inclusion of the coupled wave model introduces wave driven currents, impacts to the currents from waves, and altered mixing and bed stress patterns which impact cross-shelf sediment transport (Wright et al. 1980, Geyer et al. 2004) and potentially river plume circulation (e.g. Gerbi et al. 2013). From the three-year simulations, seasonally averaged differences between the ROMS and coupled ROMS/SWAN runs show that the inclusion of wave processes causes higher surface salinity, lower stratification, increased landward near-bed velocity, and complex differences in surface velocity patterns, with plume areas showing reduced speeds and other nearshore areas showing increased speeds (Fig. 3.20). Seasonal differences in velocity patterns are apparent between the two runs. Previous studies comparing ROMS and ROMS/SWAN models have similarly found that coupled simulations show increased surface turbulence injection from wave breaking that leads to reduced plume stratification (Gerbi et al. 2013; Rong et al. 2014; Moghimi et al. 2019). Wave-current interaction at river outflows is expected to alter wave propagation in plume areas (Olabarrieta et al. 2011), and other wave-driven circulation patterns (e.g. Stokes drift) are expected to alter the inner shelf circulation (Moulton et al. 2023).

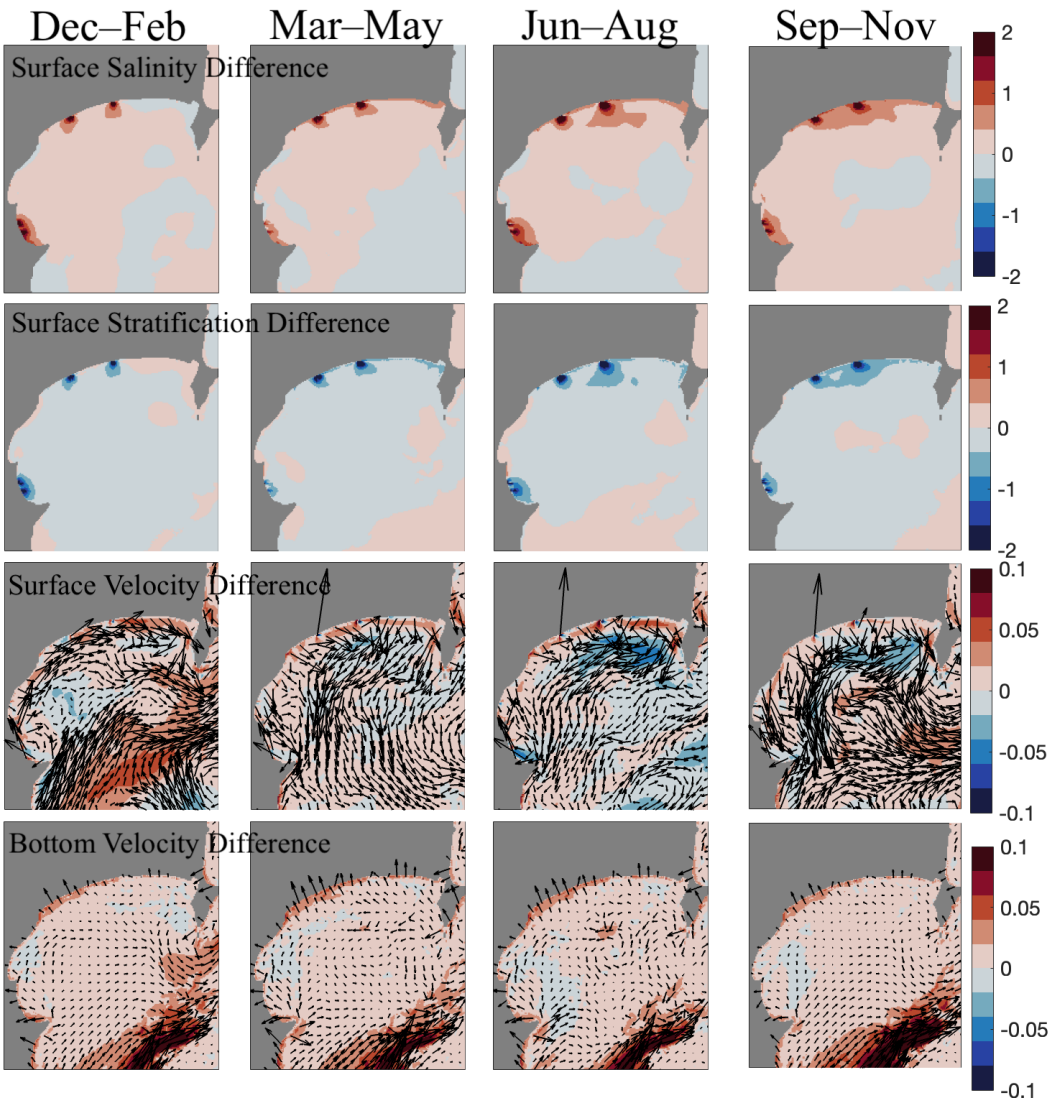

Figure 3.20 Comparison between ROMS and Coupled ROMS/SWAN runs using average seasonal values. Each row shows the surface salinity difference (Coupled – ROMS), salinity stratification difference (calculated as the difference from top to bottom), surface velocity difference, and bottom velocity difference.

The time-varying response to the inclusion of waves is assessed through a timeseries offshore of the Wairoa River which compares the vertical structure of density, velocity, and mixing in relation to varying wave conditions for the ROMS and ROMS/SWAN runs over the winter of 2018 (Fig. 3.21). The inclusion of waves generally reduces the plume thickness and magnitude of stratification (Fig. 3.21b-c). Surface cross-shore velocities show similar variability with typical differences of 0.1 m s^{-1}, with the largest differences occurring during discharge events (Fig. 3.21d). The long-shore velocity differences have greater magnitudes with typical differences of 0.2 m s^{-1} and the coupled run shows higher magnitudes (Fig. 3.21e), particularly during wave events in October and November of 2018. Higher turbulence production is seen in the coupled runs with increased surface and bed values (Fig. 3.21f-g), with typically increased buoyancy fluxes during these same periods (Fig. 3.21h-i). The

most pronounced differences between the two model runs occur during periods of increased buoyancy from rivers due to the proximity of the Wairoa River as well as during wave events. The findings suggest the including waves may additionally impact the flux of suspended sediment from rivers, as impacts to the cross-shore and long-shore currents will impact the initial sediment deposition. Other potential wave driven processes such as Stokes drift are not investigated.

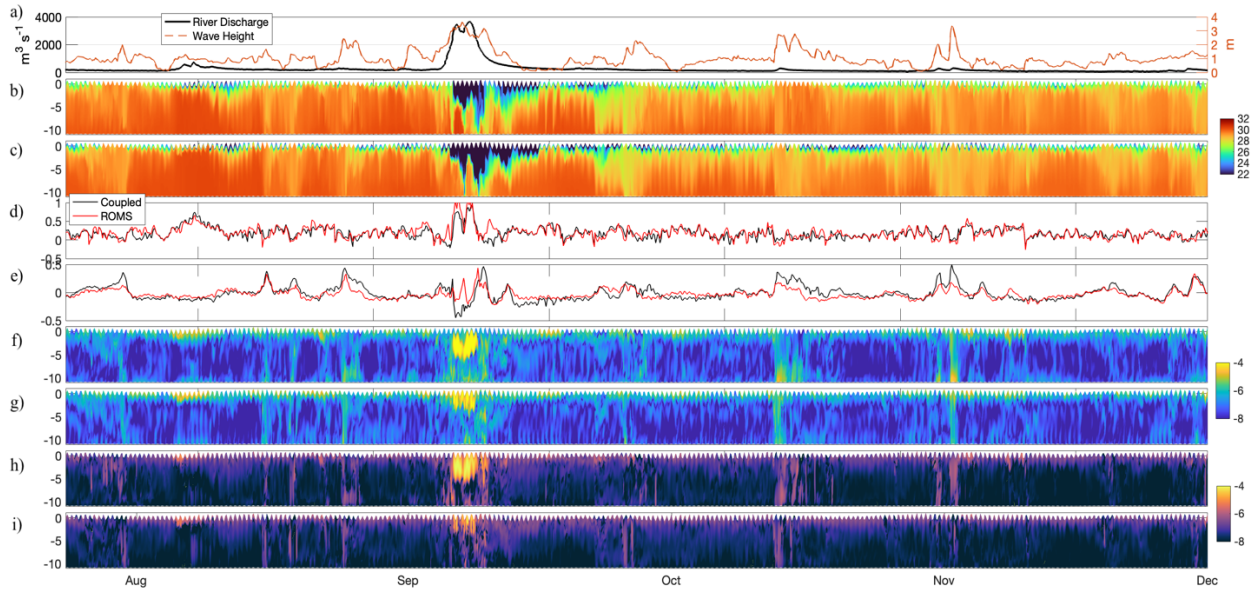

Figure 3.21 Timeseries offshore of the Wairoa River that compares the coupled ROMS/SWAN model with the ROMS only run over a select period in 2018. a) River discharge of the northern rivers (left axis; m^3 s^{-1}) and wave height offshore of the Wairoa River (right axis; m). b) Density (plus 1000; kg m^{-3}) offshore of the Wairoa River for the coupled run. c) Density (plus 1000; kg m^{-3}) offshore of the Wairoa River for the ROMS only run. d) Surface cross-shore velocity (m s^{-1}). e) Depth averaged long-shore velocity (m s^{-1}). f) Log of turbulence production for coupled and g) ROMS only. h) Log of buoyancy flux for coupled and i) ROMS only.

3.5 Discussion

3.5.1 Sediment transport from small mountainous rivers

The suspended sediment transport from river plumes was found to be largely dependent on the grain size which sets transport distances, with the majority of riverine sediment being transported distances on the order of kilometers. The erosion of bed mass is caused during elevated wave conditions (greater than ~1.5 m) which allows bottom currents to redistribute sediment. The spatial patterns in the changes in bed sediment generally reflect modifications to pre-existing bed sediment and do not necessarily reflect the transport of recently derived fluvial sediment, as the modelled magnitudes of instantaneous transport in the Bay greatly surpass the riverine flux. These findings are in qualitative agreement with previous works on small mountainous rivers in energetic settings (Geyer et al. 2004; Walsh and Nittrouer 2009; Harris et al. 2008) although specific transport metrics are not investigated here.

3.5.2. Limitations and future work

Further investigations focused specifically on the riverine sediment and near-bed currents would be able to distinguish between riverine sediment transport patterns and bed adjustment to oceanographic conditions in the Bay. The modelling of sediment transport considered here was limited by unknown sediment properties within the Bay as well as model formulations that excluded processes such as flocculation and bed consolidation. Future modelling work in Hawke Bay would be better constrained by additional measurements of the grain size distribution in rivers and identifying the prevalence of flocculated particles, and additionally resolving estuarine processes that would impact river plume dynamics.

3.6. Conclusion

A numerical model of Hawke Bay, Aotearoa New Zealand, performed well when assessed against a range of measurements, and was used to elucidate the general circulation patterns and the transport of suspended sediment from rivers. The model shows that the density structure and inner shelf circulation is heavily influenced by the input of surface buoyancy from multiple rivers, with elevated stratification present in vicinity of the major rivers throughout the year. The average circulation in the Bay reflects localized river plume circulations, superimposed on wind driven patterns and the characteristic pattern of outflow at the northern and southern ends of the Bay. Offshore of the Bay, the Wairarapa Coastal Current is present at the shelf break throughout the year and the East Cape Current can intrude into the Bay during summer months.

The river plumes are mainly influenced by wind once away from the river inlets, which can steer the river plumes and mix the surface fresh layer. The northern rivers on average flow offshore and toward the south, while the southern rivers flow offshore on average, corresponding to the influence of the average wind direction. The four main rivers in the Bay display similar magnitudes of stratification and velocity patterns, with the main difference being the orientation of the coastline in relation to the predominate southwest wind direction which alters plume processes.

The inclusion of surface waves predominantly impacts the resuspension of sediment from the bed as well as turbulent mixing of the water column. The spatial patterns of sediment concentration variability in the Bay validated well against satellite derived estimates, while the magnitude showed large biases likely associated with errors in the satellite derived estimates. Similar to previous studies of small mountainous river systems, the cross-shelf river plume transport of sediment is highly dependent on the settling velocity, with grain sizes larger than coarse silt not able to initially transit farther than a few kilometers. Waves consistently resuspend material, and the long-term sedimentation patterns are largely due to bed sediment redistribution after the sediment has initially settled from river plumes. Waves additionally modify the vertical structure of turbulence, increasing surface mixing and altering river plume circulation.

Chapter 4: The variability of cross-shelf flows offshore of a small mountainous river

Contribution of Authors

Chapter 4 presents the article "The variability of cross-shelf flows offshore of a small mountainous river" which will be submitted to the journal *JGR: Oceans* for review. Ted Conroy conceptualized the study, performed all field work and data analysis, and wrote the article. Karin R. Bryan provided feedback, supervision, and editing of the article throughout the process. Joe O'Callaghan provided assistance with the conceptualization, interpretation, and editing of the article.

4.1 Introduction

The cross-shelf flux of material across the inner shelf is a key parameter for understanding the fate of terrestrial material in the coastal ocean. A detailed understanding of the processes responsible for sediment delivery is particularly relevant for small mountainous rivers, which can yield large discharge magnitudes in episodic events to energetic coastal areas (Wright et al. 1980). Small mountainous river systems deliver disproportionate amounts of sediment to the coastal margin (relative to their catchment size) and are found worldwide on active margins (Milliman and Syvitski 1992). Timescales and magnitudes of the cross-shelf flux are relevant for long-term sediment fluxes, ecological impacts, and the management of coastal areas.

The majority of river plume studies have focused on larger river systems that operate on slower time scales and have spatial scales on the order of 10's of kilometers rather than 100's of meters to kilometers (Horner-Devine et al. 2015), while smaller scale river plumes have received less attention. River plumes from small mountainous river systems generally have narrow inlets with small estuaries, large magnitudes of discharge, and commonly outflow to energetic inner shelf environments (e.g. Geyer et al. 2000, Lemagie and Lerczak 2022). Smaller rivers have been found to be less influenced by rotation (Horner-Devine et al. 2015), although the distinction between river size and the importance of rotation is unclear at present. Smaller river plumes than considered here have been found to be influenced by tidal currents (Basdurak et al. 2020) and wave breaking (Rodriguez et al. 2018).

Using in-situ observations, the coupled inner shelf and river plume response was investigated offshore of a small mountainous river to common shelf forcings, with particular emphasis on the response of the cross-shelf velocity, density, and shear structure. The aim was to quantify the differences that occurred during storm events and varying wind conditions, and from these measurements, infer the ultimate impact on the cross-shelf sediment flux from small mountainous rivers. Observations were collected offshore of the Tukituki River in Hawke Bay, New Zealand, which drains a steep, highly erodible catchment which is regularly subjected to intense rainfall events. We use a number of data sources to quantify plume transport, mixing, and the resultant impact on cross-shelf sediment transport.

4.2 Background

4.2.1 Inner shelf and river plume circulation

River plume dynamics are controlled by the interplay between processes within the river and the currents and stratification in the receiving environment of the shelf. In turn, the currents on the inner shelf are influenced by waves, wind, tide, and regional current patterns (Lentz and Fewings 2012, Kumar et al. 2016). The interplay of processes within the river plume depend on the river

velocity at the inlet mouth, the density contrast between the outflowing water and ambient ocean water, the barotropic pressure gradient, and ambient currents created by the wind or offshore currents (Horner-Devine et al. 2015, Hetland 2005). In the near-field region, transport is generally dictated by the outflow momentum at the river mouth, modulated by tidal forcing (e.g. Basdurak et al. 2020), which transitions into the subcritical mid-field region, where lateral spreading of the plume predominately occurs and wind forcing plays a larger role in directing and mixing the plume, and is the dominant mechanism of vertical mixing in the far-field plume (Horner-Devine et al. 2015). Mixing intensity is typically highest in the near-field region due to high shear values after the plume detaches from the bed.

4.2.2 Response of river plume and inner shelf to wind forcing

The most-studied wind-driven response of river plumes has been found to be upwelling or downwelling Ekman transport (Horner-Devine et al. 2015). Upwelling winds are directed alongshore, flowing with the coast on the left in the southern hemisphere, whereas the opposite conditions cause downwelling. Upwelling winds have been shown to vertically thin and transport river plumes offshore, while downwelling winds have been shown to trap fresh water near the coast and deepen the plume layer while enhancing coastal current formation (Horner-Devine et al. 2015; Fong and Geyer 2001). The plume response to cross-shore winds has received limited attention but a few studies have found that plumes can be advected in the direction the wind is blowing (Hunter et al. 2010, Kakoulaki et al. 2014).

Similarly, inner shelf flows respond to downwelling and upwelling wind forcing with geostrophic flow in the alongshelf direction, and in the cross-shelf direction Ekman transport occurs in the surface layer and a compensating return flow is present in the lower layer. Cross-shore winds can drive sea level set up and circulation in depths less than ~30 m but do not drive alongshore geostrophic flows (Lentz and Fewings 2012). Similarly, cross-shore winds can drive a return flow in the bottom layer. Stratification limits the cross-shelf transport by limiting the Ekman depth, which inhibits penetration of the surface current surface into the water column.

4.2.3 Hawke Bay and Tukituki River

Hawke Bay is a southeast facing embayment (~40 by ~80 km), on the east coast of the North Island of New Zealand, extending from the Mahia Peninsula in the north to Cape Kidnappers (Fig. 4.1). The Bay has a gentle slope that extends to the shelf break outside of the Bay. Steep coastal mountains combined with high average rainfall rates produce significant episodic river discharge events that transport on average 11 million tons of suspended sediment to the Bay each year (Hicks et al. 2011). The Bay is exposed to a strong wave climate from the south (Komar 2010) and has a spring tidal range of 1.9 m.

The Tukituki River is in the southern Hawkes Bay, flowing from a ~2500 km^2 catchment in the Ruahine Range for ~80 km to the Pacific Ocean. The discharge is highly episodic with increased flows in winter but the potential for large events year-round. The largest recorded discharge was 3040 $m^3 s^{-1}$ while typical events occur on the order of 10^2–10^3 $m^3 s^{-1}$ and the mean discharge is 43 $m^3 s^{-1}$. The annual sediment flux from the Tukituki River is estimated to be around 1 million tons (Hicks et al. 2011). Near the river inlet, the bed is composed of gravel pebbles with gravel beach on each side of the inlet, with fine sand present offshore (White 1994). The inlet morphology is highly variable in spatial position, impacted by flood events and alongshore transport from waves, and can vary from being fully closed to an inlet width of ~300 m. The inlet was surveyed 8 days prior to the instrument deployment where the depth at the inlet was 3.5 m (below mean sea level).

A study describing the sediment and circulation properties of the Tukituki River and surrounding coastal region described the estuary as highly stratified with muddy bed sediment (predominately fine silt), with the main muddy sediment deposits located offshore of the river deeper than ~10 m (White 1994). In the river, the maximum recorded Suspended Sediment Concentration was ~2500 mg l^{-1} (Norris, 2019) and offshore of the river at the bed was around 4000 mg l^{-1} (White 1994). However, the inner shelf processes that guide the river sediment offshore are unknown.

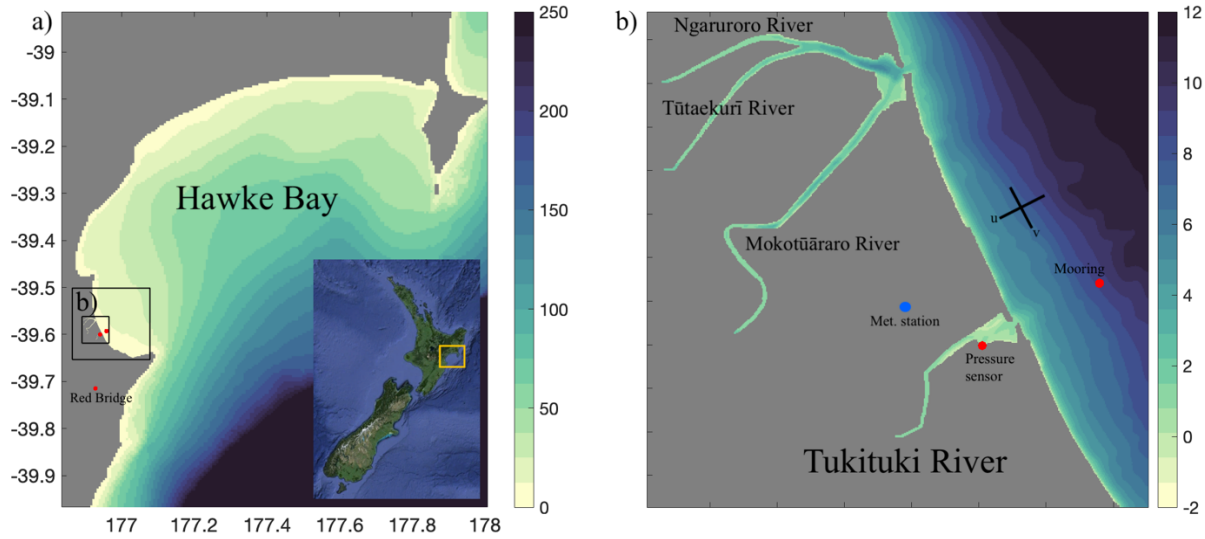

Figure 4.1 Areal overview of Hawkes Bay, Aotearoa New Zealand (shown in inset figure). The bathymetry of Hawke Bay (m) is shown on the left, and a zoomed in view of the Tukituki River area is shown on the right. To the north of the Tukituki River is the river complex of the Ngaruroro, Tūtaekurī, and Mokotūāraro Rivers. On the right image, the black cross represents the rotated coordinate system used in this study.

4.3 Methods

4.3.1 Instrument Deployment

A set of instruments was deployed in the winter of 2022 located 1 km offshore of the mouth of the Tukituki River in 8 m depth, including downward and upward facing bed mounted Acoustic Doppler Current Profilers (ADCPs), five Conductivity, Temperature and Depths Sensors (CTDs), and three Optical Backscatter Sensors (OBSs) (Fig. 4.1). The instruments were deployed for 41 days with varying sampling rates aimed at resolving river plume processes (Table 4.1).

Table 4.1 Description of instrumentation used and sampling information for the 2023 deployment offshore of the Tukituki River. Locations of instruments are shown in Fig. 4.1.

Instrument	**Depth**	**Sampling**	**Additional info**
ADCP (Nortek Signature 1000)	35 cmab looking up	Average 120 seconds every 5 minutes, 5 beam continuous burst 2 Hz. Echosounder continuous sampling	20 cm bins average, 40 cm bins burst, 1 cm bins echosounder
ADCP (Nortek Aquadopp 2 khz)	43 cmab looking down	Burst 8 Hz 2400 times every 1800 sec	25 mm bins
OBS at bed	19.5 cmab	Burst 8 Hz 2400 times every 1800 sec	High range setting
2 OBSs in water column	0.35, 1.7 m below surface	Burst 6 Hz 1024 times every 10 minutes	Auto ranging
2 RBR Concerto CTDs	0.35, 1.7 m below surface	Burst 6 Hz 1024 times every 10 minutes	High salinity bias accounted for with offset
3 Seabird Microcat 37 ODO CTDs	43 cmab, 5 mab, 50 cmbs	Sample every 10 minutes	

The Signature 1000 upward-facing ADCP was processed by removing data with correlation lower than 50% (Nortek Operations Manual for Signature 1000) as well as removing the surface layer. The density measurements show large density fluctuations between 0.35 and 1.7 m from the surface (Fig. 4.2) such that the river plume is typically surface focused with the pycnocline less than 1.7 m from the surface. The quality of ADCP data directly below the water surface was variable over the deployment, which was removed by removing data 25 cm below the surface. The Signature

measured up to 8.9 m above the instrument, while the maximum recorded level above the instrument was 9.5 m, so the near-surface velocity was not observed during several of the largest high tides.

A downward facing Aquadopp ADCP was similarly processed but stopped recording data around July 22 indicating a potential burial of the frame. Echo intensity shows that the bed was normally 17 cm below the Aquadopp sensor, implying a vertical change of 22.5 cm. Whether burial occurred because of sediment deposition or frame sinking is not known. The ADCP velocities were rotated to shore-normal coordinates. The suspended sediment concentration from OBS sensors was estimated using lab calibrations of each of the instruments using sediment sourced from a sediment trap that was located on the ADCP frame.

The two uppermost CTDs were fixed to a surface buoy such that they remained below a constant height from the water surface at 0.35 and 1.7 m below the surface, while the three other CTDs were fixed to the bed at mean heights of 4, 5, and 8.2 m below the surface. The RBR CTDs showed a continuous bias of higher salinity in comparison to the Microcat CTDs throughout the deployment. A fixed salinity bias of 0.24 and 1.48 psu were subtracted from the RBR salinity measurements, as the calibrations on the Microcat CTDs (on loan from NIWA) were more up to date. The suspended sediment concentration from the OBS sensors was estimated by calibrating the backscatter data recorded by the OBS sensors in a tank using bed sediment collected at the location of the instruments.

4.3.2 Additional Data Sources

Data for river discharge and river turbidity were sourced from Hawkes Bay Regional Council at observations station Red Bridge, located 15 km from the river mouth (https://www.hbrc.govt.nz/environment/river-levels/). The river suspended sediment concentration (SSC) was determined from a linear relationship between river turbidity and SSC in samples taken during flood events. Wind speed and direction data were sourced from the Whakatu meteorological station located 3 km inland from the river mouth (data provided by NIWA). Satellite data used here were sourced from Planet Labs and Sentinel-2. Suspended sediments from the Tukituki River contains mostly fine silt (4.3 μm) with mean settling velocities of 0.008 and 0.015 m s^{-1} (White 1994).

4.4 Results

4.4.1 Overview of collected data

Instruments were deployed on July 14 (denoted as day 3) for 41 days, the day after the largest discharge event of the deployment period, where the Tukituki River peak flow was 530 m^3 s^{-1} (Fig. 4.2a). Three additional discharge events occurred during the deployment, including on day 4 (270 m^3 s^{-1}), day 16 (260 m^3 s^{-1}), and day 30 (300 m^3 s^{-1}). During these discharge events, similar magnitudes and timing of freshwater fluxes occurred from the combined outflow of the

Tūtaekurī/Ngaruroro/Mokotūāraro Rivers to the North of the Tukituki River. Smaller discharge events occurred separately for the Ngaruroro/Tūtaekurī/Mokotūāraro Rivers on day 38 (145 m^3 s^{-1}) and for the Tukituki River on day 39 (120 m^3 s^{-1}). The magnitude of suspended sediment concentration in the Tukituki River had similar patterns to river discharge, with sharp increases to values between 500-2000 mg l^{-1} during discharge events which quickly dropped to values in the range of 20-50 mg l^{-1} during non-events.

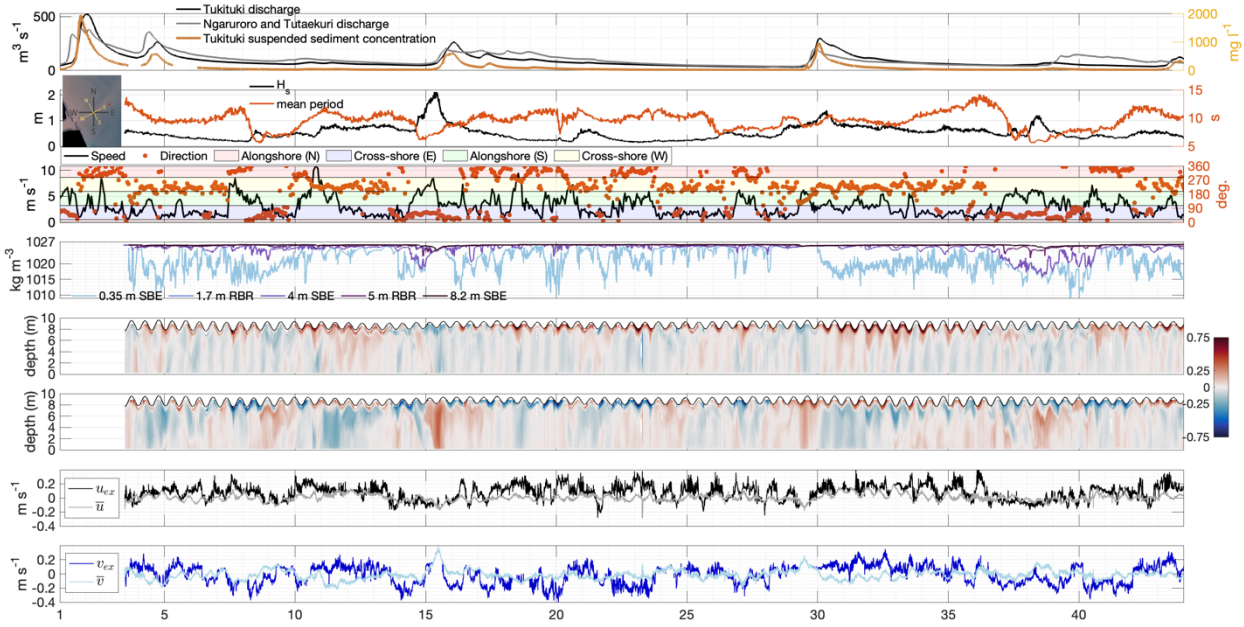

Figure 4.2 Timeseries of collected data offshore of the Tukituki River from July 12 (day 1) to August 24, 2022. a) River discharge (m^3 s^{-1}) from the Tukituki River (black), combined Ngaruroro, Tūtaekurī, and Mokotūāraro Rivers (grey), and the suspended sediment concentration (mg l^{-1}) in the Tukituki River (gold; right axis). b) Left inset panel shows the orientation of the coastline with the rotated coordinate system (yellow). The significant wave height (H_s) in m and the mean wave period (s; right axis). c) The wind speed and direction (right axis) measured at Whakatu. The wind direction axis was coloured based on the coastline orientation at the Tukituki River. d) Density (kg m^{-3}) of from CTD measurements throughout the water column. e) Cross-shelf velocity (m s^{-1}) where positive velocity is directed offshore. f) Along-shelf velocity (m s^{-1}) where positive velocity is directed northward. The surface is shown by the black line. g-h) show the cross-shelf and along-shelf exchange and depth averaged velocities (m s^{-1}).

Wave conditions generally followed the temporal variability of river discharge because the storm events were characterized by both catchment rain and offshore wind conditions that generated swell (Fig. 4.2b). Measured values of significant wave height (H_s) ranged from 0.2 to 2.1 m during the deployment and the measured mean period ranged from 5.5 to 14.2 seconds. Three moderate swell events occurred on day 15 (2.1 m), day 30 (1.4 m), and day 38 (1.2 m), with sustained increased heights from days 11-14 and days 30-36. The mean period was low (~7 s) during the first and third

swell events and elevated during the second swell (12 s) with longer period swell generally occurring during lower wave heights.

The wind speed and direction were highly variable, with multiple wind events with wind speeds greater than 5 m s^{-1} occurring over the 41-day deployment period (Fig. 4.2c). The wind direction was classified in relation to the coastline orientation (left panel in Fig. 4.2b and the right axis of Fig. 4.2c), which shows a predominate offshore wind direction (wind from the SW) with periods of onshore wind (from the NE), as well as alongshore wind in both directions. The water column density showed pronounced surface variability at 0.35 m below the surface throughout the deployment (Fig. 4.2d), while 1.7 m below the surface showed a much smaller range of density variability, indicating the plume thickness was generally less than 1.7 m . The time variability of the surface density was linked with the river discharge and tidal variability but shows additional complexity likely related to wind variability and the river inlet geometry (discussed below).

The water column velocity showed a 1–2 m surface layer throughout the deployment with increased speeds (> 0.5 m s^{-1}) during periods of high stratification and tidal oscillations (Fig. 4.2e-f). The velocity fluctuated between two-layer baroclinic flows, unidirectional flow with increased speed at the surface, and barotropic full water column velocity patterns. The cross-shelf velocity was strongest at the surface (0.2–0.8 m s^{-1}) related to the plume circulation, and weaker at depth (0.1–0.2 m s^{-1}) in comparison to the along-shelf velocity (0.1–0.4 m s^{-1}).

Depth averaged velocities ($\bar{u}, \bar{v}$) and the exchange velocities (u_{ex}, v_{ex}), defined as the average velocity from the surface to the first zero crossing at depth (Moulten et al. 2023) are shown in Fig. 4.2g-h. The cross-shelf exchange velocity u_e is primarily positive and is related to the river plume but varies in magnitude between 0.3 and -0.2 m s^{-1}, while the depth averaged cross-shelf velocity varies in range from 0.4 and -0.4 m s^{-1}. Both appear to relate to tidal oscillations and the wind speed and direction. The depth averaged velocities are slower, with $\bar{u}$ showing predominately tidal variability and $\bar{v}$ showing predominantly wind related variability.

To determine which river plume region the observations where in over the deployment, the upper layer Froude number ($Fr = u/\sqrt{g'h}$) was calculated (Hetland 2005), where u is the average cross-shelf velocity in the plume layer, h is the plume depth, and g' is the reduced gravity. In the near-field region, Fr will be maintained to be greater than 1 and the mid field plume region begins where Fr drops below 1 (Horner-Devine et al. 2015). Given that the density measurements were collected at five locations in the water column, and the largest stratification is typically present between the upper two measurement points (Fig. 4.2), the Froude number was calculated assuming the plume depth, defined as the depth of the maximum stratification, was likely between 0.35 and 1.7 m from the water surface. Using a general plume depth of 1 m and the plume velocity averaged in the

upper 1 m, the Froude number was found to be greater than 1 roughly 50% of the deployment, signifying that the mooring location sampled both the near-field and mid-field plume in time.

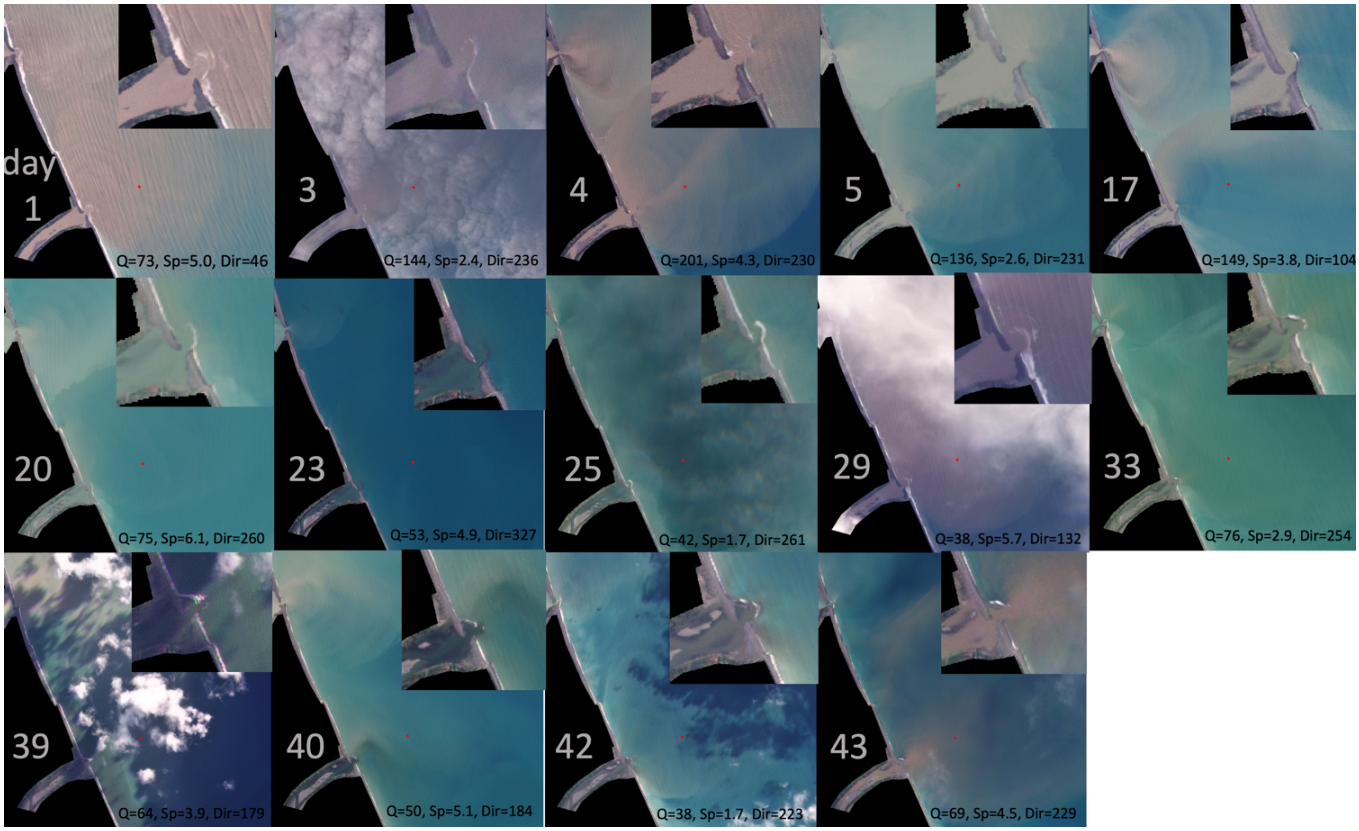

Figure 4.3 Satellite imagery focused on the Tukituki River mouth labelled by days of the deployment. The red dot indicates the location of the mooring. Imagery is sourced from Planet Labs and Sentinel-2. For each day at the time of image collection, the river discharge (Q in m^3 s^{-1}), wind speed (Sp in m s^{-1}) and direction (Dir in degrees) are labelled.

4.4.2 Inlet morphology and plume spatial variability

Satellite imagery collected over the deployment period displays a spatial overview of the Tukituki River plume throughout the deployment period and highlights the importance of the river inlet geometry in controlling the near-field river plume directionality (Fig. 4.3). The beginning period of the deployment (days 3-17) showed that the inlet had an extended submerged bar directing the plume outflow to the north, with waves breaking along the inlet bar on the southern side. Radial plumes were observed generally all days that were not impacted by the inlet geometry, such as days 29, 33, 42, and 43, as well as during days where the bulk of suspended sediment was transported northward but radial spreading occurred (days 4, 5).

Plume extents from satellite imagery suggests that the freshwater transport as recorded at the mooring may have been reduced until ~day 20 as the near-field plume was directed northward. Two

periods of similar river discharge and wind conditions are examined over multiple tidal cycles with different inlet morphologies, from day 4–8 (Fig. 4.4a) and days 29–33 (Fig. 4.4b). The discharge events had similar peak magnitudes of 270 and 300 m^3 s^{-1} respectively and offshore wind (although differing wind speeds) throughout the entire period. At the start of each event, abrupt transitions to upper layer stratification occurs along with upper layer cross-shelf offshore velocity. The main difference between the two events is the magnitude of tidal variability in the stratification and velocity patterns with greater variability when the inlet was directed north, with cross-shore velocities fluctuating between offshore and onshore for the first event and maintaining offshore flow with greater magnitude for the second. It is possible that during the first event, only buoyancy driven signals are observed, while the second event contains both the buoyancy driven spreading as well as the momentum input from the near-field plume. The upper layer Froude number shows roughly a two-fold increase from days 4–8 compared with days 29–33, with most of the period during days 29–33 the Froude number was greater than 1.

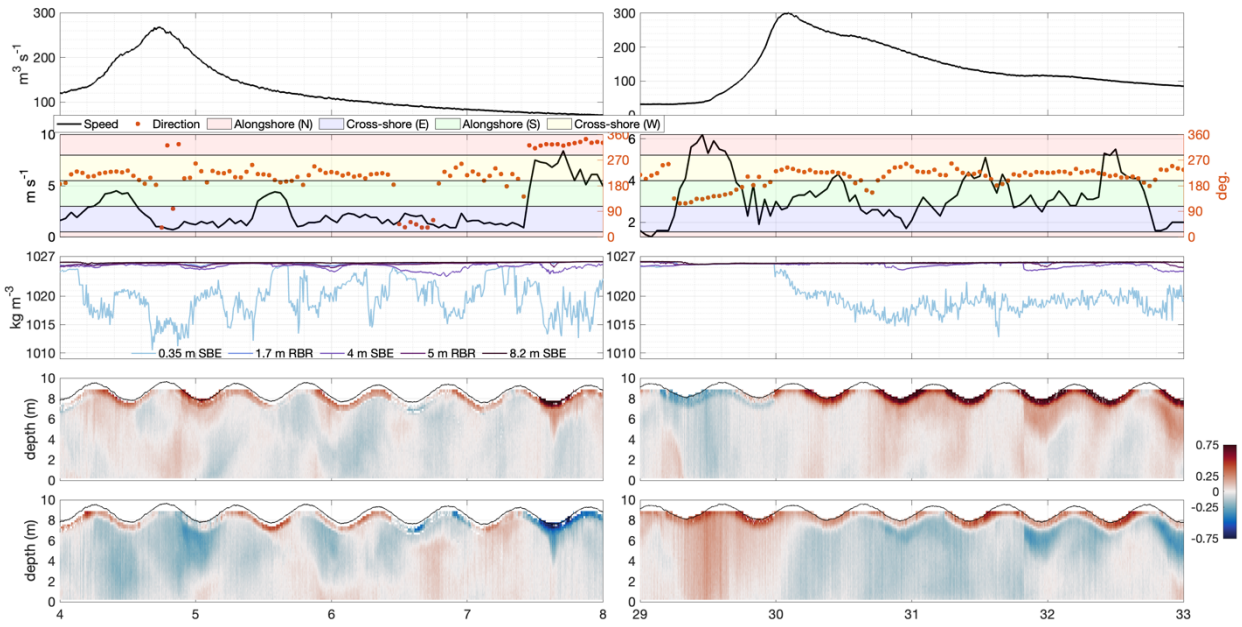

Figure 4.4 Comparison between periods with varying river inlet configurations. The northward directed inlet (left) and the uninhibited inlet (right) are shown under similar discharge and meteorological conditions. The panels include the river discharge, wind speed and direction, density, and cross-shelf and alongshelf velocity.

The timing of satellite data collection did not coincide with the largest wind events but shows a number of modest N wind occurrences (~5 m s^{-1}) where the Ngaruroro/Tūtaekurī/Mokotūāraro plume and the offshore component of the Tukituki plume is directed southward (days 17, 20, 23). Several instances of cross-shore winds with low winds speeds (< 5 m s^{-1}) were additionally captured for onshore winds (days 40 and 42) and offshore winds (days 3, 4, 5, 33, 39 and 43). For all days observed, fronts were present between the plumes of the two rivers which inhibited lateral spreading

from the Tukituki plume northward, and the plume from the Ngaruroro/Tūtaekurī/Mokotūāraro Rivers was not visually observed at the mooring location during the deployment.

4.4.3 Variability with environmental conditions

The relation between environmental conditions and river plume characteristics was assessed through linear correlation analysis between the relevant environmental forcings and main plume properties. Each relevant forcing variable, including the cross-shelf and alongshelf wind, river discharge, tidal height, wave height, and stratification was compared with the river plume response variables that included the cross-shore velocity, alongshore velocity, stratification, and surface density (Fig. 4.5). The cross-shelf wind displayed the highest correlations with the cross-shelf velocity followed by moderate correlations with the alongshelf velocity as well as density stratification. The alongshelf wind in contrast only showed correlations with the alongshelf plume velocity. However, this analysis does not take into account lagged relationships or the dominant timescales of forcing variability, which may show additional patterns regarding river plume response to environmental conditions.

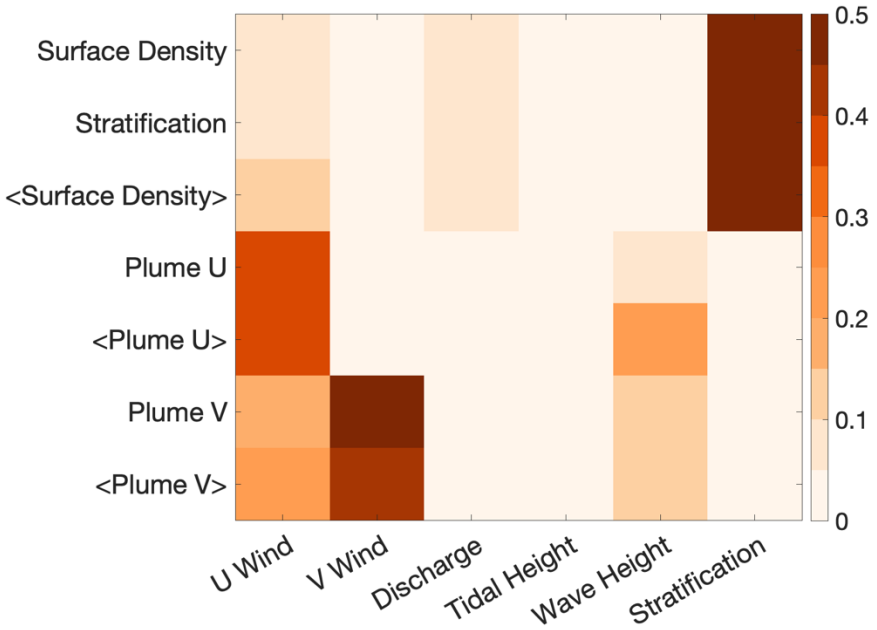

Figure 4.5 The squared linear correlation coefficient (r^2) evaluated between river plume forcing variables (x-axis) and response variables (y-axis). The brackets (< >) denote the use of a tidal filter.

4.4.4 Relation between wind and circulation

The water column velocity was strongly related to wind variability, with differing responses based on the wind direction and stratification. The predominate SW wind direction is directed offshore from the Tukituki River and occurred frequently during the deployment. During SW winds,

surface intensified cross-shore velocity was observed (Fig. 4.2e), and the alongshore velocity was generally two-layer with the surface flowing northward and at depth flowing southward.

During onshore (NE) winds, the offshore directed plume transport was absent in the cross-shore direction and flow was landward. The alongshore flow was northward (when the wind had a slight northward component), likely due to the wind orientation relative to the coastline and showed increased surface shear in comparison to the cross-shore structure, with density stratification still present. The largest decreases in bed density occurred during onshore winds.

One alongshore northward wind (downwelling) event occurred which showed barotropic northward flow and landward cross-shore flow. The plume was likely transported northward away from the mooring location as no stratification was observed. Alongshore southward (upwelling) winds show the surface plume deflecting offshore and to the right, with baroclinic structure observed in both the cross-shore and alongshore directions.

4.4.5 Plume mixing

The vertical structure was used to identify periods of increased mixing throughout the water column and how mixing was related to the interplay of stratification and wind variability. The intensity of turbulence was quantified through the shear squared, the vertical shear of horizontal velocity, defined as $S^2 = (\frac{\partial u}{\partial z})^2 + (\frac{\partial v}{\partial z})^2$. Stresses at the surface and bed drive vertical shear that mix of momentum and buoyancy dependent on the stratification. The surface and bottom boundary layer thicknesses can be described by a critical Ekman thickness which is the depth that mixing from Ekman transport can reach (Lentz and Fewings 2012), which is defined for stratified regions as $\delta = Cu_*/\sqrt{Nf}$ (Moulten et al. 2023). Here C is a constant (1.5), N is the Brunt–Väisälä frequency, and the friction velocity u_* is calculated from the bed and surface shear stress as $u_* = \sqrt{\tau/\rho_0}$. The balance between shear and stratification is represented by the Richardson number, defined as $Ri = g'\rho_z/\rho_0 u_z^2$.

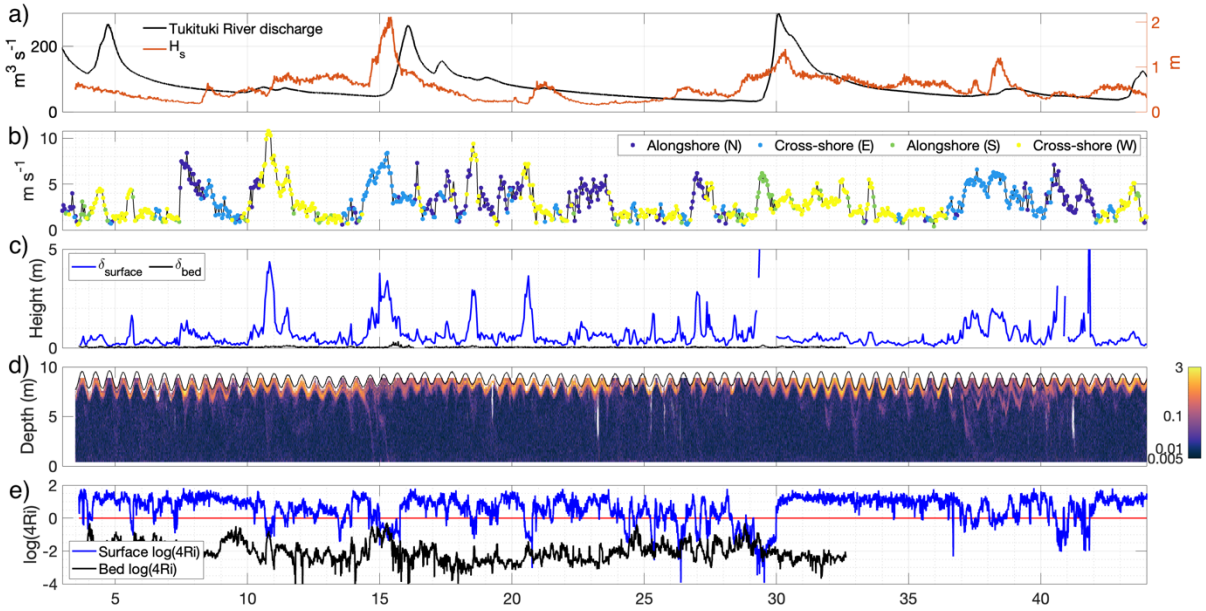

Figure 4.6 Timeseries of mixing related values. a) Tukituki River discharge (black) and significant wave height (orange). b) Wind speed and direction (right axis). c) Critical Ekman depth (m) for the surface (blue) and bottom (black). d) Shear-squared velocity (s^{-2}). e) Richardson number evaluated at the surface (between 0.35 and 1.7 m from the surface) and the closer to the bed (between 5 and 8.2 m from the surface).

The estimated critical Ekman depth at the surface over the deployment ranges from 0.2–4 m below the water surface, with wind events over 1–2-day time frames increasing the depth (Fig. 4.6c). The shear-squared consistently shows highest values in the upper 1 m of the water column (Fig. 4.6d) either at the top of the measured region or ~0.5 m below, with maximum values between 0.5–3 s^{-2} at the surface, and typical values at depth less than 0.03 s^{-2}. Enhanced shear-squared commonly propagates downward into the water column following ebb tide and reaches the bed on few occasions.

The balance between turbulent mixing and stratification is assessed through the Richardson number calculated at the surface and bed (Fig. 4.6e) and compared with an established threshold of stability of 0.25 (Horner-Devine et al. 2015). The average surface Ri is 2.4 indicating predominately stable stratification that is frequently interrupted throughout the deployment, while the average bed Ri is 0.005 and does not exceed the stability threshold during the deployment. The periods of surface Ri<0.25 directly correspond with periods of increased δ_s related to increased wind speeds. These periods show decreased magnitudes of surface S^2 but with S^2 elevated downward through the water column. The decreased magnitude of S^2 is likely due to the reduction in stratification and buoyancy induced shear flow.

4.5 Discussion

The observed circulation patterns at the mooring location were primarily dependent on 1) the river inlet geometry, 2) the river discharge magnitude, and 3) the wind speed and direction. In

particular, the wind variability impacted the cross and alongshelf velocity structure and altered the stratification variability significantly over the deployment. In this section, the response of the vertical structure of velocity, density, and mixing to varying winds is further quantified and compared to previous studies.

4.5.1 Characterizing the wind response

The average response of the velocity profiles to the four wind directions is assessed by averaging vertical profiles over the entire deployment period (Fig. 4.7). The cross-shelf velocity (Fig. 4.7a) shows the greatest offshore directed surface magnitude during offshore winds followed by upwelling winds, and weak offshore surface flow during downwelling winds. During onshore winds, the average surface velocity is landward. At depth (5–6 m from the bed), the average cross-shore velocity is landward for all wind directions with weak speeds. The alongshore winds drive the highest surface alongshore velocities in their respective directions, while offshore wind drives a surface northward velocity and onshore wind drives a surface southward velocity (Fig. 4.7b). The average of the subtidal velocities showed similar patterns as Fig. 4.7.

These results are similar to previous studies that documented increased cross-shore plume velocity during upwelling and downwelling winds (Fong and Geyer 2001, Horner Devine et al. 2015). However, the greatest offshore directed flow occurs during offshore winds on average, which has not been commonly reported (Horner-Devine et al. 2015). Given that the mooring location recorded the near-field plume for roughly half of the deployment, signifying a time-variation of the Rossby number, it is likely that during times where inertia dominates (in the near-field plume), the cross-shelf velocity is less prone to Ekman dynamics and cross-shelf winds can enhance the cross-shelf plume velocity.

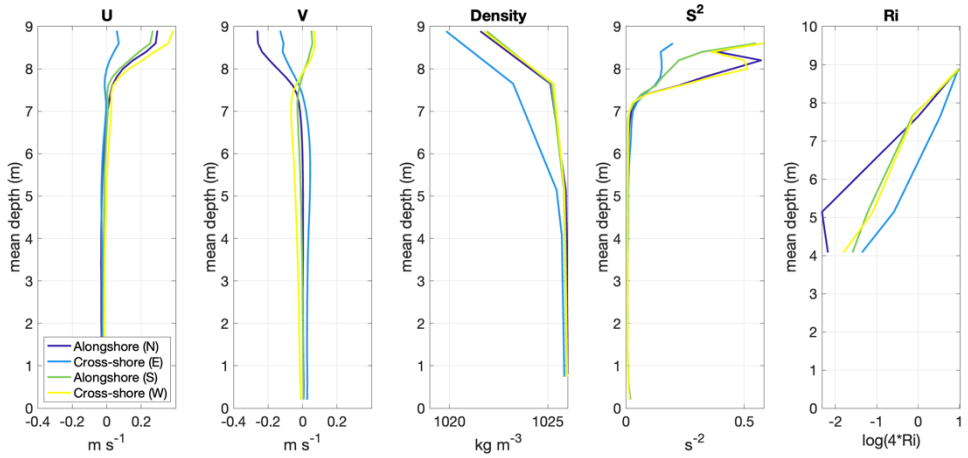

Figure 4.7 Average velocity profiles with to respect to wind direction over the entire deployment. The wind directions are relative to the coastline orientation (shown in Fig 4.2). The y-axis plots the mean depth (m) of the sigma coordinates.

Density profiles are similar for all wind directions with high stratification at the surface, except for onshore winds which show lower density at the surface CTD and throughout the water column (Fig. 4.7c). Closer inspection of the variability between onshore winds and density (Fig. 4.2) shows that density decreases with depth and the plume thickness increases (Fig. 4.7c). Shear-squared profiles show the largest surface shear during offshore and upwelling winds, with lower magnitudes during downwelling and onshore winds (Fig. 4.7d). The mean profiles of Ri show upper water column stable stratification for all wind directions, with higher values at depth again seen for onshore winds (Fig. 4.7e).

4.5.2 Mixing response

The highest shear conditions during the deployment occurred when magnitude of cross-shore plume velocity is the strongest, which corresponded to times of offshore and upwelling winds. The variation of the Richardson number also varies with the wind conditions but does not solely vary with the wind speed or the shear intensity, as the near-surface Ri shows scatter when directly compared with the Ekman depth for Ri values less than 0.25, and additionally does not show a clear relation with wind direction (Fig. 4.8).

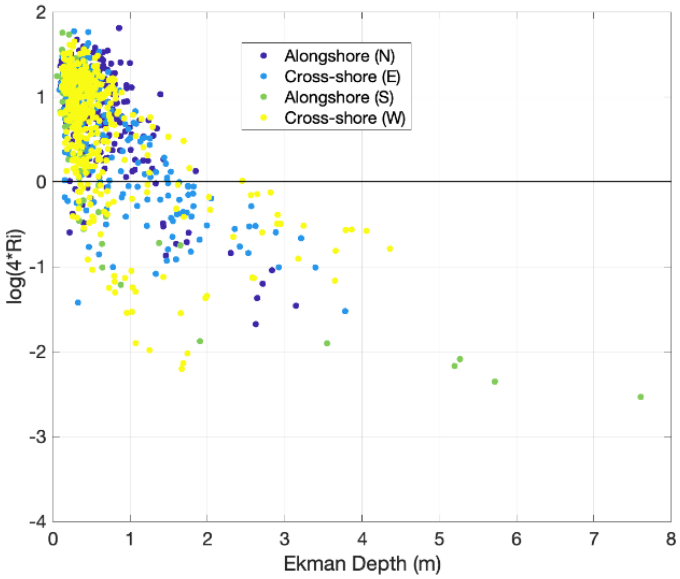

Figure 4.8 The calculated surface Ekman depth (m) compared with the Richardson number (near-surface), coloured by wind direction.

4.5.3 Cross-shore sediment transport

The upper water column suspended sediment concentration ranged from 5-125 mg l^{-1} and was primarily related to variability in the river discharge, while the near bed suspended sediment concentration varied on the order of 1000's of mg l^{-1} and was related to both the river discharge and wave variability (Fig. 4.9a,b). The impact of the observed cross-shelf circulation on the sediment

transport is assessed by comparison with the raw echo magnitude (Fig. 4.9c), the measured SSC values throughout the water column (Fig. 4.9d), and the computed cross-shelf sediment flux at three locations in the water column (Fig. 4.9e,f). In the surface plume layer, the SSC is highly episodic, linked with variations in the river discharge, and is small during non-event time periods. The discharge event on day 16 recorded the highest SSC values at the mooring while the day 4 and day 30 discharge events reached much smaller fractions of the river SSC (~40 mg l^{-1}).

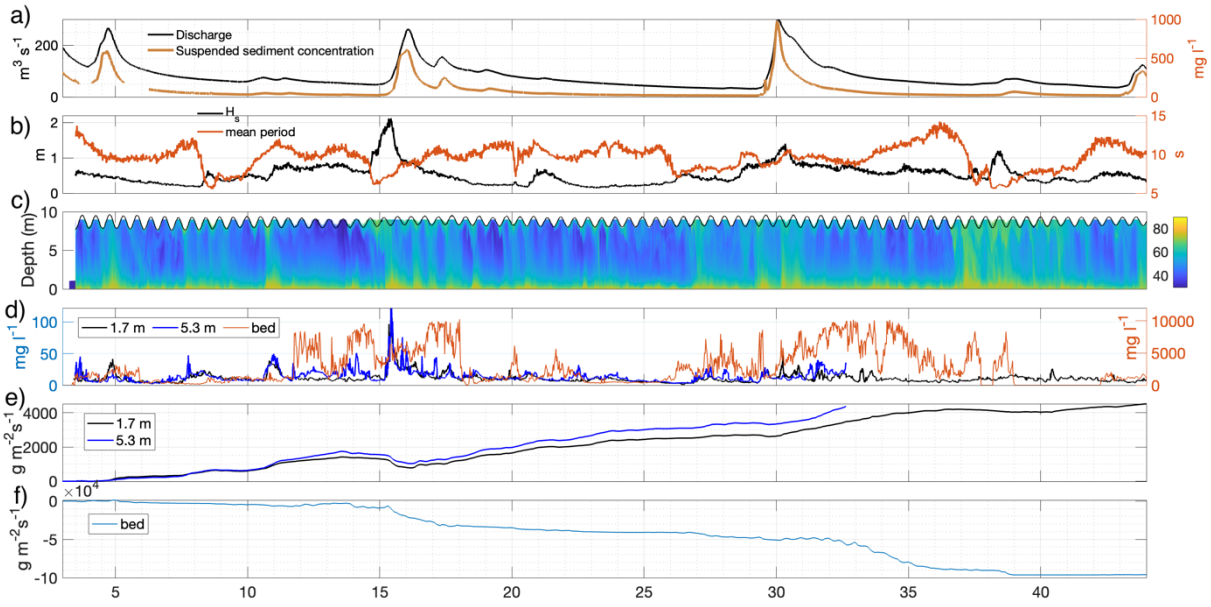

Figure 4.9 Timeseries of suspended sediment concentration and sediment fluxes. a) Tukituki river discharge and suspended sediment concentration. b) Significant wave height and period. c) Echo magnitude (from 0 to 100). d) Suspended sediment concentrations (mg l^{-1}, note that the bed measurement is on the right axis). e) The cumulative near surface cross-shelf sediment fluxes (g $m^{-2}s^{-1}$) and f) the cumulative near bed cross-shelf sediment flux (g $m^{-2}s^{-1}$).

Elevated surface SSC values are followed by subsurface increases in echo intensity (Fig. 4.9c) indicating sediment deposition to the bed. High echo intensity is present from the bed throughout the deployment, which elevates through the water column during increases in wave height. The cumulative cross-shore sediment fluxes for the surface layers show offshore directed transport for the deployment apart from the discharge event on day 16 when onshore winds directed the surface layer landward.

In contrast, the cross-shore transport at the bed was landward for the entire deployment (Fig. 4.9f) and the flux magnitude was an order of magnitude greater than the cross-shore surface flux. For all wind directions, the average near bed cross-shelf velocity is landward (Fig. 4.7a), while the average near bed alongshelf velocity is strongest for cross-shore winds; southward for offshore winds and northward for onshore winds (Fig. 4.7b). Previous work suggests that muddy deposits are

primarily located greater than 10 m depth (White 1994). The circulation at the mooring location suggests that suspended sediment is consistently transported landward at depth, and north or south depending on the water column circulation. Given that the predominant wind direction is offshore which induces a southward alongshore current (Fig. 4.7b), sediment is likely transported southward for a majority of the time.

4.5.4 Scale dependence of river plume

The Tukituki River has smaller time and space scales than the majority of river plumes investigated elsewhere (Horner-Devine et al. 2015, MacCready et al. 2010, Hetland 2010). Smaller plumes have been shown to be less impacted by rotation (Cole et al. 2019), impacted by tidal processes (Basdurak et al. 2020, Spicer et al. 2021), and potentially be influenced by cross-shore winds (Kakoulaki et al. 2014). In this study, radial plumes are observed in satellite imagery with no bulge formation and there was no alongshelf oriented tidal modulation of a low discharge (~10 m^3 s^{-1}) river plume as in Basdurak et al. (2020).

Here, oceanward cross-shore winds were found to impact the cross-shelf velocity structure throughout the deployment in addition to upwelling winds, suggesting that the Tukituki River plume may be an intermediate sized river plume with unique characteristics. It is likely that the measurements collected here reflect the time varying properties of the near-field and midfield plume where rotation has varying magnitudes of relative importance. However, these measurements also signify that cross-shore winds, in particular oceanward directed winds, can accelerate the river plume oceanward at speeds greater than during upwelling winds. In addition, the magnitude of shear-squared observed here is relatively high in comparison to reported values from other river plumes, with values measured here of 0.5-3 s^{-2}. Horner-Devine et al. (2015) reports high shear values in the near-field plume on the order of 1 s^{-2}. It would be beneficial for future studies to integrate these results into a river plume classification to add to the existing classification performed by Horner-Devine et al. (2015).

4.6 Conclusion

A deployment offshore of the Tukituki River captured a large range of conditions including multiple discharge events, wind events from a range of directions, and moderate swell conditions. The instrument location was positioned in the near-field river plume for roughly half of the time which is a region of the river plume that has not been sampled comprehensively in past studies. Satellite imagery revealed that the inlet morphology substantially varied over the deployment period which influenced the directionality of the near-field river plume.

The response to varying wind magnitude and direction was characterised in terms of the vertical structure of velocity, stratification, and intensities of shear-driven mixing. Variations in the

wind direction resulted in distinct vertical profiles of cross-shore and alongshore velocity, with similar results as compared with previous studies for upwelling and downwelling winds, but with stronger than expected relations with onshore and offshore winds. The shear-driven mixing of the river plume was found to be strongly related to the wind stress. Finally, the impact of the cross-shelf circulation on the cross-shelf sediment transport was assessed through computing fluxes throughout the water column. It was found that throughout the deployment period the upper water column transported river derived sediment oceanward, but at near the bed, high landward transport of sediment occurred due to the high sediment concentrations found there due to resuspension combined with the persistent landward near bed flow. Together, these results add a conceptual framework for small mountainous river systems and the sediment transport resultant from river plume circulation.

Chapter 5: General Conclusions

5.1 Main findings of thesis

This thesis set out to describe the dynamics of small mountainous river plumes and detail how suspended sediment from these rivers is transited across the inner shelf on multiple spatial scales, from observations of the near-field plume of the Tukituki River to Bay-wide remote sensing observations, and time scales, from individual discharge events to multi-year periods. Particular emphasis was placed on understanding the drivers of river plume variability, including directionality, mixing, and the transport of suspended sediment. The thesis determined the main drivers of circulation and sediment transport patterns in Hawke Bay, as well as provided globally-relevant information regarding small mountainous river plume circulation, mixing, and the transport of suspended sediment across the inner shelf.

The thesis combined multiple different methodologies with datasets, including the wealth of spatiotemporal information available from satellite remote sensing (Chapter 2), detailed information from numerical ocean modelling (Chapter 3), and highly detailed observations of these processes (Chapter 4). These methods produced new insights regarding **1.** circulation in Hawke Bay, **2.** suspended sediment transport from small mountainous river plumes, and **3.** the relation between wind and plume dynamics in small mountainous river plumes, as elucidated in more detail below.

1. **Hawke Bay circulation**

The circulation in Hawke Bay was found to be heavily influenced by buoyancy input from rivers (Chapter 1), creating density stratification over broad regions of the Bay, with commonly outward-directed radial plumes and buoyancy-driven coastal currents that generally occur in the northern Bay (Fig. 5.1). Similar to past estimates of circulation (e.g. Ridgeway and Stanton 1969), outflow occurs on average at each headland of the Bay (Fig. 5.1), although no strong inflow in the middle of the Bay is observed as was previously suggested (Ridgeway and Stanton 1969). The Wairarapa coastal current is present offshore of the Bay throughout the year, allowing cooler, denser water (relative to the East Cape Current) to be transported into the Bay. The time dependent circulation in the Bay is heavily dependent on wind conditions and the river discharge. Throughout the nearshore of the Bay, the alongshore velocity patterns were driven primarily by wind forcing, while cross-shore velocity was more influenced by buoyancy input from rivers.

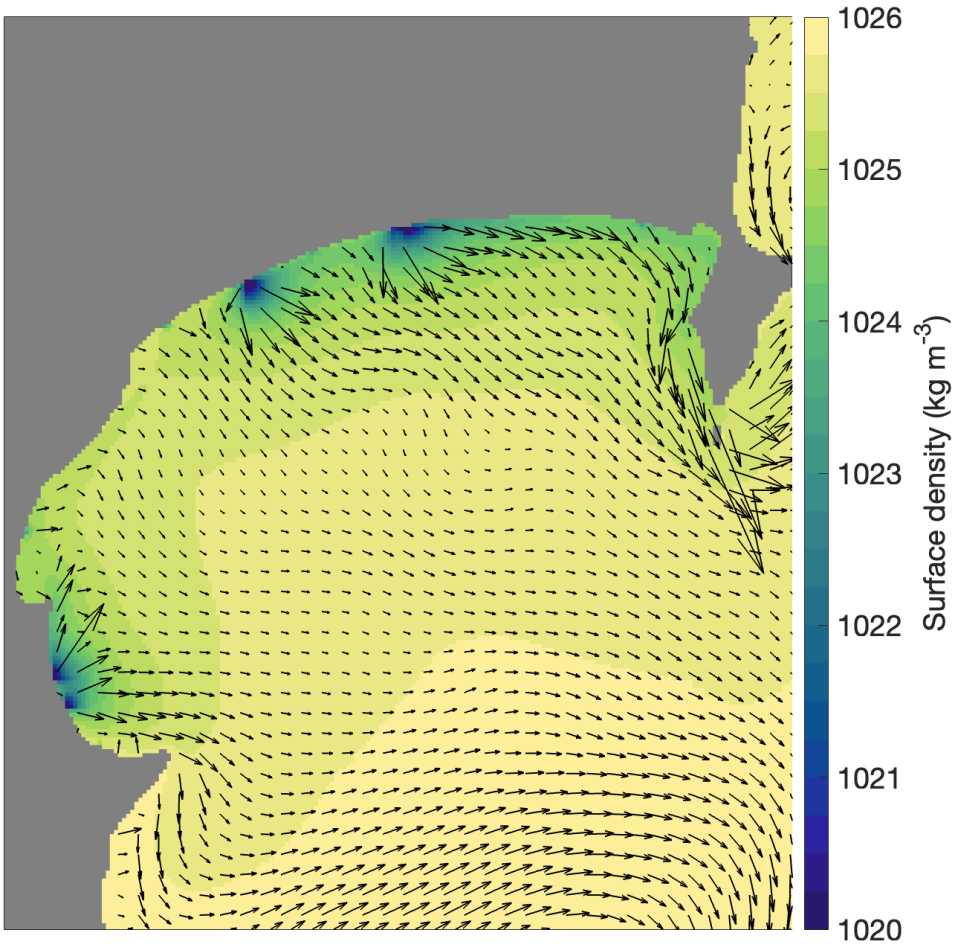

Figure 5.1 The mean surface density and circulation from 2017 to 2019. Mean surface density (coloured; kg m^{-3}) and surface currents (black arrows) in Hawke Bay from 2017 to 2019.

2. Sediment transport in Hawke Bay

The sediment transport in Hawke Bay is initially driven by surface advection from river plumes, with common length scales of surface transport ranging from 2 to 6 km from river inlets, determined from remote sensing (Fig. 5.2). The surface sediment concentration was found to be most linked to temporal variations in river discharge, with secondary impacts from wave resuspension. Wind is important for directing river plumes and was not shown to impact sediment resuspension at the surface. Similar to studies on other rivers, a strong dependence of transport distances on varying particle sizes was found (e.g. Geyer et al. 2004). Fine silt and clay sediments were found to be dispersive throughout the Bay, while coarse silt and aggregated material was only able to be transported a few kilometers from the river mouths through river plumes.

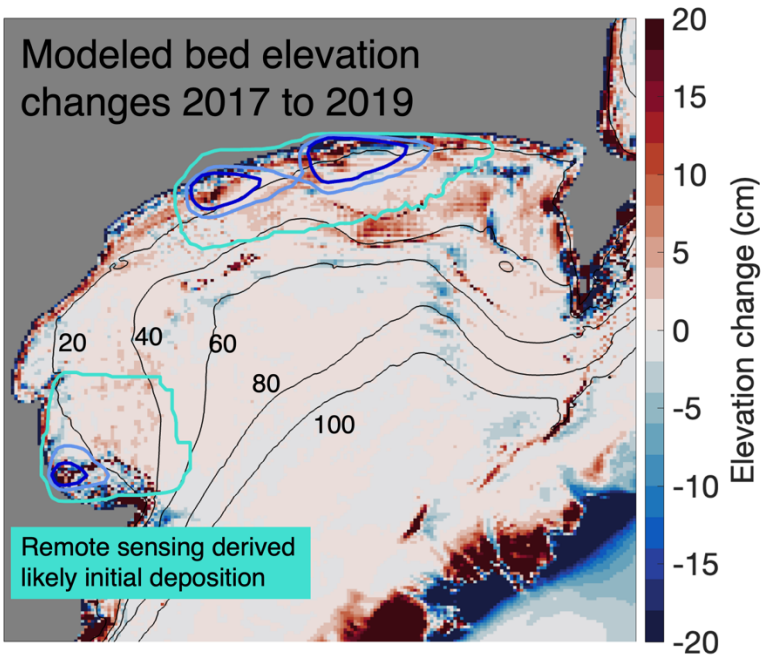

Figure 5.2 The bed sediment deposition from the numerical model (cm) over the period of 2017 to 2019. Depth contours are shown in 20 m intervals. In blue contours, the probabilities of occurrence of the 5 mg l^{-1}TSS value are shown, sourced from Chapter 2.

While sediment from the rivers can settle nearshore if there are small wave heights, the bed stress in the nearshore commonly exceeds thresholds for fine sediment resuspension. Discharge events were shown to produce deposition rates in the range of 1 to 10 cm, however, most fine sediment was transported to depths greater than 40 m over longer time periods. For example, the regions of likely initial sediment deposition (Chapter 2) are broadly representative of longer term sediment accumulation regions (Chapter 3) in offshore depths outside areas of high bed stress. Measurements from offshore of the Tukituki River (Chapter 4) highlight that the near bed velocity is often flowing landward, in opposition to the surface plume layer, which can transport sediment sourced from river plumes and resuspended sediment landward.

3. River plume relation with wind variability

Wind was found to set river plume directionality and is an important component for river plume mixing throughout the Bay, observed from remote sensing, observations, and numerical modelling. The dominant wind direction is from the SW, although the wind displays a broad range of directionality (Fig 5.3), and due to the varying coastline orientation at the major river inlets (Fig. 5.3), a wind direction that is directed offshore in the southern region of the Bay would be directed along the coastline towards the Mahia Peninsula for the northern region, for example. From the remote sensing results (Chapter 2) and the numerical model (Fig. 5.3; Chapter 3), river plumes transport was shown to correspond linearly with wind directions, and the buoyancy flux varied with wind speed (Chapter

3). Offshore of the Tukituki River, the observations (Chapter 4) showed distinct responses of the cross-shore and alongshore velocity profiles, stratification, and mixing to upwelling, downwelling, and cross-shelf winds. The vertical structure observed in the Tukituki River plume is likely found throughout the other rivers in the Bay, but with different probabilities of occurrence due to the varying coastline orientation throughout the Bay.

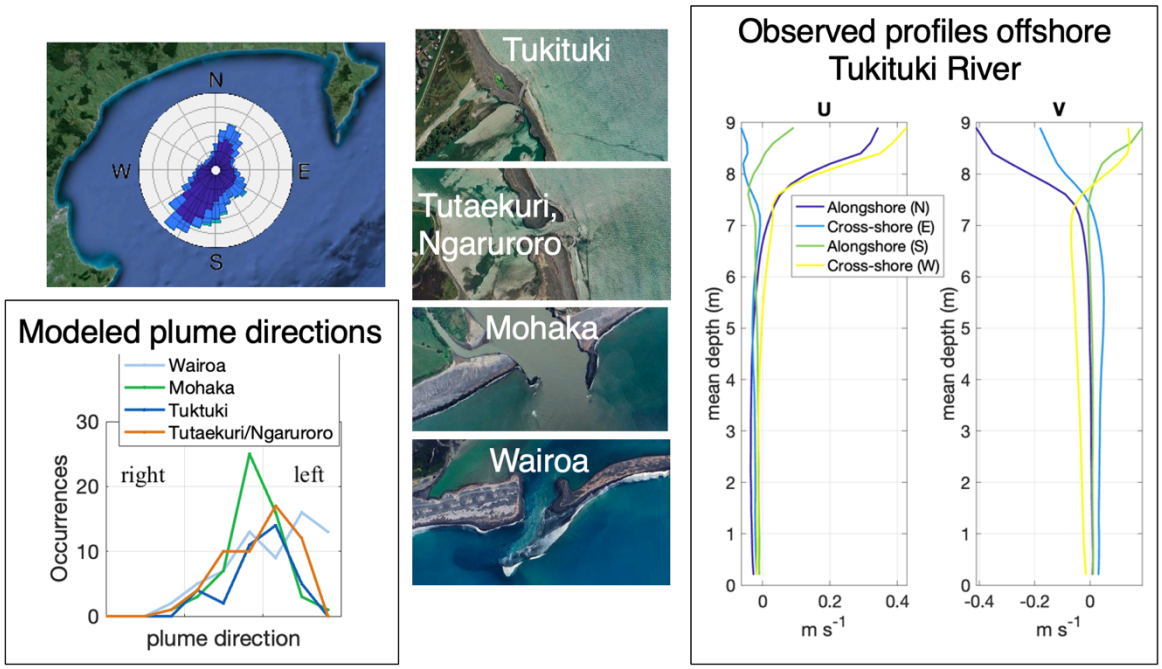

Figure 5.3 The relation between wind and river plume characteristics throughout Hawke Bay. The upper left shows the wind rose from Napier Airport, the bottom left shows modelled river plume directions. The middle panels show the major rivers inlet orientations, and the right plot shows the observed vertical profiles of cross-shore and alongshore velocity in relation to varying wind directions as measured offshore of the Tukituki River.

5.2 Limitations of current work

This thesis used multiple methodologies to take advantage of differing approaches, although each methodology has limitations related either the method itself or the feasibility to be completed during this thesis. The remote sensing analysis would benefit from a TSS algorithm that was created with observations that included a higher range of TSS, as the model shows that the surface SSC can be in range the hundreds of mg l^{-1} during discharge events.

The numerical model showed that the sediment size is a key determinant in setting transport distances from rivers. However, the grain sizes used in Chapter 3 represent the best estimate of characteristic particle sizes in the Bay based on limited measurements. Additional measurements on grain size in rivers, in the Bay, and observations of aggregated particles would add certainty in determining transit patterns from rivers. Additionally, the numerical model simulated river outflows as point sources to the coastal ocean and did not resolve the dynamics of estuaries. This likely induced

greater fresh water delivery to the coast than in nature at times when there is a salt intrusion into the estuaries. The model also did not accurately simulate the momentum flux from rivers as the inlet width is typically much smaller than the model grid size of 500 m. This additions would make the numerical model more realistic but likely would not change the main conclusions of this thesis, as these are derived from multiple lines of evidence.

5.3 Relevance of thesis

Both the terrestrial and marine environment of the Hawkes Bay region can be severely impacted by flood events as exemplified by the devastating effects of Cyclone Gabrielle in 2023, showing the importance of understanding the underlying circulation and sediment transport patterns in small mountainous river systems. The knowledge base generated by this thesis will help inform management strategies and the potential threat to marine ecosystems from sediment loading and seafloor disturbance during discharge events. Locally, this thesis added substantially to our understanding of the characteristics of coastal processes in Hawke Bay, but also informed understanding of small mountainous river systems globally, the characterisation of surface sediment transport from river plumes from remote sensing, and relations between varying wind directions and river plume vertical structure.

References

Albuquerque, J., Antolínez, J.A., Gorman, R.M., Méndez, F.J. and Coco, G., 2021. Seas and swells throughout New Zealand: A new partitioned hindcast. Ocean Modelling, 168, p.101897.

Atkin, E., 2022. Report of Survey: Tukituki River and Entrance. eCoast report prepared for the University of Waikato and the Hawkes Bay Regional Council.

Aurin, D., Mannino, A. and Franz, B., 2013. Spatially resolving ocean color and sediment dispersion in river plumes, coastal systems, and continental shelf waters. Remote Sensing of Environment, 137, pp.212-225.

Basdurak, N.B., Largier, J.L. and Nidzieko, N.J., 2020. Modeling the dynamics of small-scale river and creek plumes in tidal waters. Journal of Geophysical Research: Oceans, 125(7), p.e2019JC015737.

Bever, A.J., McNinch, J.E. and Harris, C.K., 2011. Hydrodynamics and sediment-transport in the nearshore of Poverty Bay, New Zealand: Observations of nearshore sediment segregation and oceanic storms. Continental Shelf Research, 31(6), pp.507-526.

Bever, A.J. and Harris, C.K., 2014. Storm and fair-weather driven sediment-transport within Poverty Bay, New Zealand, evaluated using coupled numerical models. Continental Shelf Research, 86, pp.34-51.

Bostock, H., Jenkins, C., Mackay, K., Carter, L., Nodder, S., Orpin, A., Pallentin, A. and Wysoczanski, R., 2019. Distribution of surficial sediments in the ocean around New Zealand/Aotearoa. Part B: continental shelf. New Zealand Journal of Geology and Geophysics, 62(1), pp.24-45.

Booij, N.R.R.C., Ris, R.C. and Holthuijsen, L.H., 1999. A third-generation wave model for coastal regions: 1. Model description and validation. Journal of geophysical research: Oceans, 104(C4), pp.7649-7666.

Bradford, J.M., 1980. Hydrology, plankton and nutrients in Hawke Bay, September 1976. New Zealand Oceanographic Institute.

Chappell, P.R. 2013. The climate and weather of Hawke's Bay. NIWA Science and Technology Series 58, 44 pp.

Chiswell, S.M., 2002. Wairarapa coastal current influence on sea surface temperature in Hawke Bay, New Zealand. New Zealand Journal of Marine and Freshwater Research, 36(2), pp.267-279.

Cole, K.L. and Hetland, R.D., 2016. The effects of rotation and river discharge on net mixing in small-mouth Kelvin number plumes. Journal of Physical Oceanography, 46(5), pp.1421-1436.

Constantin, S., Doxaran, D., Derkacheva, A., Novoa, S. and Lavigne, H., 2018. Multi-temporal dynamics of suspended particulate matter in a macro-tidal river Plume (the Gironde) as observed by satellite data. Estuarine, Coastal and Shelf Science, 202, pp.172-184.

de Souza, J.M., Suanda, S.H., Couto, P.P., Smith, R.O., Kerry, C. and Roughan, M., 2022. Moana Ocean Hindcast–a 25+ years simulation for New Zealand Waters using the ROMS v3. 9 model. EGUsphere, 2022, pp.1-34.

Dogliotti, A.I., Ruddick, K. and Guerrero, R., 2016. Seasonal and inter-annual turbidity variability in the Río de la Plata from 15 years of MODIS: El Niño dilution effect. Estuarine, Coastal and Shelf Science, 182, pp.27-39.

Eyles, G. and Fahey, B., 2006. The Pakuratahi land use study. Hawkes Bay Regional Council Report 3861.

Feng, L., Hu, C. and Li, J., 2018. Can MODIS land reflectance products be used for estuarine and inland waters?. Water Resources Research, 54(5), pp.3583-3601.

Fong, D.A. and Geyer, W.R., 2001. Response of a river plume during an upwelling favorable wind event. Journal of Geophysical Research: Oceans, 106(C1), pp.1067-1084.

Gangloff, A., Verney, R., Doxaran, D., Ody, A. and Estournel, C., 2017. Investigating Rhône River plume (Gulf of Lions, France) dynamics using metrics analysis from the MERIS 300m Ocean Color archive (2002–2012). Continental shelf research, 144, pp.98-111.

Gerbi, G.P., Chant, R.J. and Wilkin, J.L., 2013. Breaking surface wave effects on river plume dynamics during upwelling-favorable winds. Journal of physical oceanography, 43(9), pp.1959-1980.

Geyer, W.R., Hill, P., Milligan, T. and Traykovski, P., 2000. The structure of the Eel River plume during floods. Continental Shelf Research, 20(16), pp.2067-2093.

Geyer, W.R., Hill, P.S. and Kineke, G.C., 2004. The transport, transformation and dispersal of sediment by buoyant coastal flows. Continental Shelf Research, 24(7-8), pp.927-949.

Godoi, V.A., Bryan, K.R. and Gorman, R.M., 2016. Regional influence of climate patterns on the wave climate of the southwestern Pacific: The New Zealand region. Journal of Geophysical Research: Oceans, 121(6), pp.4056-4076.

Grabowski, R.C., Droppo, I.G. and Wharton, G., 2011. Erodibility of cohesive sediment: The importance of sediment properties. Earth-Science Reviews, 105(3-4), pp.101-120.

Haidvogel, D.B., Arango, H., Budgell, W.P., Cornuelle, B.D., Curchitser, E., Di Lorenzo, E., Fennel, K., Geyer, W.R., Hermann, A.J., Lanerolle, L. and Levin, J., 2008. Ocean forecasting in terrain-following coordinates: Formulation and skill assessment of the Regional Ocean Modeling System. Journal of computational physics, 227(7), pp.3595-3624.

Hale, R.P. and Ogston, A.S., 2015. In situ observations of wave-supported fluid-mud generation and deposition on an active continental margin. Journal of Geophysical Research: Earth Surface, 120(11), pp.2357-2373.

Harris, C.K., Sherwood, C.R., Signell, R.P., Bever, A.J. and Warner, J.C., 2008. Sediment dispersal in the northwestern Adriatic Sea. Journal of Geophysical Research: Oceans, 113(C11).

Hersbach, H., Bell, B., Berrisford, P., Hirahara, S., Horányi, A., Muñoz-Sabater, J., Nicolas, J., Peubey, C., Radu, R., Schepers, D. and Simmons, A., 2020. The ERA5 global reanalysis. Quarterly Journal of the Royal Meteorological Society, 146(730), pp.1999-2049.

Hetland, R.D., 2005. Relating river plume structure to vertical mixing. Journal of Physical Oceanography, 35(9), pp.1667-1688.

Hetland, R.D. and Hsu, T.J., 2013. Freshwater and sediment dispersal in large river plumes. Biogeochemical Dynamics at Large River-Coastal Interfaces: Linkages with Global Climate Change, edited by: Bianchi, TS, Allison, MA, and Cai, W.-J., Springer, New York, USA, pp.55-85.

Hickey, B.M., Kudela, R.M., Nash, J.D., Bruland, K.W., Peterson, W.T., MacCready, P., Lessard, E.J., Jay, D.A., Banas, N.S., Baptista, A.M. and Dever, E.P., 2010. River influences on shelf ecosystems: introduction and synthesis. Journal of Geophysical Research: Oceans, 115(C2).

Hicks, D.M., Shankar, U., McKerchar, A.I., Basher, L., Lynn, I., Page, M. and Jessen, M., 2011. Suspended sediment yields from New Zealand rivers. Journal of Hydrology (New Zealand), pp.81-142.

Hill, P.S., Milligan, T.G. and Geyer, W.R., 2000. Controls on effective settling velocity of suspended sediment in the Eel River flood plume. Continental shelf research, 20(16), pp.2095-2111.

Horner-Devine, A.R., Hetland, R.D. and MacDonald, D.G., 2015. Mixing and transport in coastal river plumes. Annual Review of Fluid Mechanics, 47, pp.569-594.

Hunter, E.J., Chant, R.J., Wilkin, J.L. and Kohut, J., 2010. High-frequency forcing and subtidal response of the Hudson River plume. Journal of Geophysical Research: Oceans, 115(C7).

Kakoulaki, G., MacDonald, D. and Horner-Devine, A.R., 2014. The role of wind in the near field and midfield of a river plume. Geophysical Research Letters, 41(14), pp.5132-5138.

Kerry, C., Roughan, M. and De Souza, J., 2023. Characterising the variability of boundary currents and ocean heat content around New Zealand using a multi-decadal high-resolution regional ocean model. Journal of Geophysical Research: Oceans, p.e2022JC018624.

Kirk, J.T., 1994. Light and photosynthesis in aquatic ecosystems. Cambridge university press.

Kniskern, T.A., Kuehl, S.A., Harris, C.K. and Carter, L., 2010. Sediment accumulation patterns and fine-scale strata formation on the Waiapu River shelf, New Zealand. Marine Geology, 270(1-4), pp.188-201.

Komar, P.D., 2010. Shoreline evolution and management of Hawke's Bay, New Zealand: tectonics, coastal processes, and human impacts. Journal of Coastal Research, 26(1 (261)), pp.143-156.

Kuehl, S.A., Alexander, C.R., Blair, N.E., Harris, C.K., Marsaglia, K.M., Ogston, A.S., Orpin, A.R., Roering, J.J., Bever, A.J., Bilderback, E.L. and Carter, L., 2016. A source-to-sink perspective of the Waipaoa River margin. Earth-Science Reviews, 153, pp.301-334.

Kumar, N. and Feddersen, F., 2017. The effect of Stokes drift and transient rip currents on the inner shelf. Part II: With stratification. Journal of Physical Oceanography, 47(1), pp.243-260.

Kumar, N., Feddersen, F., Suanda, S., Uchiyama, Y. and McWilliams, J., 2016. Mid-to inner-shelf coupled ROMS–SWAN model–data comparison of currents and temperature: Diurnal and semidiurnal variability. Journal of Physical Oceanography, 46(3), pp.841-862.

Lee, Z., Pahlevan, N., Ahn, Y.H., Greb, S. and O'Donnell, D., 2013. Robust approach to directly measuring water-leaving radiance in the field. Applied Optics, 52(8), pp.1693-1701.

Lehmann, M.K., Gurlin, D., Pahlevan, N., Alikas, K., Conroy, T., Anstee, J., Balasubramanian, S.V., Barbosa, C.C., Binding, C., Bracher, A. and Bresciani, M., 2023. GLORIA-A globally representative hyperspectral in situ dataset for optical sensing of water quality. Scientific Data, 10(1), p.100.

Lemagie, E. and Lerczak, J., 2020. The evolution of a buoyant river plume in response to a pulse of high discharge from a small midlatitude river. Journal of Physical Oceanography, 50(7), pp.1915-1935.

Lentz, S.J. and Fewings, M.R., 2012. The wind-and wave-driven inner-shelf circulation. Annual review of marine science, 4, pp.317-343.

Many, G., Bourrin, F., de Madron, X.D., Ody, A., Doxaran, D. and Cauchy, P., 2018. Glider and satellite monitoring of the variability of the suspended particle distribution and size in the Rhône ROFI. Progress in oceanography, 163, pp.123-135.

McKee, B.A., Aller, R.C., Allison, M.A., Bianchi, T.S. and Kineke, G.C., 2004. Transport and transformation of dissolved and particulate materials on continental margins influenced by major rivers: benthic boundary layer and seabed processes. Continental Shelf Research, 24(7-8), pp.899-926.

McSweeney, S.L., Kennedy, D.M., Rutherfurd, I.D. and Stout, J.C., 2017. Intermittently Closed/Open Lakes and Lagoons: Their global distribution and boundary conditions. Geomorphology, 292, pp.142-152.

Milligan, T.G., Hill, P.S. and Law, B.A., 2007. Flocculation and the loss of sediment from the Po River plume. Continental Shelf Research, 27(3-4), pp.309-321.

Milliman, J.D. and Syvitski, J.P., 1992. Geomorphic/tectonic control of sediment discharge to the ocean: the importance of small mountainous rivers. The journal of Geology, 100(5), pp.525-544.

Moghimi, S., Özkan-Haller, H.T., Akan, Ç. and Jurisa, J.T., 2019. Mechanistic analysis of the wave-current interaction in the plume region of a partially mixed tidal inlet. Ocean Modelling, 134, pp.110-126.

Moriarty, J.M., Harris, C.K. and Hadfield, M.G., 2015. Event-to-seasonal sediment dispersal on the Waipaoa River Shelf, New Zealand: A numerical modeling study. Continental Shelf Research, 110, pp.108-123.

Moulton, M., Suanda, S.H., Garwood, J.C., Kumar, N., Fewings, M.R. and Pringle, J.M., 2023. Exchange of plankton, pollutants, and particles across the nearshore region. Annual Review of Marine Science, 15, pp.167-202.

Murphy, A.H., 1988. Skill scores based on the mean square error and their relationships to the correlation coefficient. Monthly weather review, 116(12), pp.2417-2424.

Nechad, B., Dogliotti, A., Ruddick, K. and Doxaran, D., 2016, May. Particulate backscattering and suspended matter concentration retrieval from remote-sensed turbidity in various coastal and riverine turbid waters. In Living Planet Symposium, Proceedings of the conference held (pp. 9-13).

Norris, T., 2019. Sediment monitoring using automatic ISCO samplers for State of the Environment reporting in Hawke's Bay. Report from the Hawkes Bay Regional Council. HBRC Report No. RM19-245-5398.

O'Callaghan, J., 2019. Spatial mapping of subsurface oxygen depletion in Hawke Bay. NIWA client report number 2019213WN.

O'Callaghan, J.M. and Stevens, C.L., 2017. Evaluating the surface response of discharge events in a New Zealand Gulf-ROFI. Frontiers in Marine Science, 4, p.232.

Olabarrieta, M., Warner, J.C. and Kumar, N., 2011. Wave-current interaction in Willapa Bay. Journal of Geophysical Research: Oceans, 116(C12).

Pantin, H.M., 1966. Sedimentation in Hawke Bay No. Bulletin 171 New Zealand Department of Science and Industrial Research.

Pawlowicz, R., Di Costanzo, R., Halverson, M., Devred, E. and Johannessen, S., 2017. Advection, surface area, and sediment load of the Fraser River plume under variable wind and river forcing. Atmosphere-Ocean, 55(4-5), pp.293-313.

Paquet, F., Proust, J.N., Barnes, P.M. and Pettinga, J.R., 2009. Inner-forearc sequence architecture in response to climatic and tectonic forcing since 150 ka: Hawke's Bay, New Zealand. Journal of Sedimentary Research, 79(3), pp.97-124.

Ridgway, N. M., 1960. Surface water movements in Hawke Bay, New Zealand, New Zealand Journal of Geology and Geophysics 3:253-261.

Ridgway N. M. and Stanton B. R., 1969. Some hydrological features of Hawke Bay and nearby shelf waters, New Zealand Journal of Marine and Freshwater Research 3: 545-559

Rodriguez, A.R., Giddings, S.N. and Kumar, N., 2018. Impacts of nearshore wave-current interaction on transport and mixing of small-scale buoyant plumes. Geophysical Research Letters, 45(16), pp.8379-8389.

Rong, Z., Hetland, R.D., Zhang, W. and Zhang, X., 2014. Current–wave interaction in the Mississippi–Atchafalaya river plume on the Texas–Louisiana shelf. Ocean Modelling, 84, pp.67-83.

Saldías, G.S., Sobarzo, M., Largier, J., Moffat, C. and Letelier, R., 2012. Seasonal variability of turbid river plumes off central Chile based on high-resolution MODIS imagery. Remote Sensing of Environment, 123, pp.220-233.

Smolarkiewicz, P.K. and Margolin, L.G., 1998. MPDATA: A finite-difference solver for geophysical flows. Journal of Computational Physics, 140(2), pp.459-480.

Soulsby, R.L. and Whitehouse, R.J., 1997, January. Threshold of sediment motion in coastal environments. In Pacific Coasts and Ports' 97: Proceedings of the 13th Australasian Coastal and Ocean Engineering Conference and the 6th Australasian Port and Harbour Conference; Volume 1 (pp. 145-150). Christchurch, NZ: Centre for Advanced Engineering, University of Canterbury.

Spicer, P., Cole, K.L., Huguenard, K., MacDonald, D.G. and Whitney, M.M., 2021. The effect of bottom-generated tidal mixing on tidally pulsed river plumes. Journal of Physical Oceanography, 51(7), pp.2223-2241.

Stevens, C.L., O'Callaghan, J.M., Chiswell, S.M. and Hadfield, M.G., 2021. Physical oceanography of New Zealand/Aotearoa shelf seas–a review. New Zealand Journal of Marine and Freshwater Research, 55(1), pp.6-45.

Suanda, S.H., Feddersen, F., Spydell, M.S. and Kumar, N., 2018. The effect of barotropic and baroclinic tides on three-dimensional coastal dispersion. Geophysical Research Letters, 45(20), pp.11-235.

Thrush, S.F., Hewitt, J.E., Cummings, V.J., Ellis, J.I., Hatton, C., Lohrer, A. and Norkko, A.J.F.I.E., 2004. Muddy waters: elevating sediment input to coastal and estuarine habitats. Frontiers in Ecology and the Environment, 2(6), pp.299-306.

Traykovski, P., Geyer, W.R., Irish, J.D. and Lynch, J.F., 2000. The role of wave-induced density-driven fluid mud flows for cross-shelf transport on the Eel River continental shelf. Continental shelf research, 20(16), pp.2113-2140.

Walsh, J.P. and Nittrouer, C.A., 2009. Understanding fine-grained river-sediment dispersal on continental margins. Marine Geology, 263(1-4), pp.34-45.

Warner, J.C., Sherwood, C.R., Signell, R.P., Harris, C.K. and Arango, H.G., 2008. Development of a three-dimensional, regional, coupled wave, current, and sediment-transport model. Computers & geosciences, 34(10), pp.1284-1306.

Warrick, J.A., Xu, J., Noble, M.A. and Lee, H.J., 2008. Rapid formation of hyperpycnal sediment gravity currents offshore of a semi-arid California river. Continental Shelf Research, 28(8), pp.991-1009.

White, J.L., 1994. Coastal Processes. Nearshore Suspended Sediment in Hawke Bay. Report to the Hawke Bay Regional Council. Technical Services Department, Hawkes Bay Regional Council, TS, 94(3).

Wright LD, Nittrouer CA., 1995. Dispersal of river sediments in coastal seas: six contrasting cases. Estuaries. Sep;18:494-508.

Wright, L.D., Thom, B.G. and Higgins, R.J., 1980. Wave influences on river-mouth depositional process: examples from Australia and Papua New Guinea. Estuarine and coastal marine science, 11(3), pp.263-277.

Wu, X., Feddersen, F., Giddings, S.N., Kumar, N. and Gopalakrishnan, G., 2020. Mechanisms of Mid-to Outer-Shelf Transport of Shoreline-Released Tracers. Journal of Physical Oceanography, 50(7), pp.1813-1837.

Yu, X., Lee, Z., Shang, Z., Lin, H. and Lin, G., 2021. A simple and robust shade correction scheme for remote sensing reflectance obtained by the skylight-blocked approach. Optics Express, 29(1), pp.470-486.